Supporting Information for

Enhanced catalytic performance derived from coordination-driven structural switching between homometallic complexes and heterometallic polymeric materials

*Gracjan Kurpik, Anna Walczak, Grzegorz Markiewicz, Jack Harrowfield and Artur R. Stefankiewicz**

Table of contents

1. Materials and methods

Chemicals and solvents were purchased from commercial suppliers (mainly Merck and Fluorochem) and used without further purification. NMR solvents were purchased from Deutero GmbH and used as received.

NMR spectra were acquired on Bruker Fourier 300 MHz and Bruker Avance IIIHD 600 MHz spectrometers at 298 K and referenced on solvent residual peaks. All NMR data were processed with Mestrelab Research *MNova* software. ESI-MS spectra were recorded on a Bruker HD Impact spectrometer in positive ion mode. Theoretical MS spectra were predicted using Mestrelab Research *MNova* software. ATR-FTIR spectra were recorded on Thermo Fisher Nicolet iS50 FT-IR spectrometer. TG analysis was performed using a STA4000 (Perkin Elmer–Waltham) instrument between 30 and 600 ^{o}C in a N_2 atmosphere with a flow rate of 20 mL min^{-1} and a heating rate of 10 ^{o}C min^{-1}. Powder XRD patterns were recorded on a BRUKER D8-Focus Bragg-Brentano X-ray powder diffractometer equipped with a Cu sealed tube (λ = 1.54178Å) at room temperature. The scans were collected in the 2θ range of 5-50^{o}. Catalytic reaction products were identified with gas chromatograph Varian 450-GC coupled to mass spectrometer Bruker 320-MS.

2. Synthetic procedures

2.1. Synthesis of ligand HL

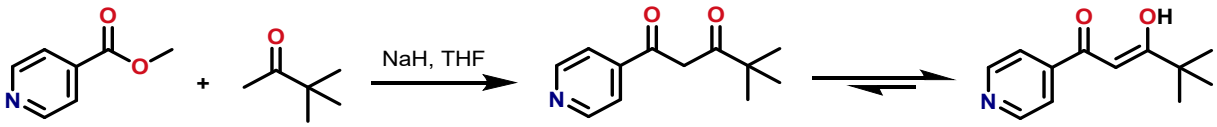

Scheme S1. Synthesis of the ligand H**L**.

The ligand H**L** (4,4-dimethyl-1-(pyridin-4-yl)pentane-1,3-dione) was prepared by Claisen condensation, following a literature procedure and involving the reaction between methyl isonicotinate and 3,3-dimethyl-2-butanone in the presence of sodium hydride. The ^{1}H NMR signals were in a good accordance with the literature data.[1]

^{1}H NMR (300 MHz, $CDCl_3$) δ = 16.09 (s, 1H), 8.75 (dd, *J* = 5.8, 1.6 Hz, 2H), 7.69 (dd, *J* = 6.1, 1.8 Hz, 2H), 6.34 (s, 1H), 4.19 (s, 0.04H), 1.26 (s, 9H).

2.2. Synthesis of the complexes based on HL

2.2.1. $[Ag(HL)_2]NO_3$ (C1)

To a solution of H**L** (82.1 mg, 0.40 mmol) in EtOH/DCM (1:1, *v/v*, 2 mL) $AgNO_3$ (34.0 mg, 0.20 mmol) was added. The mixture was stirred at room temperature for 18 h. After, the solvent was evaporated under reduced pressure. The solid residue was redissolved in DCM (0.5 mL) and precipitated by adding *n*-hexane (5 mL). The product was centrifuged off, washed with *n*-hexane (2 × 5 mL), and dried in vacuo. Yield: 77.8 mg, 67%.

^{1}H NMR (300 MHz, $CDCl_3$) δ = 16.00 (s, 2H, H^5), 8.77 (d, *J* = 6.5 Hz, 4H, H^1), 7.80 (d, *J* = 6.5 Hz, 4H, H^2), 6.36 (s, 2H, H^3), 1.27 (s, 18H, H^4).

ESI-MS calcd. for $[Ag(HL)_2]^+$ $[M\text{-}NO_3]^+$: *m/z* = 517.1251, observed: *m/z* = 517.1216.

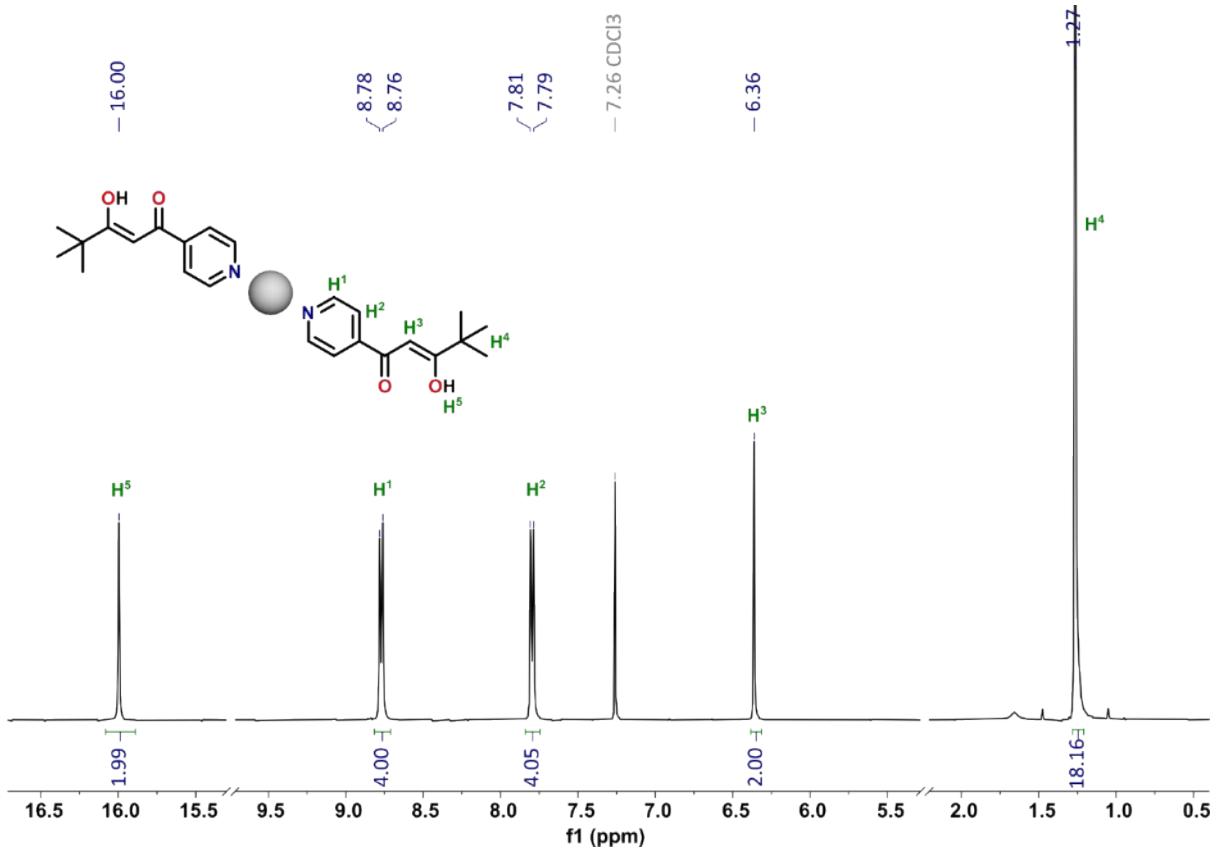

Figure S1. ^{1}H NMR spectrum (300 MHz, $CDCl_3$) of the complex $[Ag(HL)_2]NO_3$ (**C1**).

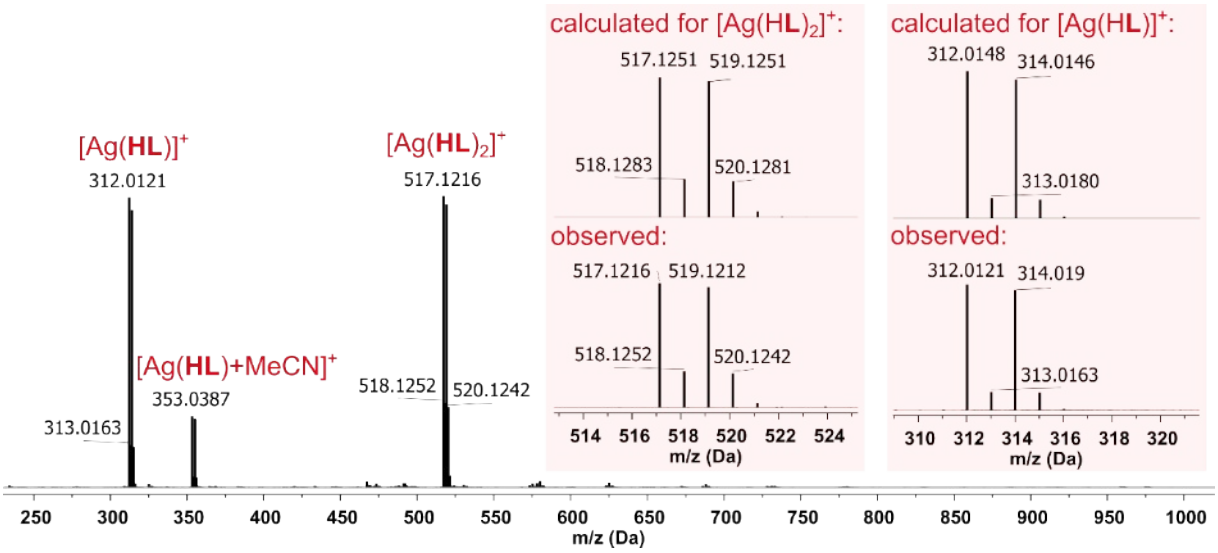

Figure S2. ESI-MS spectrum of the complex $[Ag(HL)_2]NO_3$ (**C1**).

2.2.2. $[Pd(HL)_4](NO_3)_2$ (C3)

The complex $[Pd(HL)_4](NO_3)_2$ was prepared according to a known literature procedure. The ^{1}H NMR signals were in a good accordance with the literature data.[1]

^{1}H NMR (300 MHz, $CDCl_3$) δ = 15.67 (s, 4H), 9.75 (d, *J* = 6.8 Hz, 8H), 7.83 (d, *J* = 6.8 Hz, 8H), 6.25 (s, 4H), 1.20 (s, 36H).

2.2.3. [PdL_2] (C6)

The complex [Pd**L**$_2$] was prepared according to a known literature procedure. The ^{1}H NMR signals were in a good accordance with the literature data.[1]

^{1}H NMR (300 MHz, $CDCl_3$) δ = 8.70 (d, *J* = 4.6 Hz, 4H), 7.65 (d, *J* = 4.5 Hz, 4H), 6.24 (d, *J* = 9.2 Hz, 2H), 1.26 (d, *J* = 4.2 Hz, 18H).

2.2.4. [Pd(en)(H**L**)$_2$](NO$_3$)$_2$ (C2)

A solution of H**L** (5.0 mg, 0.024 mmol) in CD_3CN (0.5 mL) was added to [Pd(en)$(NO_3)_2$] (3.5 mg, 0.012 mmol) in a NMR tube. The reaction mixture was placed in an ultrasonic bath at 50 °C. After 30 minutes, the ^{1}H NMR spectrum was measured.

^{1}H NMR (600 MHz, CD_3CN) δ = 15.81 (s, 2H, H^5), 8.94 (d, *J* = 6.8 Hz, 4H, H^1), 7.95 (d, *J* = 6.8 Hz, 4H, H^2), 6.58 (s, 2H, H^3), 4.90 (s, 4H, H^7), 2.85 (s, 4H, H^6), 1.21 (s, 18H, H^4).

ESI-MS calcd. for [Pd(en)(H**L**)$_2$(NO$_3$)+2MeCN]$^+$ [M-NO$_3$+2MeCN]$^+$: *m/z* = 720.2343, observed: *m/z* = 720.2297; calcd. for [Pd**L**$_2$+MeCN+H]$^+$ [M-2NO$_3$+MeCN+H]$^+$: *m/z* = 556.1432, observed: *m/z* = 556.1453.

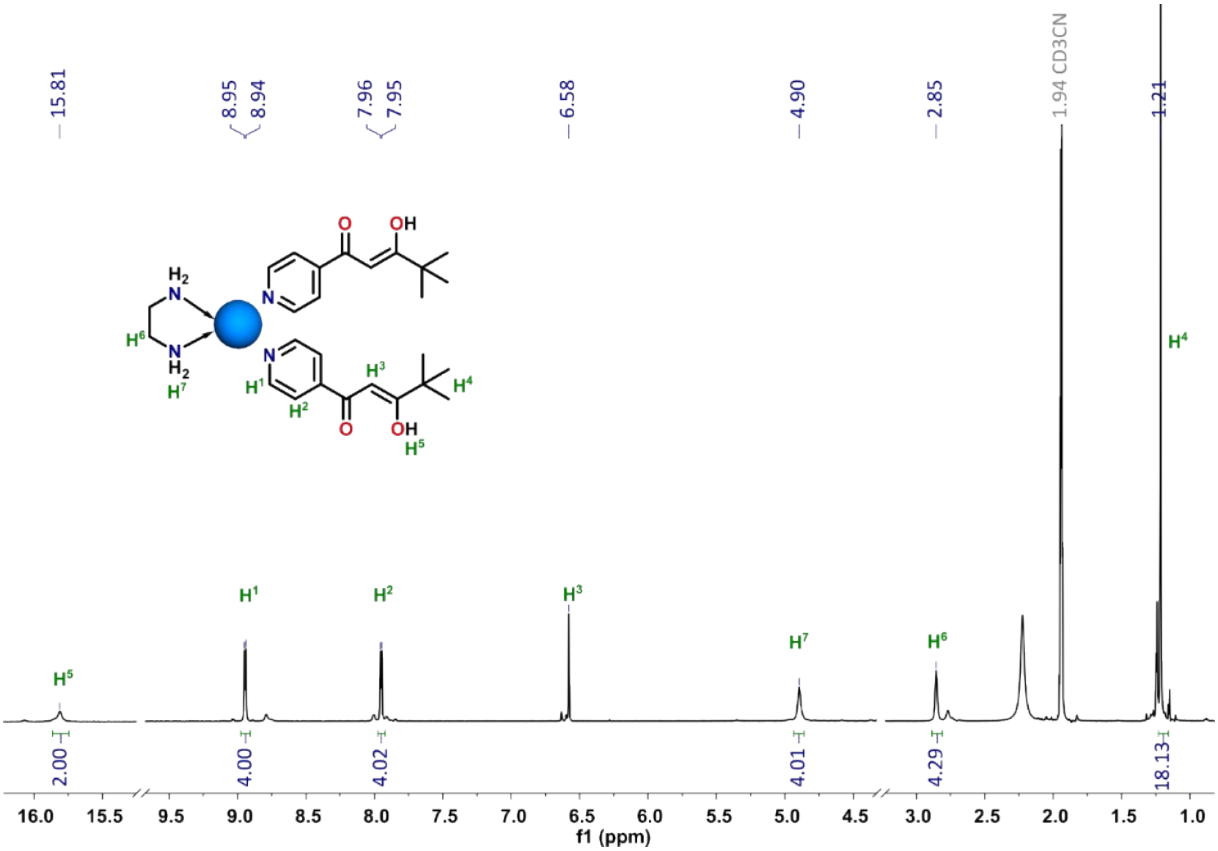

Figure S3. ^{1}H NMR spectrum (600 MHz, CD_3CN) of the complex [Pd(en)(H**L**)$_2$](NO$_3$)$_2$ (**C2**).

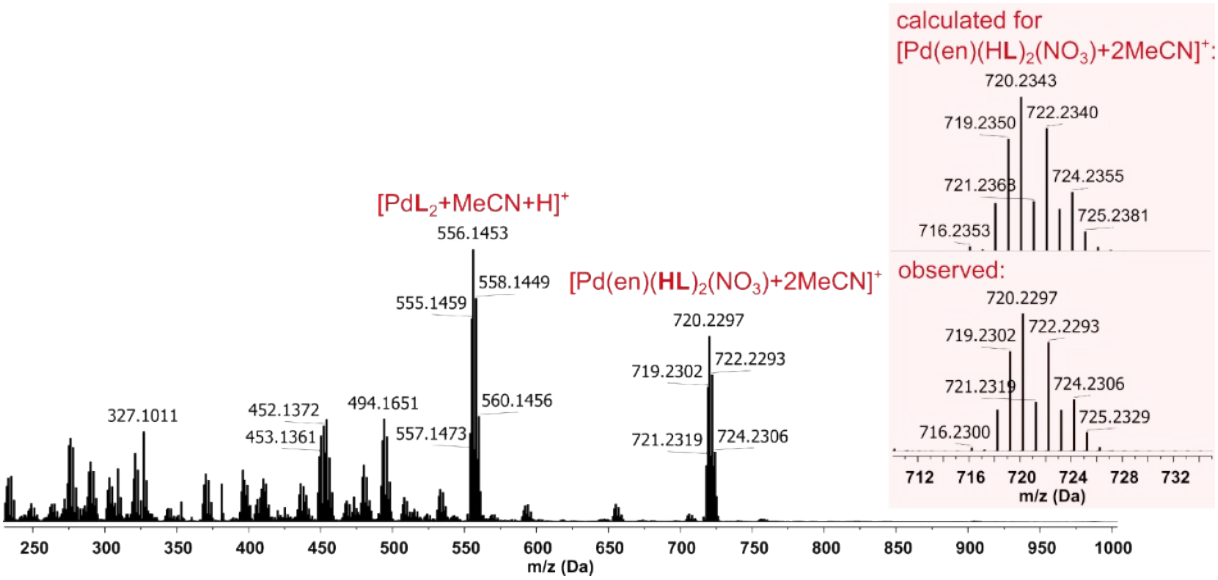

Figure S4. ESI-MS spectrum of the complex [Pd(en)(H**L**)$_2$](NO$_3$)$_2$ (**C2**).

2.2.5. [Pd(en)L]NO$_3$ (C5)

To a ligand H**L** (5.0 mg, 0.024 mmol) dissolved in CD$_3$CN (0.5 mL) Et$_3$N (10.0 µL, 0.072 mmol) was added. After, the solution of deprotonated ligand was added to [Pd(en)(NO$_3$)$_2$] (3.5 mg, 0.012 mmol) in a NMR tube. The reaction mixture was placed in an ultrasonic bath at 50 °C. After 30 minutes, the ^{1}H NMR spectrum was measured.

^{1}H NMR (300 MHz, CD$_3$CN) δ = 8.68 (d, *J* = 4.8 Hz, 2H), 7.70 (d, *J* = 4.0 Hz, 2H), 6.34 (s, 1H), 4.40 (d, *J* = 12.3 Hz, 4H), 1.19 (s, 9H).

ESI-MS calcd. for [Pd(en)**L**]$^+$ [M-NO$_3$]$^+$: *m/z* = 370.0747, observed: *m/z* = 370.0743.

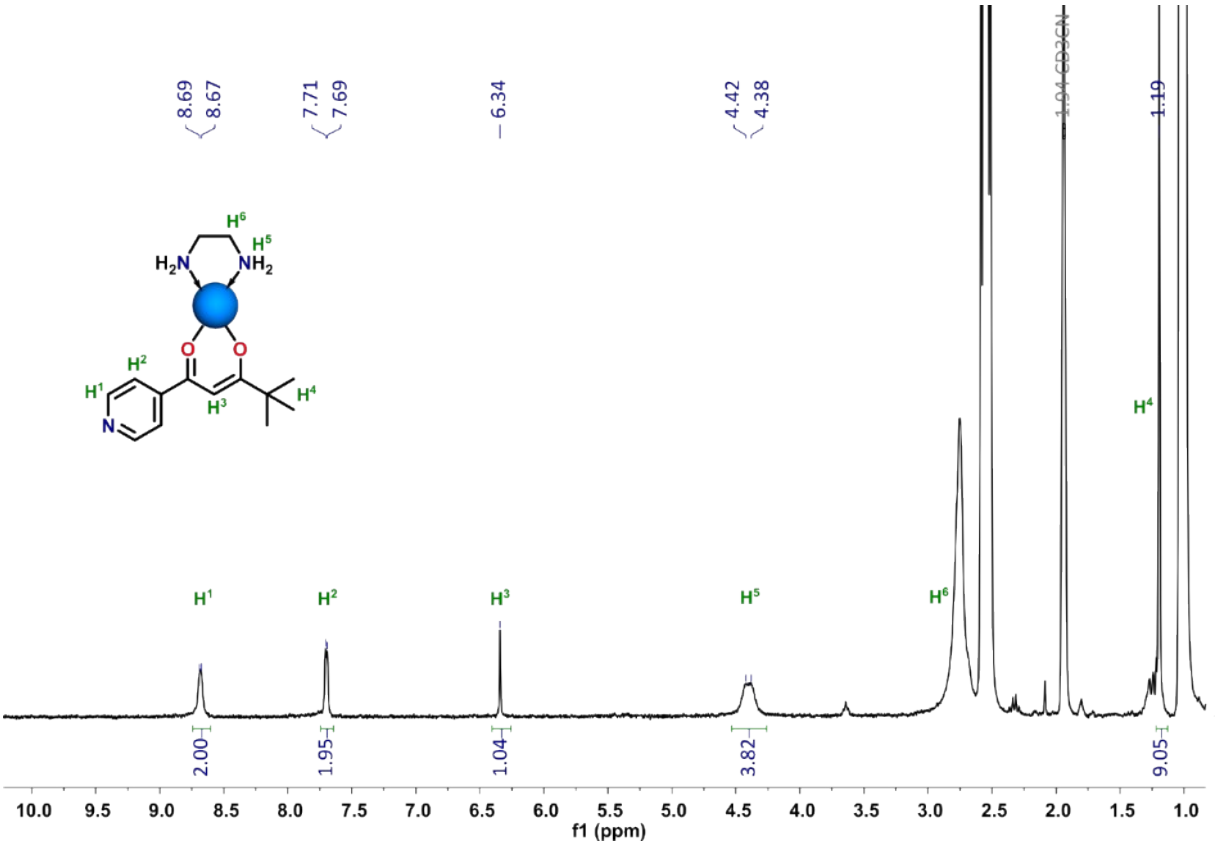

Figure S5. ^{1}H NMR spectrum (300 MHz, CD_3CN) of the complex [Pd(en)**L**]NO_3 (**C5**).

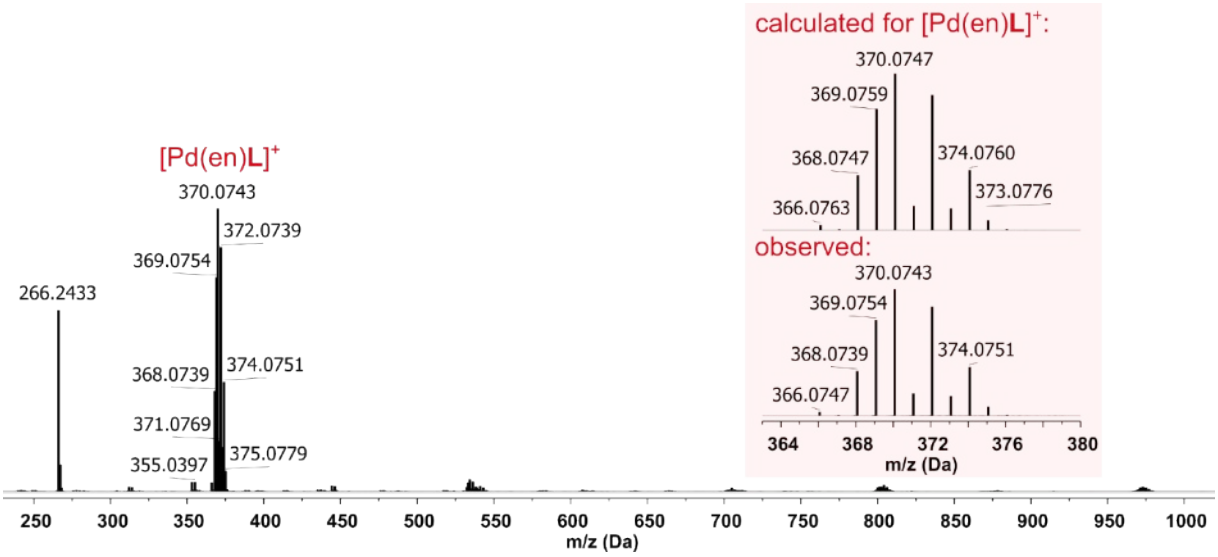

Figure S6. ESI-MS spectrum of the complex [Pd(en)**L**]NO_3 (**C5**).

2.2.6. $[Pt(HL)_4](NO_3)_2$ (C4)

The complex $[Pt(HL)_4](NO_3)_2$ was prepared according to a known literature procedure. The ^{1}H NMR signals were in a good accordance with the literature data.[2]

^{1}H NMR (300 MHz, $CDCl_3$) δ = 15.65 (s, 4H), 9.70 (d, *J* = 6.9 Hz, 8H), 7.86 (d, *J* = 6.9 Hz, 8H), 6.29 (s, 4H), 1.20 (s, 36H).

2.3. Synthesis of the coordination polymers based on HL

2.3.1. Polymer P1

A solution of AgOTf (5.0 mg, 0.019 mmol) or $AgNO_3$ (3.2 mg, 0.019 mmol) in MeOH (1 mL) was added to [Pd**L**$_2$] (10.0 mg, 0.019 mmol) dissolved in $CHCl_3$ (1 mL). The reaction mixture was stirred at room temperature for 18 h. After, the brown precipitate was centrifuged off, washed with MeOH (5 mL) and Et_2O (2 × 5 mL), and dried in vacuo. Yield: 5.8 mg, 48%.

ESI-MS calcd. for $C_{24}H_{29}N_2O_4Pd^+$ [Pd**L**$_2$+H$^+$]$^+$: *m/z* = 515.1166, observed: *m/z* = 515.1164; calcd. for $C_{24}H_{28}AgN_2O_4Pd^+$ [PdAg**L**$_2$]$^+$: *m/z* = 623.0136, observed: *m/z* = 623.0134; calcd. for $C_{26}H_{31}AgN_3O_4Pd^+$ [PdAg**L**$_2$+MeCN]$^+$: *m/z* = 664.0402, observed: *m/z* = 664.0399; calcd. for $C_{26}H_{34}AgN_2O_5PdS^+$ [PdAg**L**$_2$+DMSO]$^+$: *m/z* = 701.0275, observed: *m/z* = 701.0271; calcd. for $C_{72}H_{85}AgN_6O_{12}Pd_3^{2+}$ [Pd$_3$Ag**L**$_6$+H$^+$]$^{2+}$: *m/z* = 826.1206, observed: *m/z* = 826.1187; calcd. for $C_{72}H_{84}Ag_2N_6O_{12}Pd_3^{2+}$ [Pd$_3$Ag$_2$**L**$_6$]$^{2+}$: *m/z* = 880.0692, observed: *m/z* = 880.0696; calcd. for $C_{48}H_{56}AgN_4O_8Pd^{2+}$ [Pd$_2$Ag**L**$_4$]$^+$: *m/z* = 1137.1237, observed: *m/z* = 1137.1229; calcd. for $C_{60}H_{70}N_5O_{10}Pd_3^+$ [Pd$_3$**L**$_5$]$^+$: *m/z* = 1340.2261, observed: *m/z* = 1340.2252; calcd. for $C_{72}H_{84}AgN_6O_{12}Pd_3^+$ [Pd$_3$Ag**L**$_6$]$^+$: *m/z* = 1653.2341, observed: *m/z* = 1653.2323.

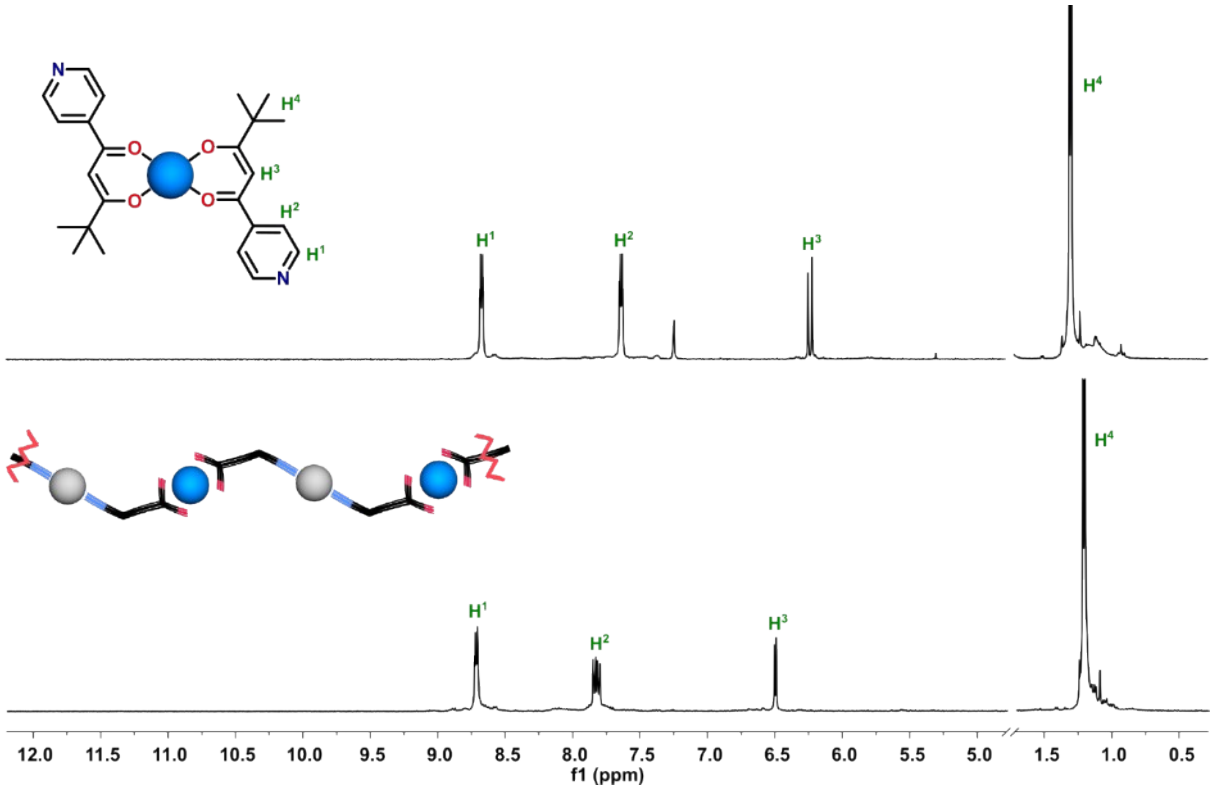

Figure S7. The comparison of ^{1}H NMR spectra (300 MHz, $CDCl_3$/DMSO-d_6) of the monomer [Pd**L**$_2$] (**C6**) and the polymer **P1**.

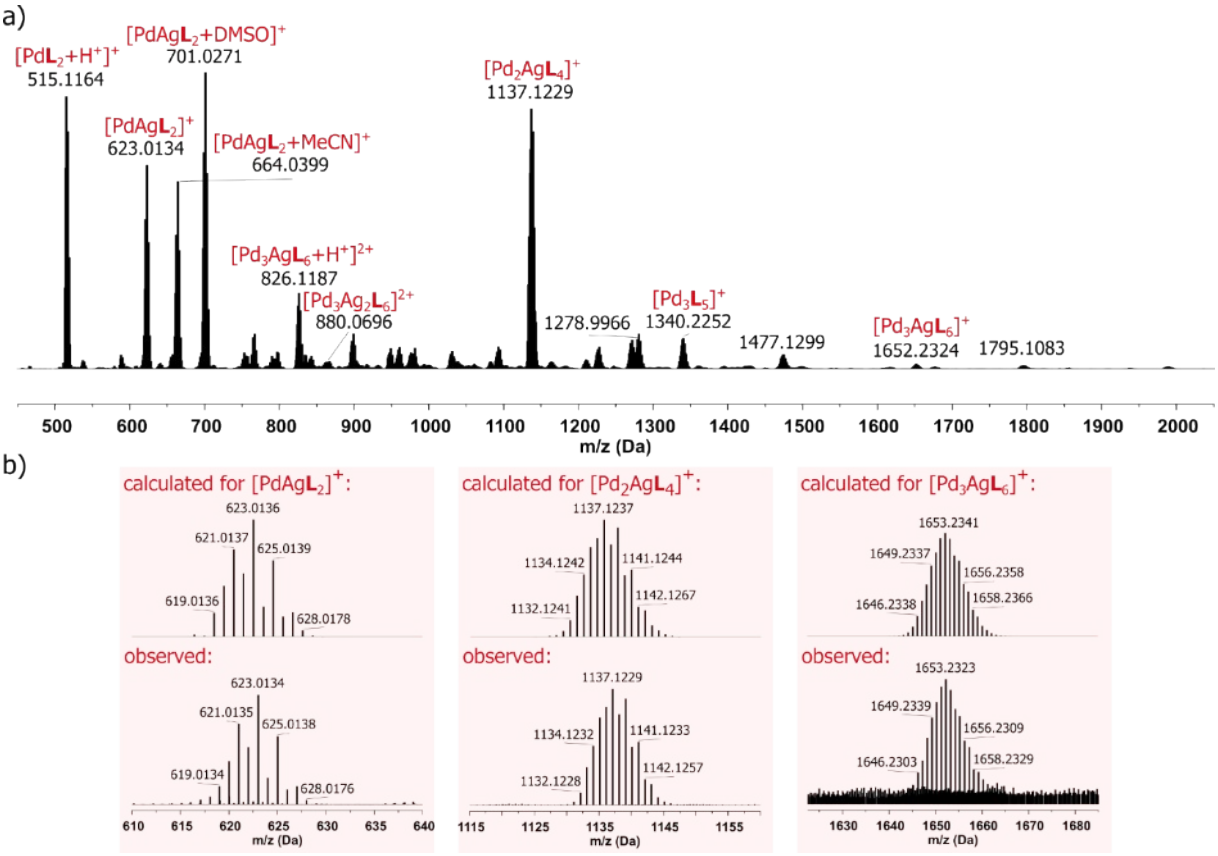

Figure S8. a) ESI-MS spectrum of the polymer **P1** in the 450-2050 Da region. b) ESI-MS analysis of **P1**, showing the theoretical isotope model (top) and the observed data (bottom) for the selected mass distributions.

2.3.2. Polymer P2

[Pd**L**$_2$] (10 mg, 0.019 mmol) was added to a suspension of $PtCl_2$ (5.2 mg, 0.019 mmol) in MeCN (3 mL). The resulting mixture was heated under reflux for 24 h. After, the mixture was cooled to room temperature. The orange precipitate was centrifuged off, washed with MeCN (5 mL) and Et_2O (2 × 5 mL), and dried in vacuo. Yield: 11.1 mg, 73%.

ESI-MS calcd. for $C_{24}H_{28}N_2NaO_4Pd^+$ [Pd**L**$_2$+Na$^+$]$^+$: *m/z* = 537.0984, observed: *m/z* = 537.0986; calcd. for $C_{48}H_{56}Cl_4N_4Na_2O_8Pd_2Pt_2^{2+}$ [Pd_2Pt_2**L**$_4$$Cl_4$+2Na$^+$]$^{2+}$: *m/z* = 803.9999, observed: *m/z* = 803.9997; calcd. for $C_{26}H_{34}Cl_2N_2NaO_5PdPtS^+$ [PdPt**L**$_2$$Cl_2$+DMSO+Na$^+$]$^+$: *m/z* = 881.0131, observed: *m/z* = 881.0136; calcd. for $C_{66}H_{90}Cl_3N_5O_{13}Pd_2Pt_2S_3^{2+}$ [Pd_2Pt_2**L**$_5$$Cl_3$+3DMSO+2H$^+$]$^{2+}$: *m/z* = 982.6559, observed: *m/z* = 982.6543; calcd. for $C_{72}H_{84}Cl_4N_6Na_2O_{12}Pd_3Pt_2^{2+}$ [Pd_3Pt**L**$_6$$Cl_4$+2Na$^+$]$^{2+}$: *m/z* = 1060.0547, observed: *m/z* = 1060.0537; calcd. for $C_{48}H_{56}Cl_4N_4NaO_8Pd_2Pt_2^+$ [Pd_2Pt_2**L**$_4$$Cl_4$+Na$^+$]$^+$: *m/z* = 1584.0104, observed: *m/z* = 1584.0108; calcd. for $C_{50}H_{60}Cl_4N_5O_8Pd_2Pt_2^+$ [Pd_2Pt_2**L**$_4$$Cl_4$+MeCN+H$^+$]$^+$: *m/z* = 1603.0550, observed: *m/z* = 1603.0509; calcd. for $C_{50}H_{62}Cl_4N_4NaO_9Pd_2Pt_2S^+$ [Pd_2Pt_2**L**$_4$$Cl_4$+DMSO+Na$^+$]$^+$: *m/z* = 1663.0241, observed: *m/z* = 1663.0296.

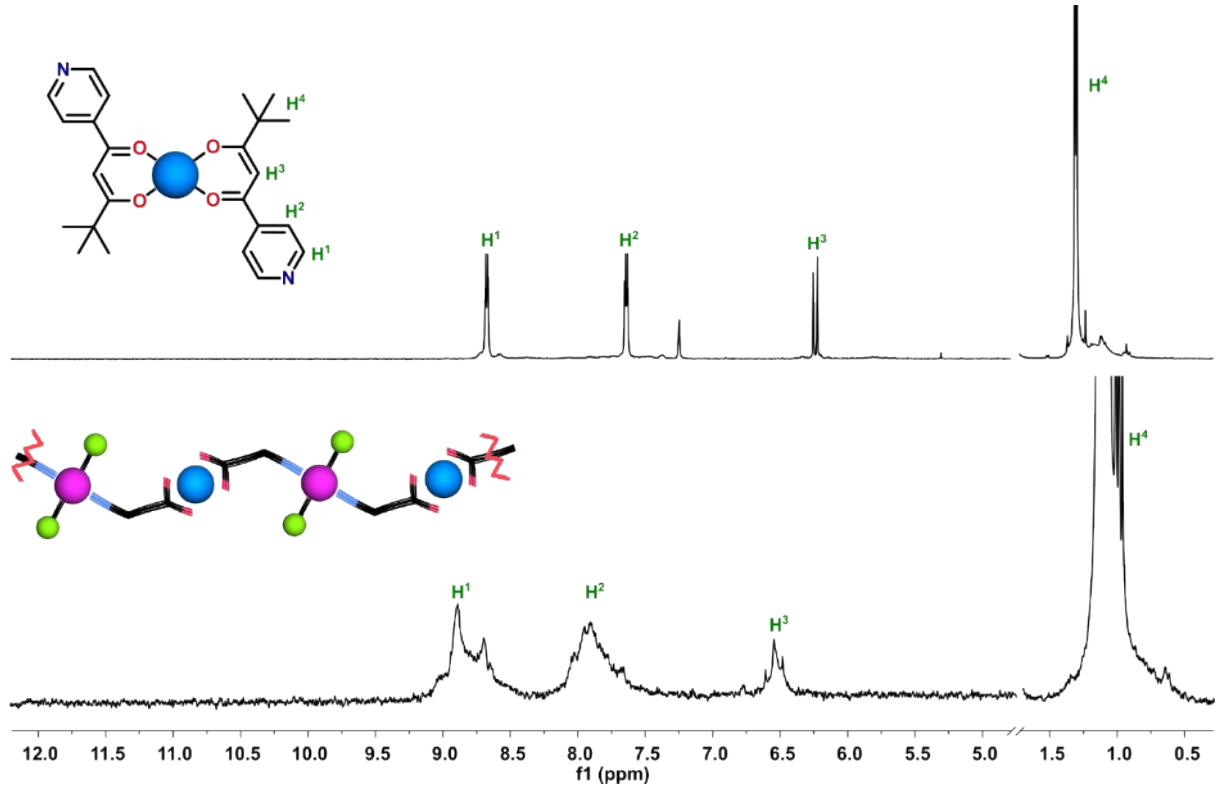

Figure S9. The comparison of ^{1}H NMR spectra (300 MHz, $CDCl_3$/DMSO-d_6) of the monomer [Pd**L**$_2$] (**C6**) and the polymer **P2**.

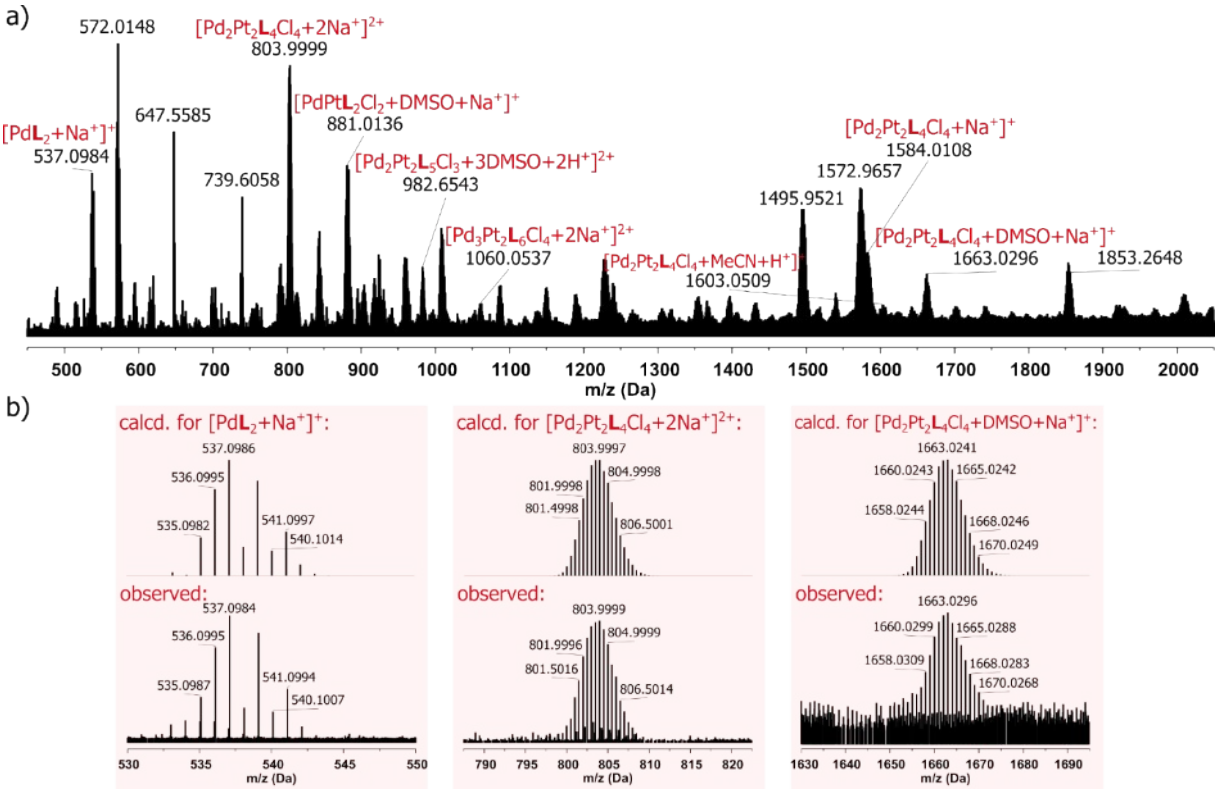

Figure S10. a) ESI-MS spectrum of the polymer **P2** in the 450-2050 Da region. b) ESI-MS analysis of **P2**, showing the theoretical isotope model (top) and the observed data (bottom) for the selected mass distributions.

2.3.3. Polymer P3

To $[Pt(H\mathbf{L})_4](NO_3)_2$ (5.0 mg, 0.004 mmol) dissolved in MeCN (3 mL), Et_3N (2.5 µL, 0.017 mmol) was added. After, $Pd(NO_3)_2{\cdot}2H_2O$ (2.4 mg, 0.009 mmol) was added to a solution of the deprotonated complex. The resulting mixture was heated for 3 h and then the solvent was evaporated under reduced pressure. The solid residue was washed with MeCN (5 mL), MeOH (5 mL) and Et_2O (2 × 5 mL), and dried in vacuo. Yield: 4.0 mg, 74%.

ESI-MS calcd. for $C_{24}H_{29}N_2O_4Pd^+$ $[Pd\mathbf{L}_2+H^+]^+$: *m/z* = 515.1166, observed: *m/z* = 515.1144; calcd. for $C_{48}H_{61}N_6O_{14}Pt^+$ $[Pt(H\mathbf{L})_4(NO_3)_2+H^+]^+$: *m/z* = 1139.5867, observed: *m/z* = 1139.6823; calcd. for $C_{60}H_{71}N_5NaO_{10}PdPt^+$ $[PdPt\mathbf{L}_5+H^++Na^+]^+$: *m/z* = 1347.3805, observed: *m/z* = 1347.4365; calcd. for $C_{74}H_{93}N_6O_{13}PdPtS^+$ $[PdPt\mathbf{L}_6+DMSO+3H^+]^+$: *m/z* = 1607.5222, observed: *m/z* = 1607.1030; calcd. for $C_{76}H_{90}N_8Na_3O_{12}PdPt^+$ $[PdPt\mathbf{L}_6+2MeCN+3Na^+]^+$: *m/z* = 1667.5074, observed: *m/z* = 1667.4175.

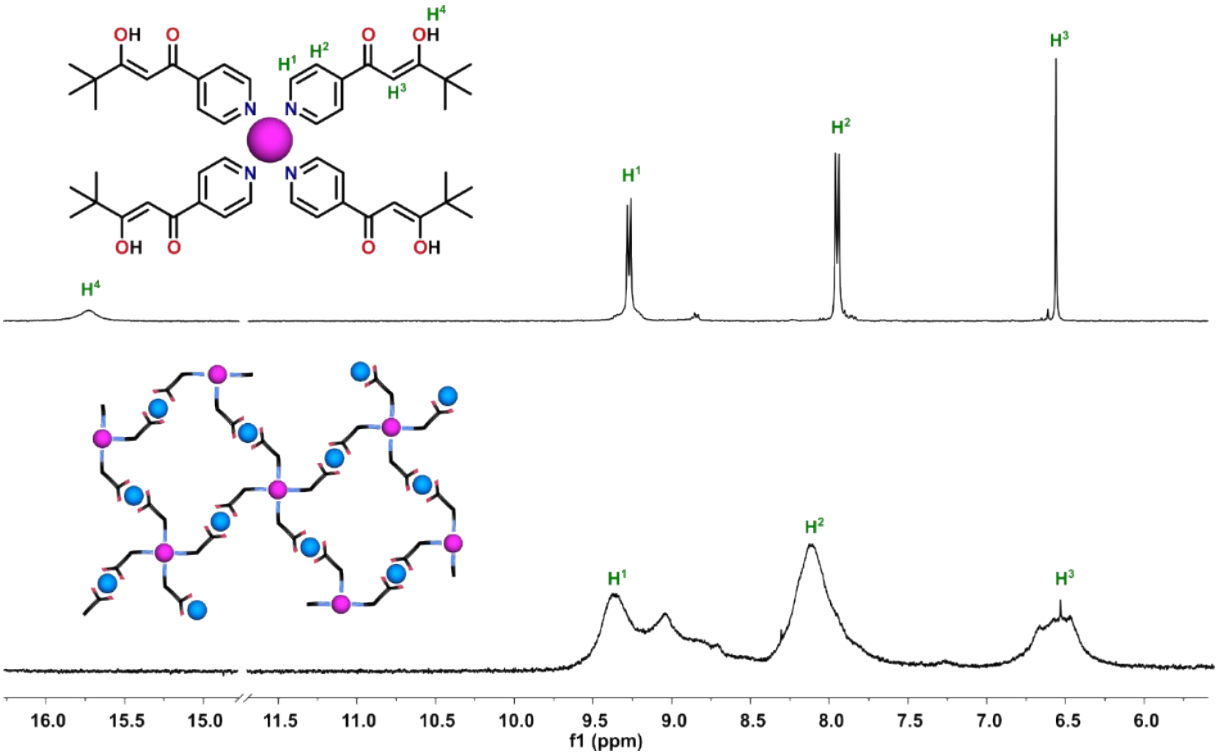

Figure S11. The comparison of ^{1}H NMR spectra (300 MHz, DMSO-d_6) of the monomer $[Pt(H\mathbf{L})_4](NO_3)_2$ (**C4**) and the polymer **P3**.

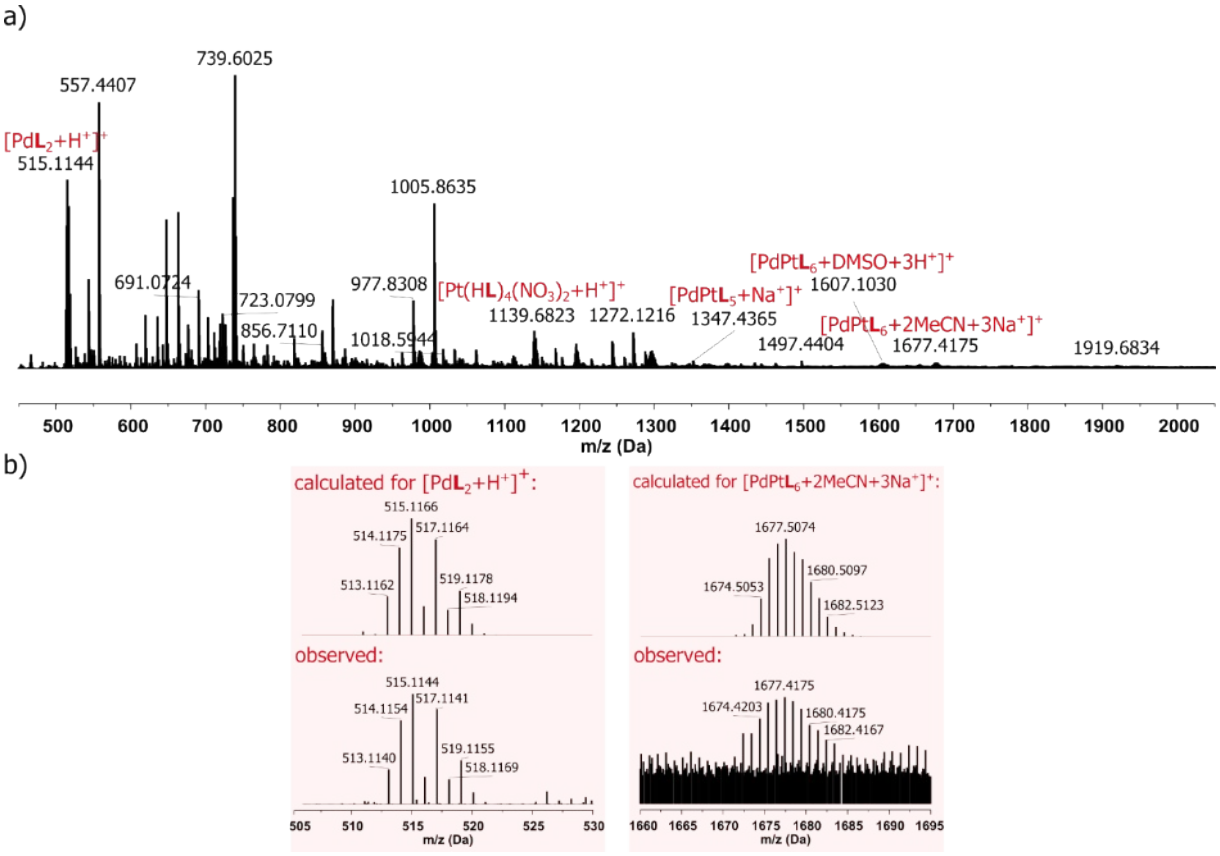

Figure S12. a) ESI-MS spectrum of the polymer **P3** in the 450-2050 Da region. b) ESI-MS analysis of **P3**, showing the theoretical isotope model (top) and the observed data (bottom) for the selected mass distributions.

3. Description of the X-ray structure of the complex C1

X-ray structure determinations for the complex **C1** was performed on a 4-circle Xcalibur EosS2 diffractometer (Agilent Technologies) equipped with a CCD (Charge-coupled Device) detector. X-ray data were collected at room temperature using graphite-monochromated MoKα radiation (λ = 0.71073 Å) with the ω-scan technique. Data reduction, UB-matrix determination and absorption correction were performed with the CrysAlisPro software.[3] Using Olex2,[4] the structures were solved by direct methods with ShelXT[5] and refined by full-matrix least-squares against F^2 with the program SHELXL[6] refinement package based on Least Squares minimization. All non-hydrogen atoms were refined anisotropically. The H-atoms were located in idealized positions by molecular geometry and refined as riding groups with $U_{iso}(H)$ = 1.2 $U_{eq}(C)$ 1.5 $U_{eq}(O)$. Selected structural parameters are reported in Table S1.

The data have been deposited in the Cambridge Crystallographic Data Collection (CCDC), deposition numbers CCDC **2244267**. These data can be obtained free of charge via www.ccdc.cam.ac.uk/data_request/cif, or by emailing data_request@ccdc.cam.ac.uk, or by contacting The Cambridge Crystallographic Data Centre, 12, Union Road, Cambridge CB2.

Alert level B

PLAT242_ALERT_2_B Low 'MainMol' Ueq as Compared to Neighbors of N009 Check

Response: The atom is located in a position where either thermal motion or multiple positions are possible. The enlarged displacement parameters are indicative of the probable thermal motion or disorder which results in this alert.

PLAT242_ALERT_2_B Low ’MainMol’ Ueq as Compared to Neighbors of C9 Check

Response: The atom is located in a position where either thermal motion or multiple positions are possible. The enlarged displacement parameters are indicative of the probable thermal motion or disorder which results in this alert.

PLAT430_ALERT_2_B Short Inter D...A Contact O2 ..O2 . 2.74 Ang. 2-x,2-y,1-z = 3_776 Check

Response: Alert is the result of intermolecular bonding in beta-diketone units.

PLAT910_ALERT_3_B Missing # of FCF Reflection(s) Below Theta(Min). 14 Note

Response: Probably missing due to the beam stop (this is likely due to using Mo radiation and the geometry of our goniometer).

Table S1. Crystal data and structure refinement for the complex **C1**.

Identification code	$[Ag(H\mathbf{L})_2]NO_3$ (**C1**)
CCDC number	**2244267**
Empirical formula	$C_{48}H_{60}Ag_2N_6O_{14}$
Formula weight	1160.76
Temperature/K	293(2)
Crystal system	monoclinic
Space group	$P2_1/n$
a/Å	17.9156(11)
b/Å	8.6942(4)
c/Å	18.8300(14)
α/°	90
β/°	117.921(8)
γ/°	90
Volume/Å^3	2591.6(3)
Z	2
ρ_{calc}g/cm^3	1.487
μ/mm^{-1}	0.824
F(000)	1192.0
Crystal size/mm^3	0.1 × 0.02 × 0.02
Radiation	MoKα (λ = 0.71073)
2Θ range for data collection/°	6.962 to 58.44
Index ranges	-22 ≤ h ≤ 23, -10 ≤ k ≤ 11, -23 ≤ l ≤ 24
Reflections collected	23174
Independent reflections	6122 [R_{int} = 0.0293, R_{sigma} = 0.0316]
Data/restraints/parameters	6122/0/414
Goodness-of-fit on F^2	1.014
Final R indexes [I>=2σ (I)]	R_1 = 0.0443, wR_2 = 0.0899
Final R indexes [all data]	R_1 = 0.0700, wR_2 = 0.1012
Largest diff. peak/hole / e Å^{-3}	0.43/-0.43

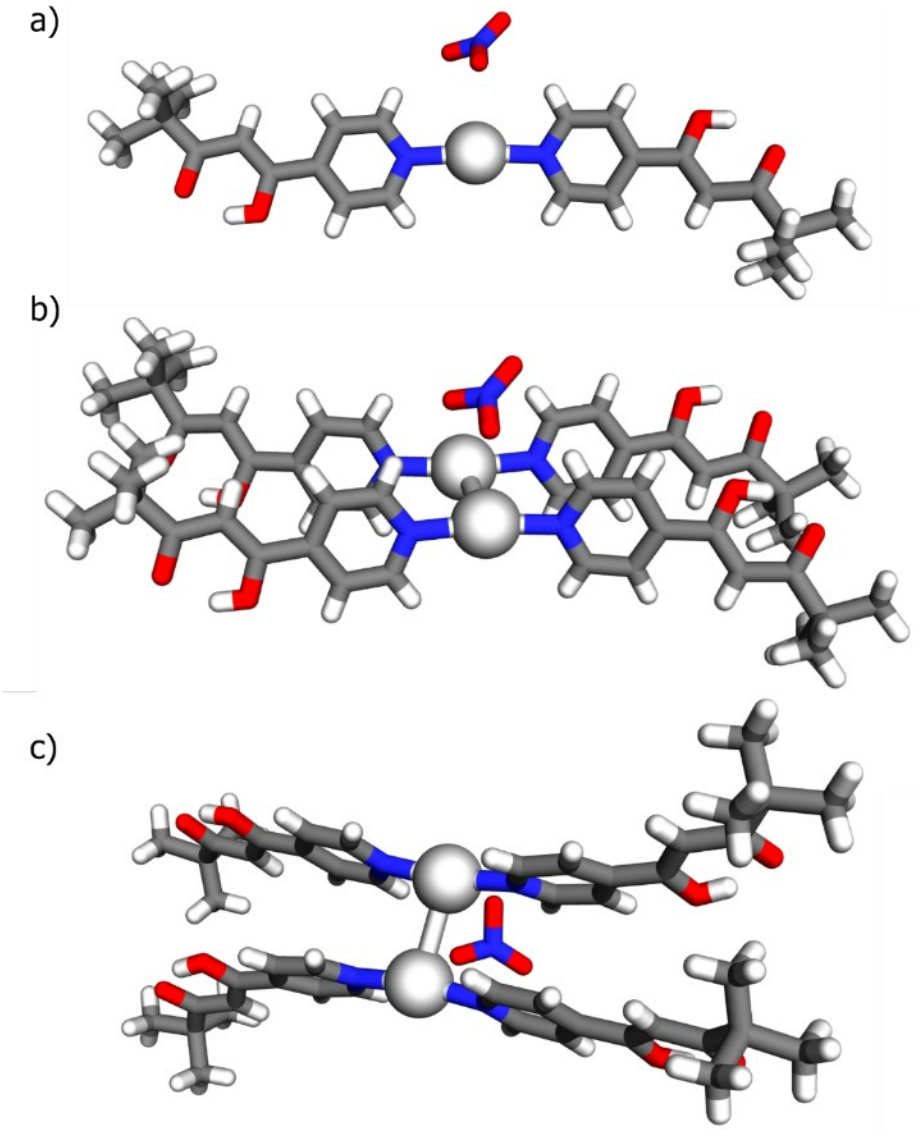

Figure S13. X-ray structures of the complex **C1** in monomer (a) and dimer forms (bc).

4. ^{1}H NMR titrations showing the supramolecular transformations

4.1. ^{1}H NMR titration of C1 with Et_3N

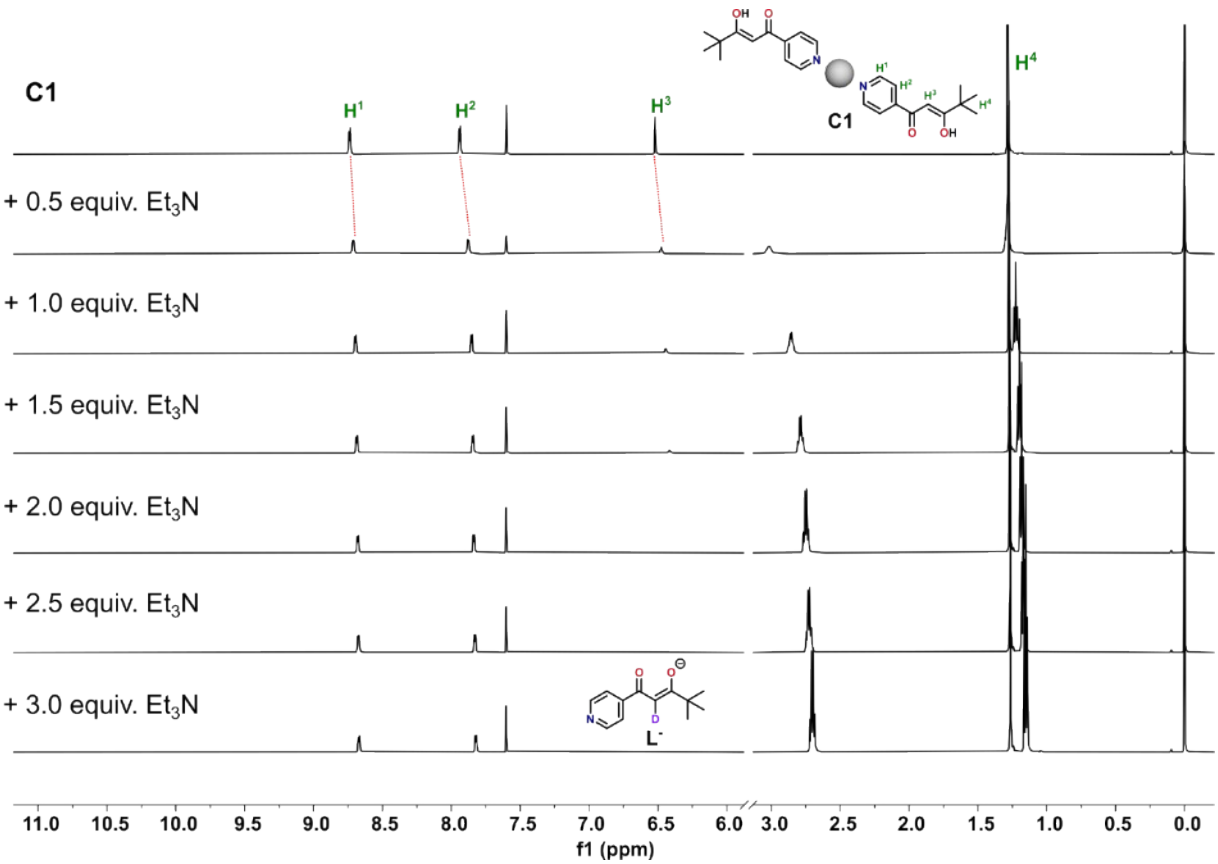

Figure S14. ^{1}H NMR titration spectra (600 MHz, $CDCl_3/CD_3OD$) of the complex **C1** upon addition of different equivalents of Et_3N.

4.2. ^{1}H NMR titration of C1 with $Pd(NO_3)_2$

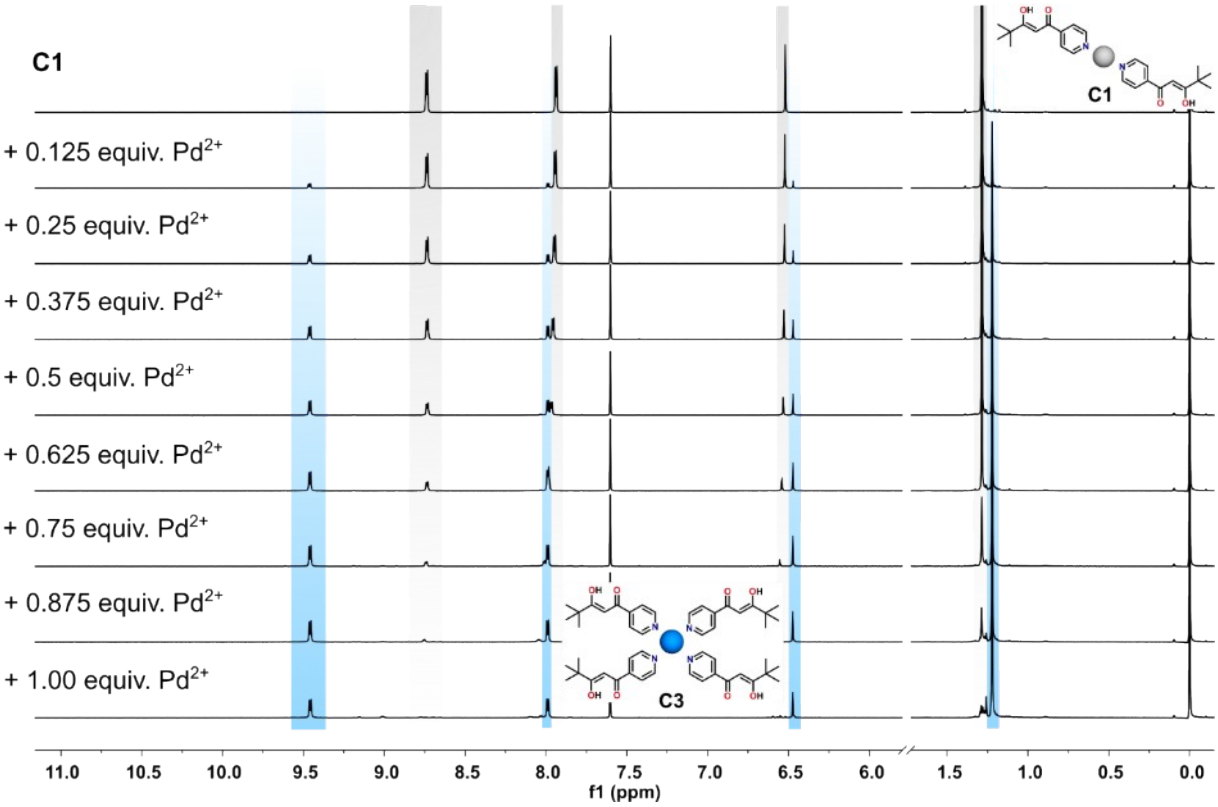

Figure S15. ^{1}H NMR titration spectra (600 MHz, $CDCl_3/CD_3OD$) of the complex **C1** with $Pd(NO_3)_2$.

4.3. ^{1}H NMR titration of C1 with $[Pd(en)(NO_3)_2]$

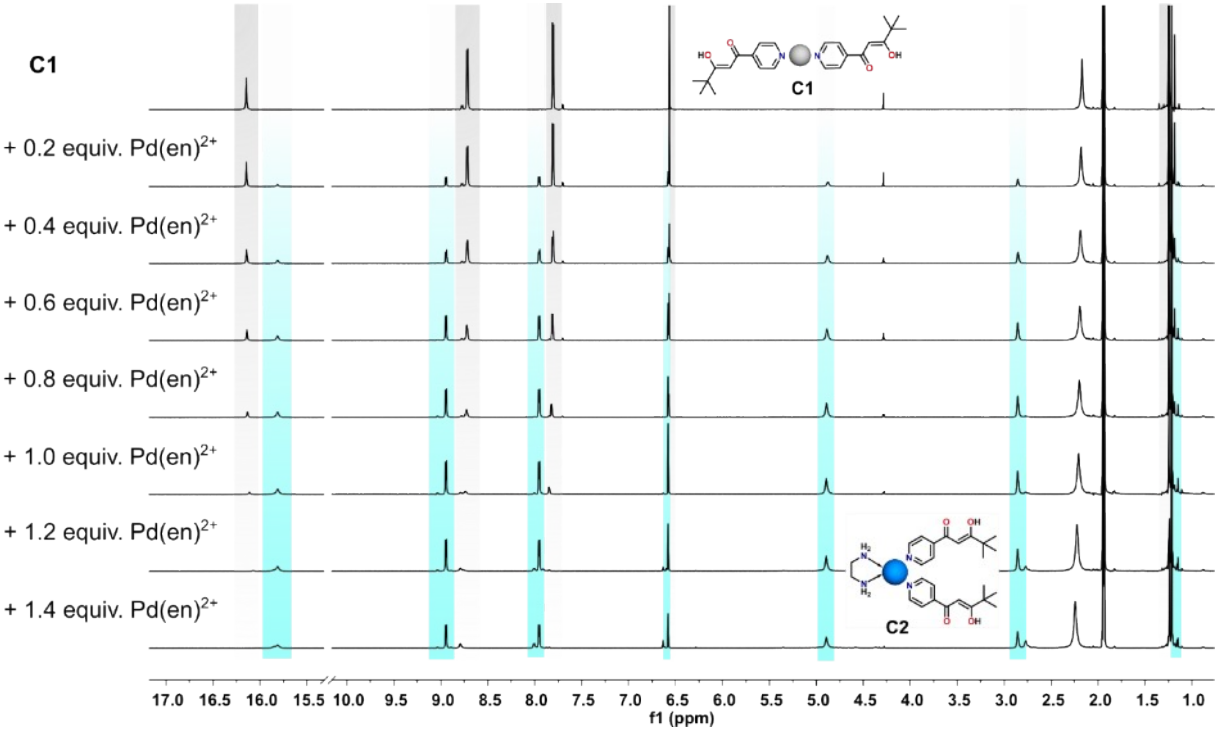

Figure S16. ^{1}H NMR titration spectra (600 MHz, CD_3CN) of the complex **C1** with $[Pd(en)(NO_3)_2]$.

4.4. ^{1}H NMR titration of C1 with $Pt(NO_3)_2$

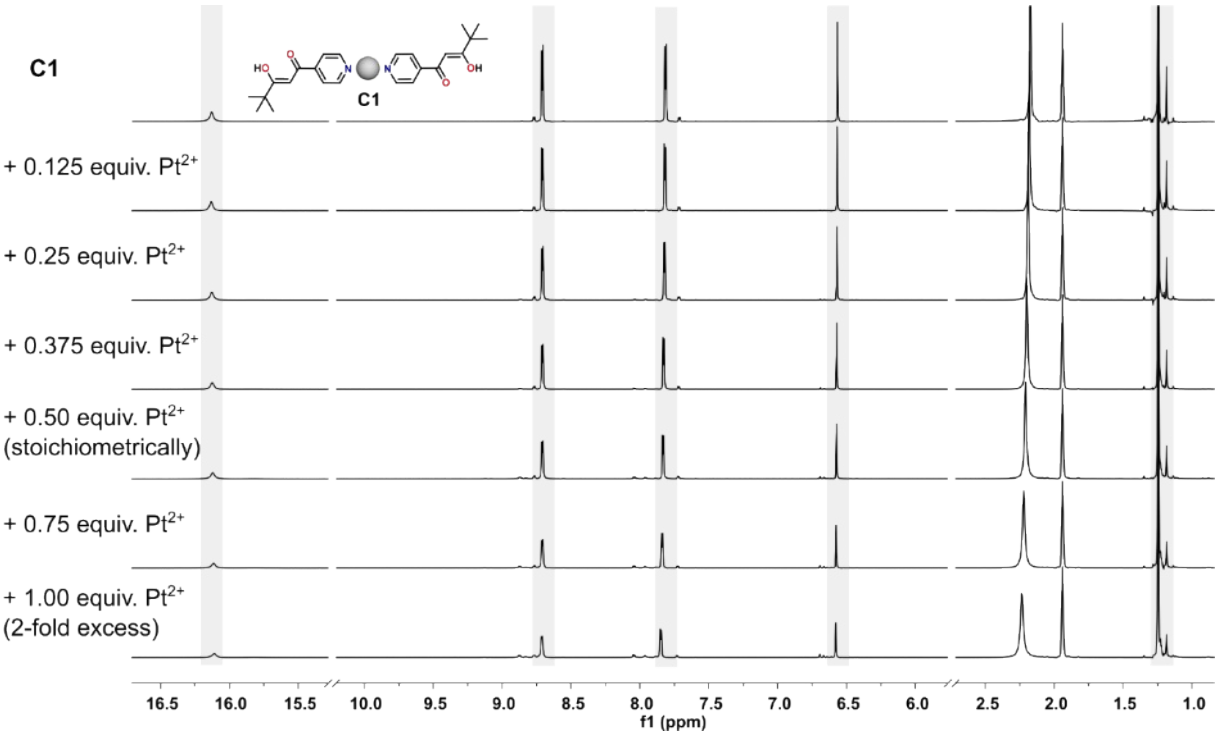

Figure S17. ^{1}H NMR titration spectra (600 MHz, CD_3CN) of the complex **C1** with $Pt(NO_3)_2$.

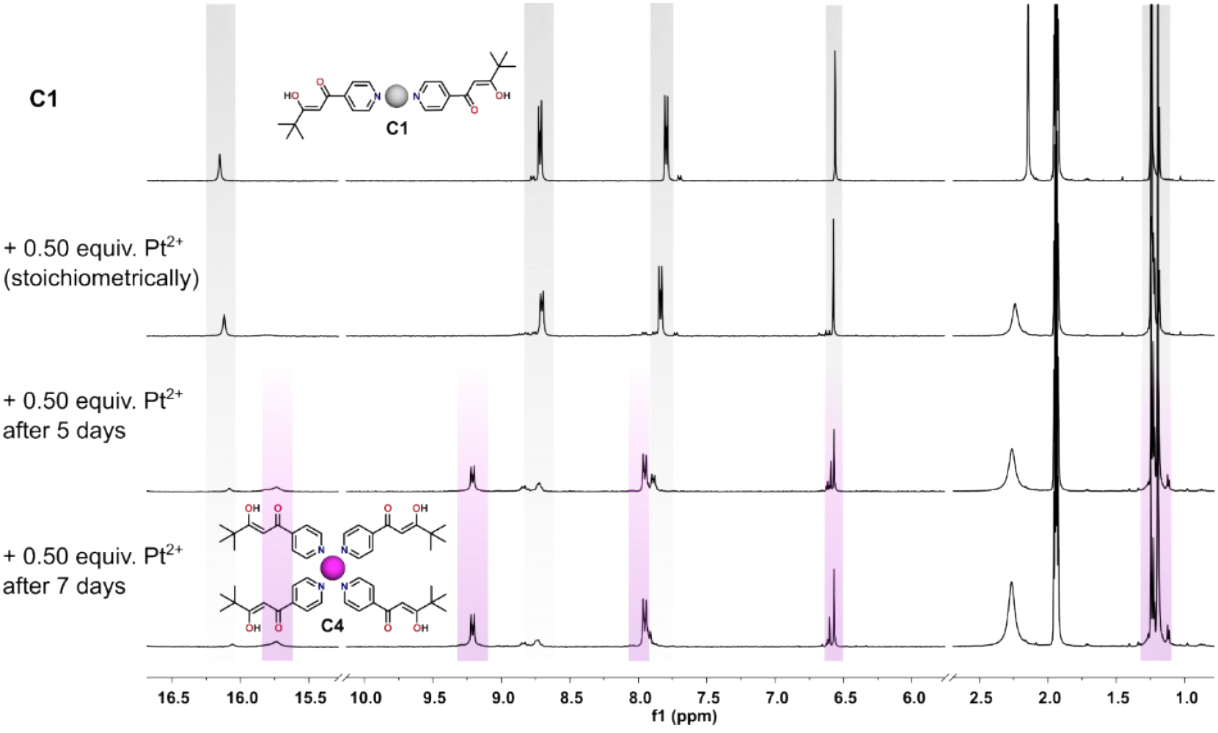

Figure S18. ^{1}H NMR spectra (600 MHz, CD_3CN) showing the transformation of the complex **C1** into **C4**.

4.5. ^{1}H NMR titration of C2 with Et_3N

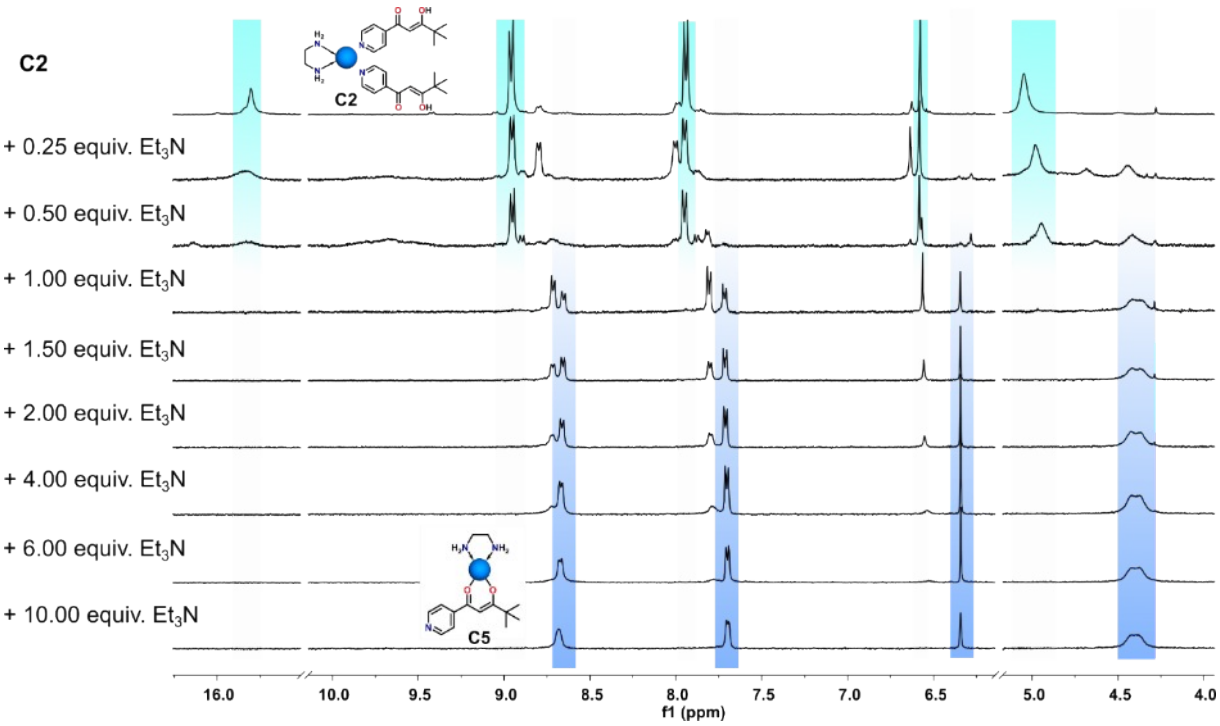

Figure S19. ^{1}H NMR titration spectra (300 MHz, CD_3CN) of the complex **C2** upon addition of different equivalents of Et_3N.

4.6. ^{1}H NMR titration of C6 with AgOTf

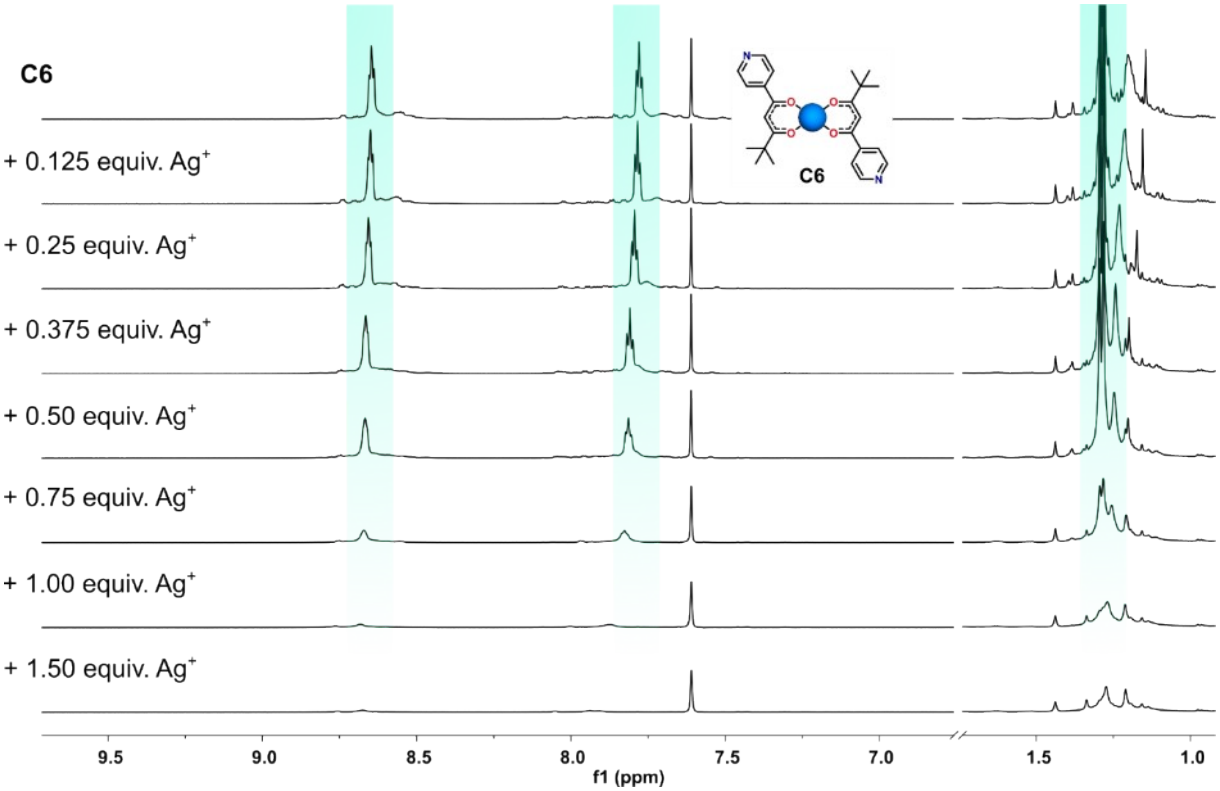

Figure S20. ^{1}H NMR titration spectra (600 MHz, $CDCl_3/CD_3OD$) of the complex **C6** with AgOTf.

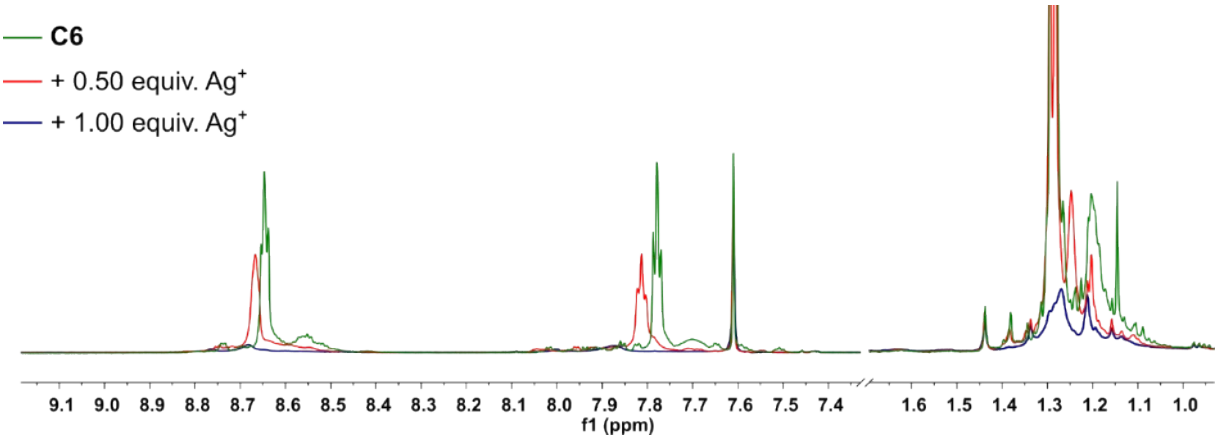

Figure S21. The imposition of ^{1}H NMR spectra (600 MHz, $CDCl_3/CD_3OD$) showing gradual decrease in the intensity of the signals derived from the complex **C6** after adding sequential portions of AgOTf.

5. ^{1}H NMR spectra of control experiments

5.1. Reaction between the C6 analogue and $AgNO_3$

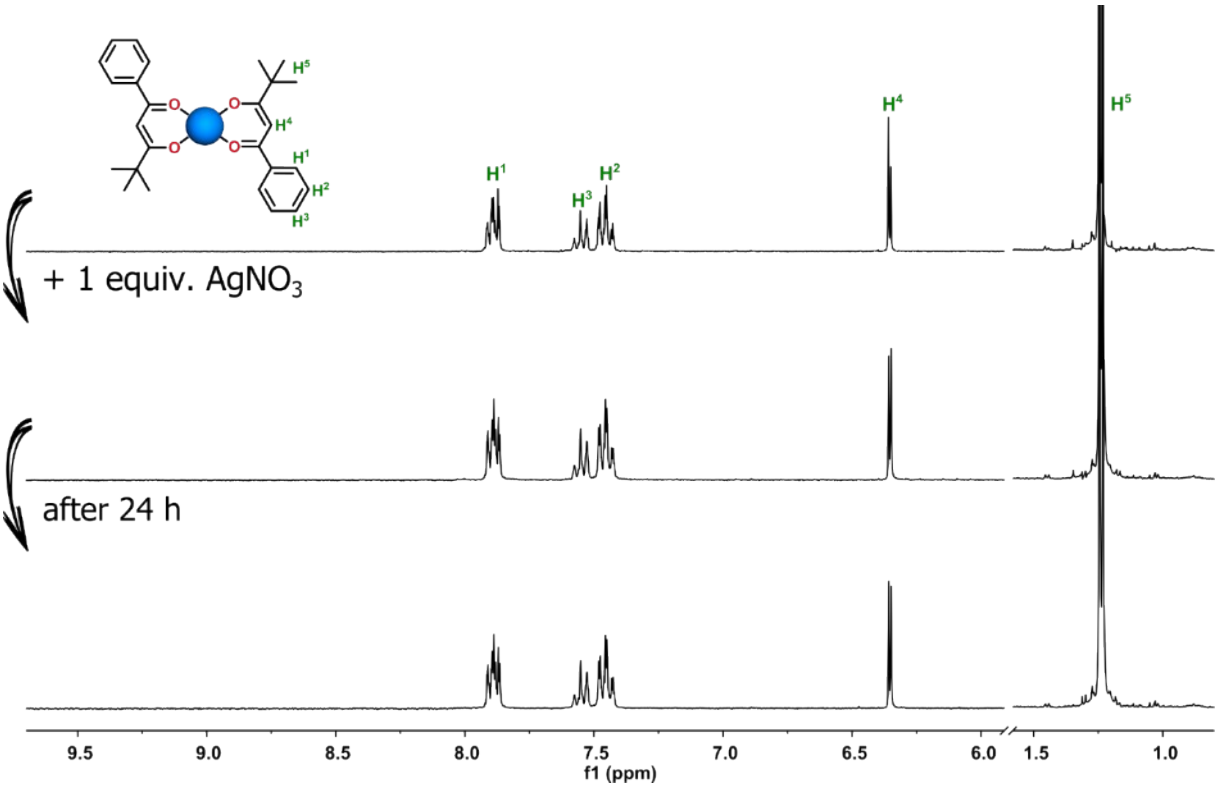

Figure S22. ^{1}H NMR spectra (300 MHz, CD_3CN) of the analogue of the complex **C6**, showing no difference after addition of $AgNO_3$.

5.2. Reaction between the C6 analogue and $PtCl_2$

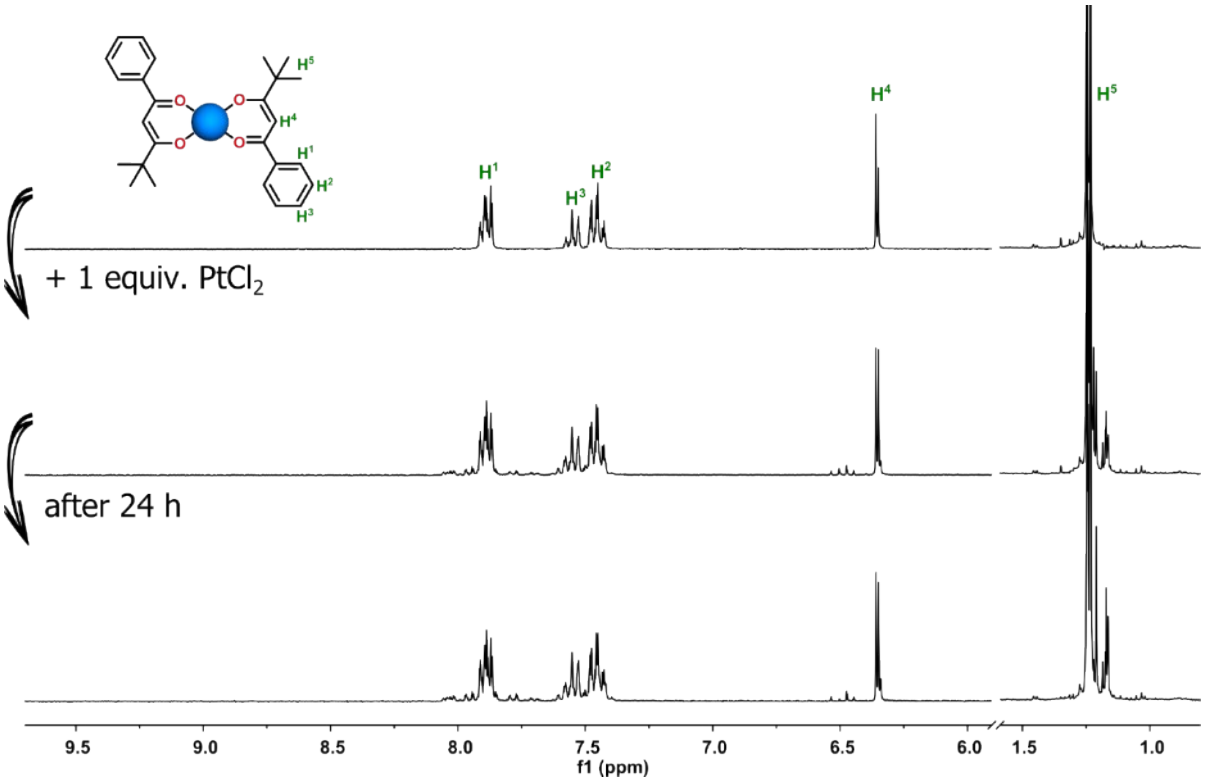

Figure S23. ^{1}H NMR spectra (300 MHz, CD_3CN) of the analogue of the complex **C6**, showing no difference after addition of $PtCl_2$.

5.3. Reaction between the C4 analogue and $Pd(NO_3)_2$

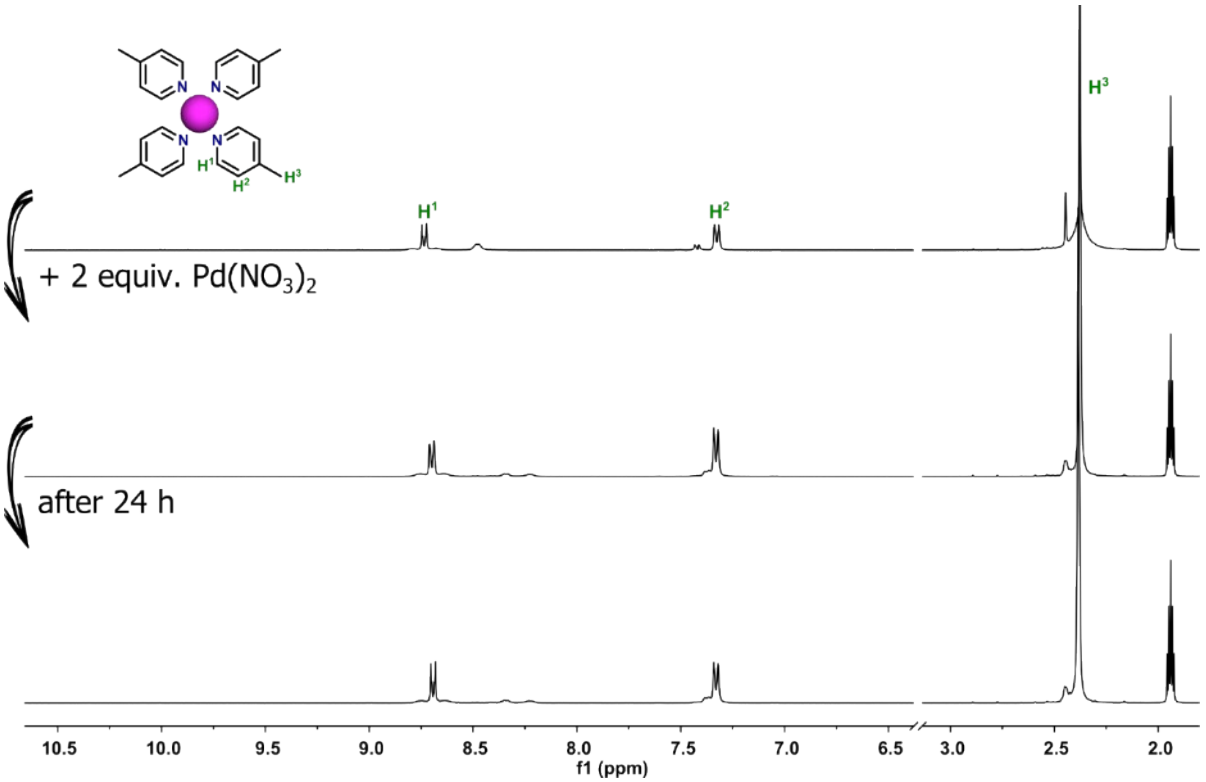

Figure S24. ^{1}H NMR spectra (300 MHz, CD_3CN) of the analogue of the complex **C4**, showing no difference after addition of $Pd(NO_3)_2$.

6. ICP-MS analysis of the polymers P1-P3

Table S2. The results of ICP-MS analysis of the polymers **P1**-**P3**.[a]

	Ag [ppm]		Pd [ppm]		Pt [ppm]	
	found [%]	calcd. [%]	found [%]	calcd. [%]	found [%]	calcd. [%]
P1	22.0	15.8	10.3	15.5	-	-
P2	-	-	10.5	13.6	26.7	25.0
P3	-	-	19.7	17.4	13.5	15.9

[a] The solutions were prepared by digesting the appropriate sample in aqua regia or concentrated nitric acid.

7. XPS analysis of the polymers P1-P3

7.1. Polymer P1

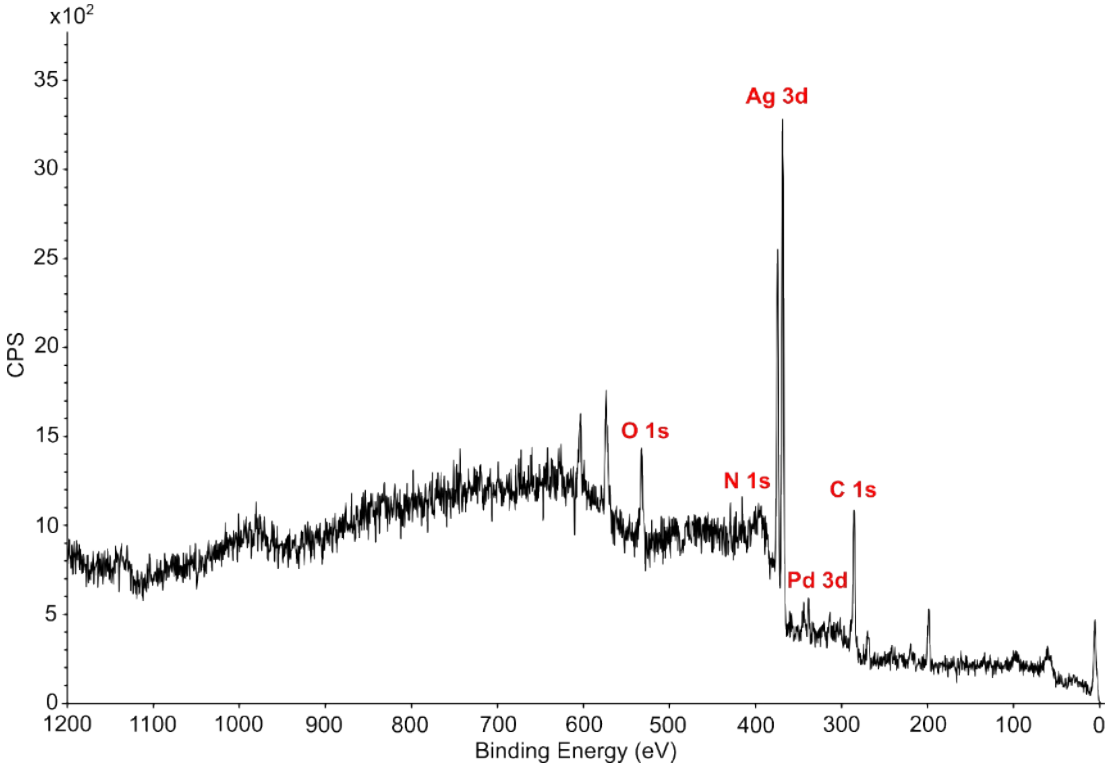

Figure S25. XPS spectrum of the polymer **P1**.

7.2. Polymer P2

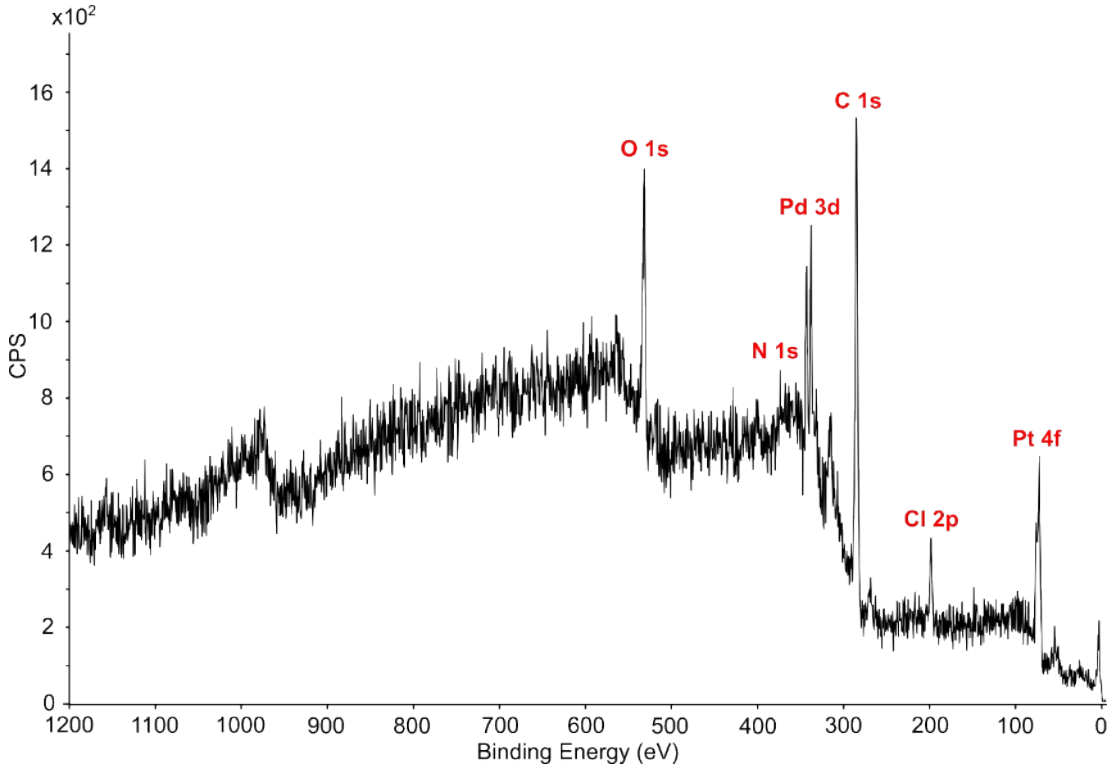

Figure S26. XPS spectrum of the polymer **P2**.

7.3. Polymer P3

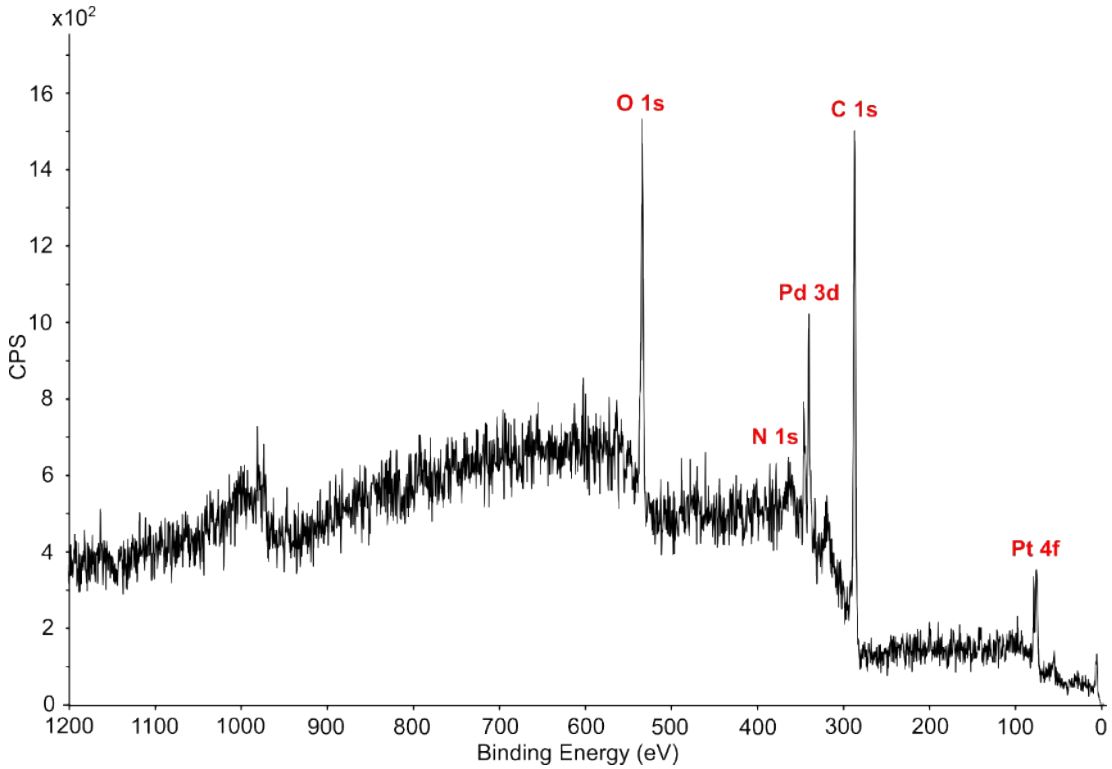

Figure S27. XPS spectrum of the polymer **P3**.

8. ATR-FTIR analysis of the coordination compounds

8.1. ATR-FTIR spectra of the coordination compounds

8.1.1. Ligand HL

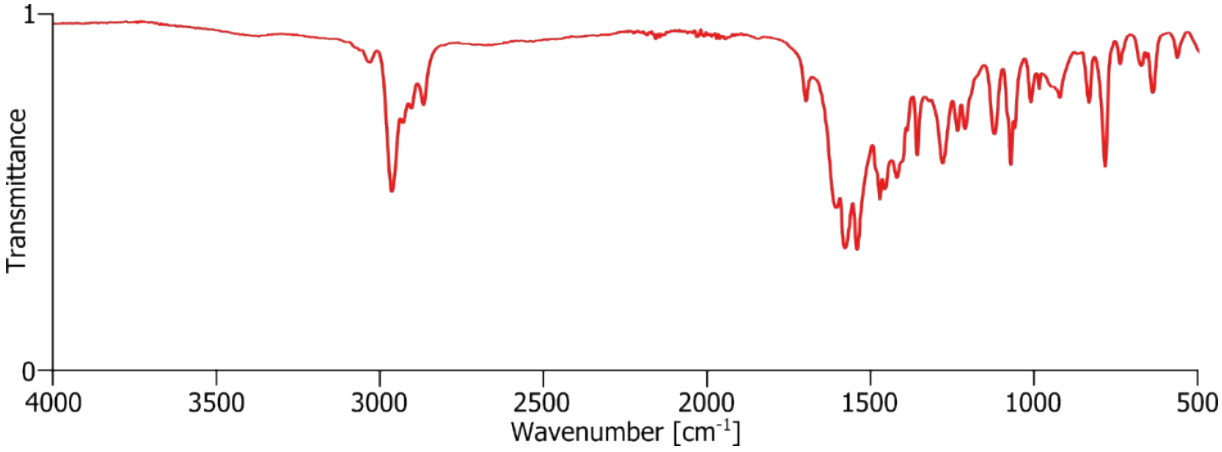

Figure S28. ATR-FTIR spectrum of the ligand H**L**.

8.1.2. Complex C1

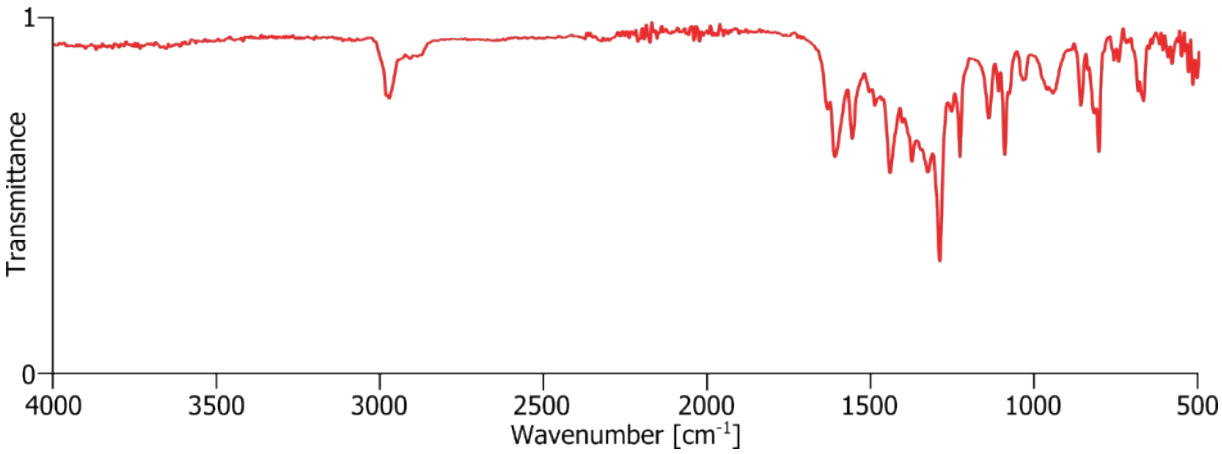

Figure S29. ATR-FTIR spectrum of the complex **C1**.

8.1.3. Complex C4

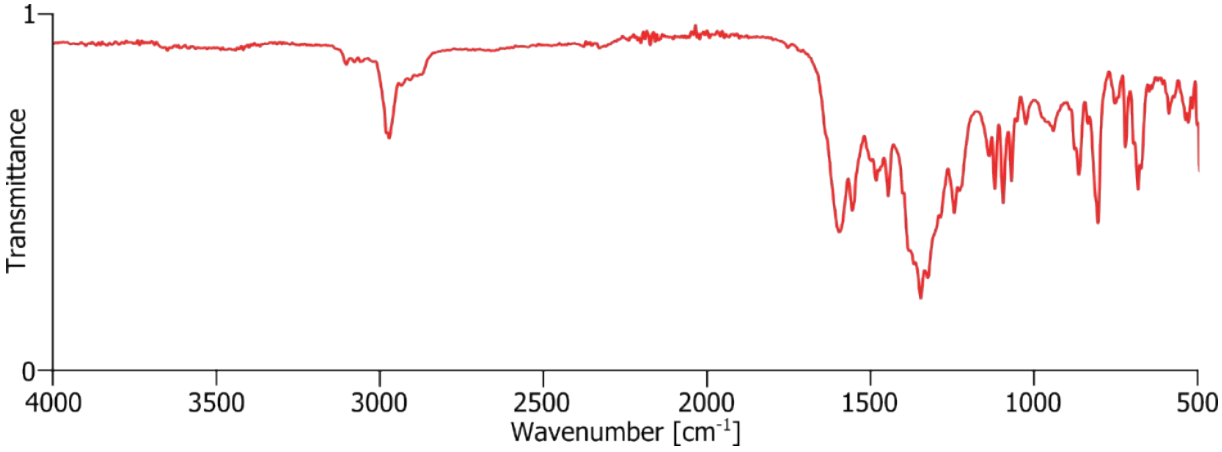

Figure S30. ATR-FTIR spectrum of the complex **C4**.

8.1.4. Complex C6

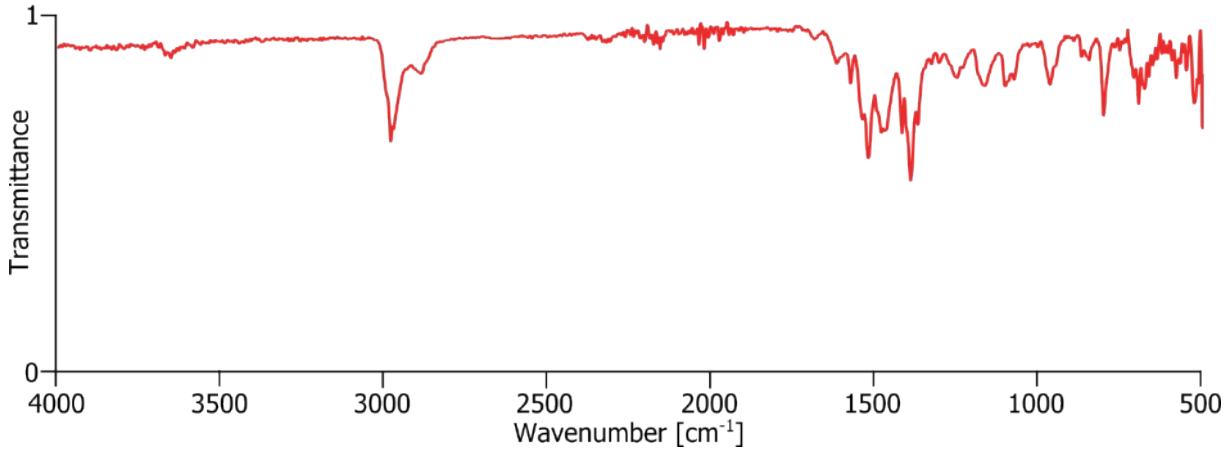

Figure S31. ATR-FTIR spectrum of the complex **C6**.

8.1.5. Polymer P1

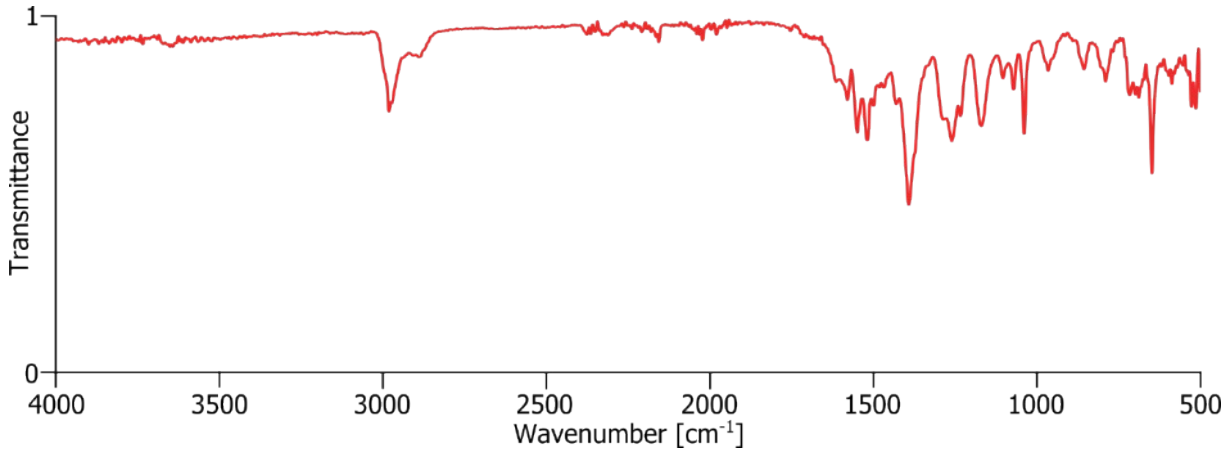

Figure S32. ATR-FTIR spectrum of the polymer **P1**.

8.1.6. Polymer P2

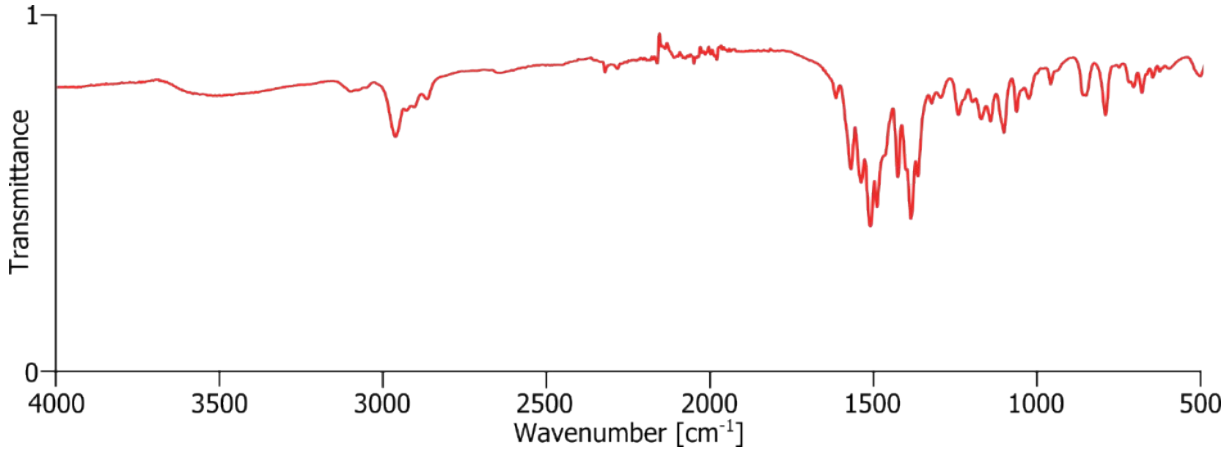

Figure S33. ATR-FTIR spectrum of the polymer **P2**.

8.1.7. Polymer P3

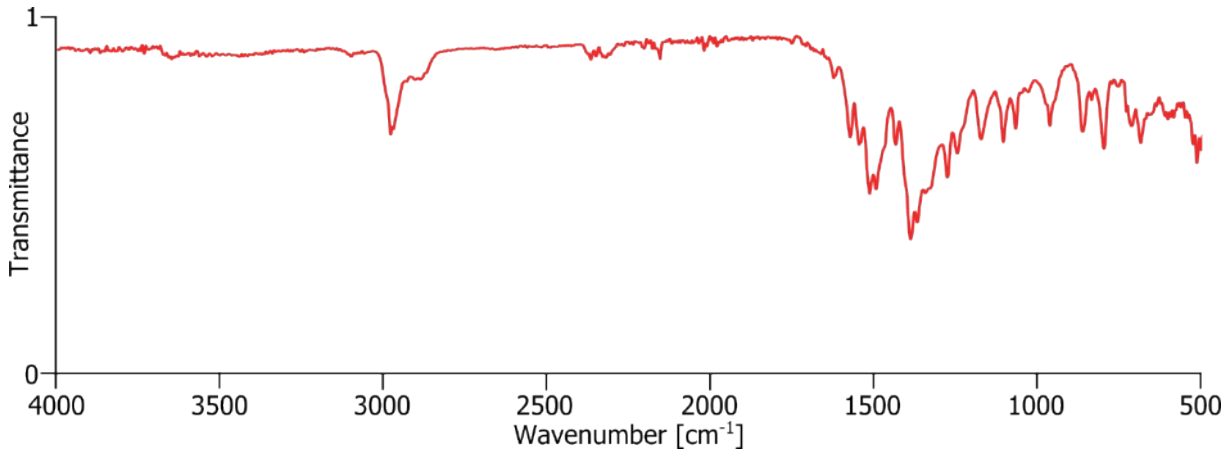

Figure S34. ATR-FTIR spectrum of the polymer **P3**.

8.2. Assignment of the absorption bands in the ligand structure

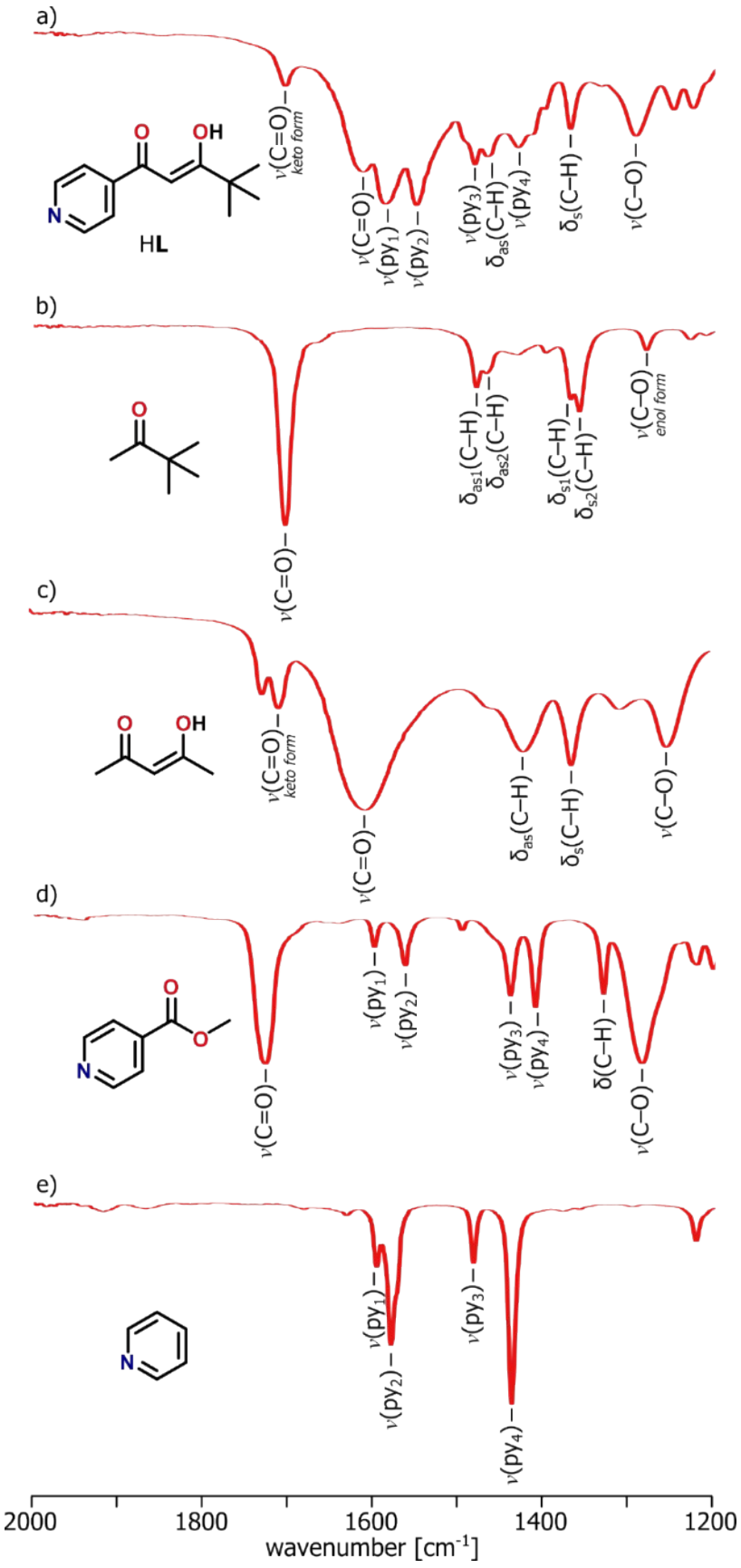

Figure S35. ATR-FTIR spectra in the 2000-1200 cm^{-1} region of: a) the ligand H**L**; b) 3,3-dimethyl-2-butanone; c) acetylacetone; d) methyl isonicotinate; e) pyridine.

8.3. Comparison of the FTIR spectra between the ligand HL and complexes

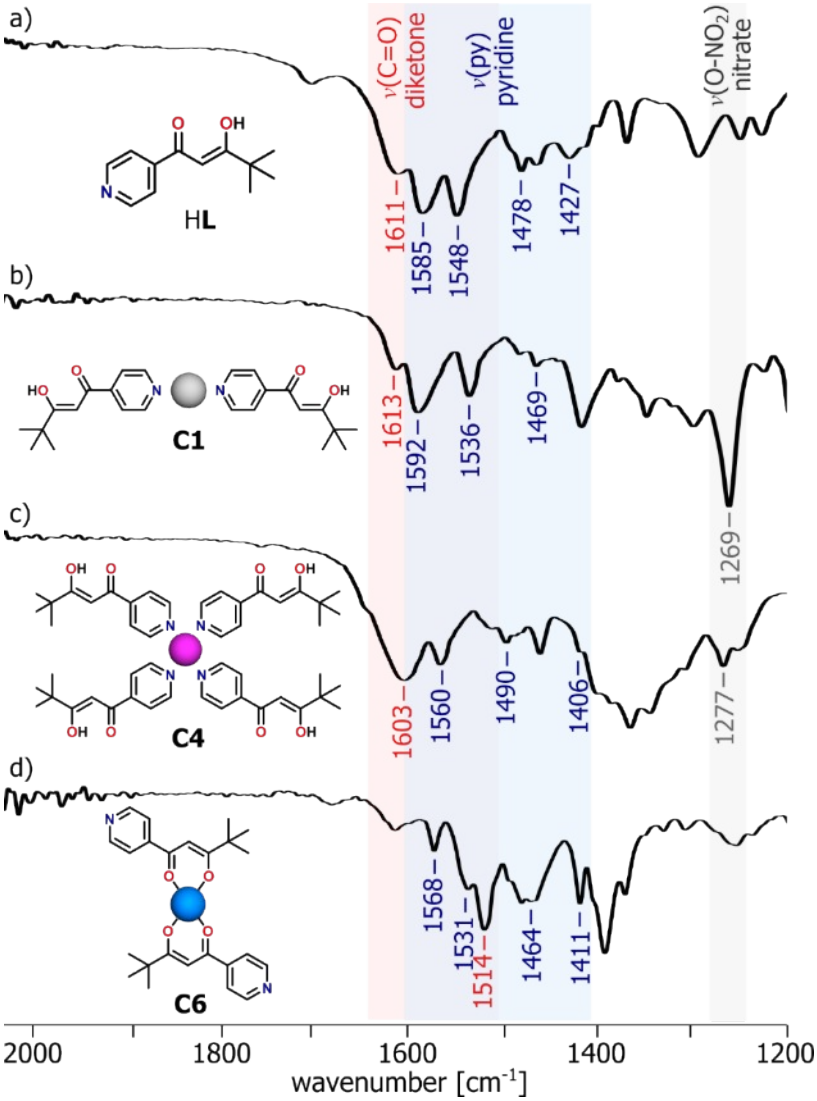

Figure S36. ATR-FTIR spectra in the 2000-1200 cm^{-1} region of: a) the ligand H**L**; b) **C1**; c) **C4**; d) **C6,** showing the involvement of the specific functional groups in metal binding.

9. Powder X-Ray diffraction patterns of the coordination compounds

9.1. Complex C1

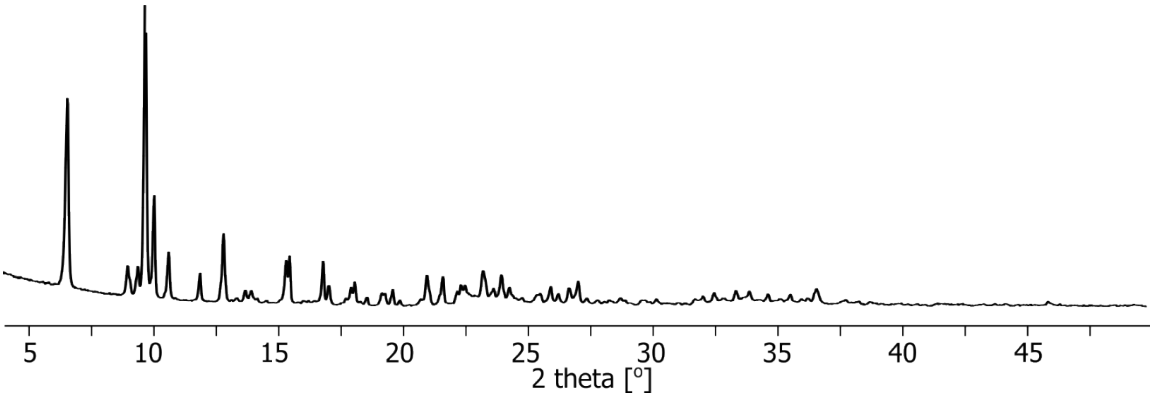

Figure S37. Powder X-ray diffraction pattern of the complex **C1**.

9.2. Complex C4

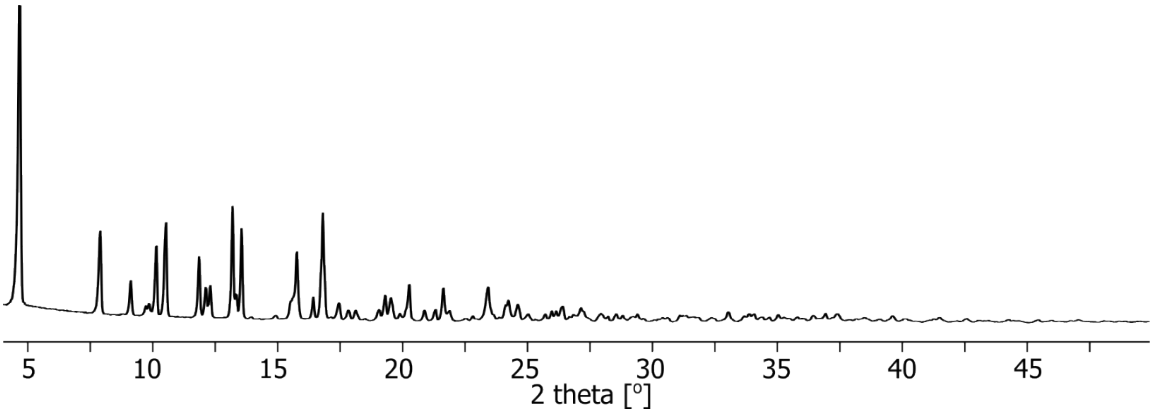

Figure S38. Powder X-ray diffraction pattern of the complex **C4**.

9.3. Complex C6

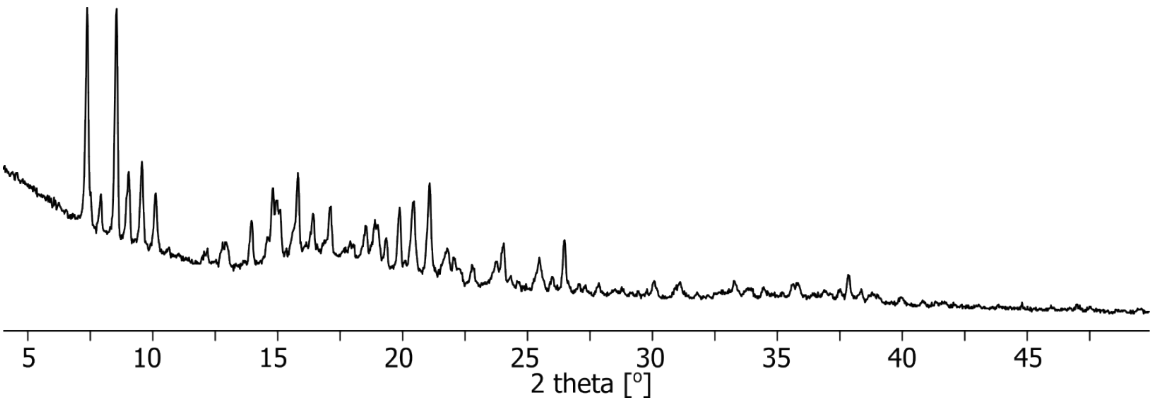

Figure S39. Powder X-ray diffraction pattern of the complex **C6**.

9.4. Polymer P1

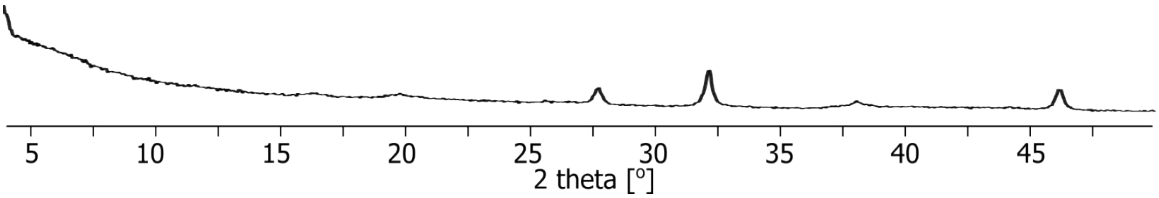

Figure S40. Powder X-ray diffraction pattern of the polymer **P1**.

9.5. Polymer P2

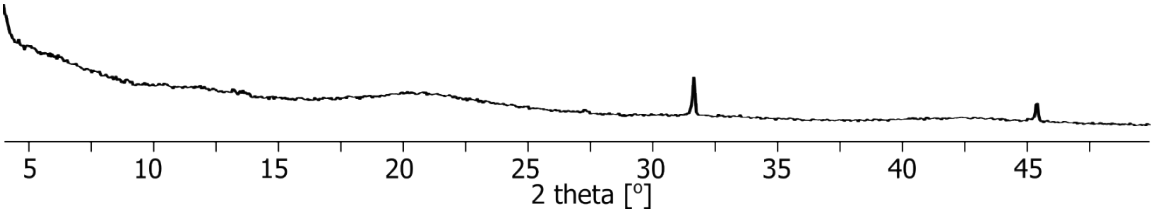

Figure S41. Powder X-ray diffraction pattern of the polymer **P2**.

9.6. Polymer P3

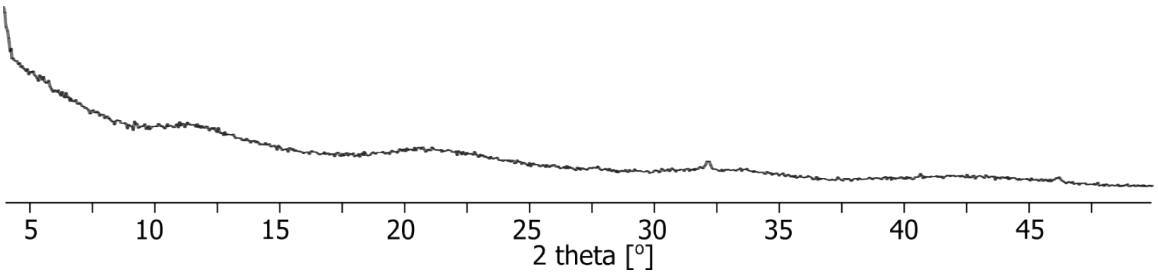

Figure S42. Powder X-ray diffraction pattern of the polymer **P3**.

10. SEM and EDS analysis of the coordination compounds

10.1. Polymer P1

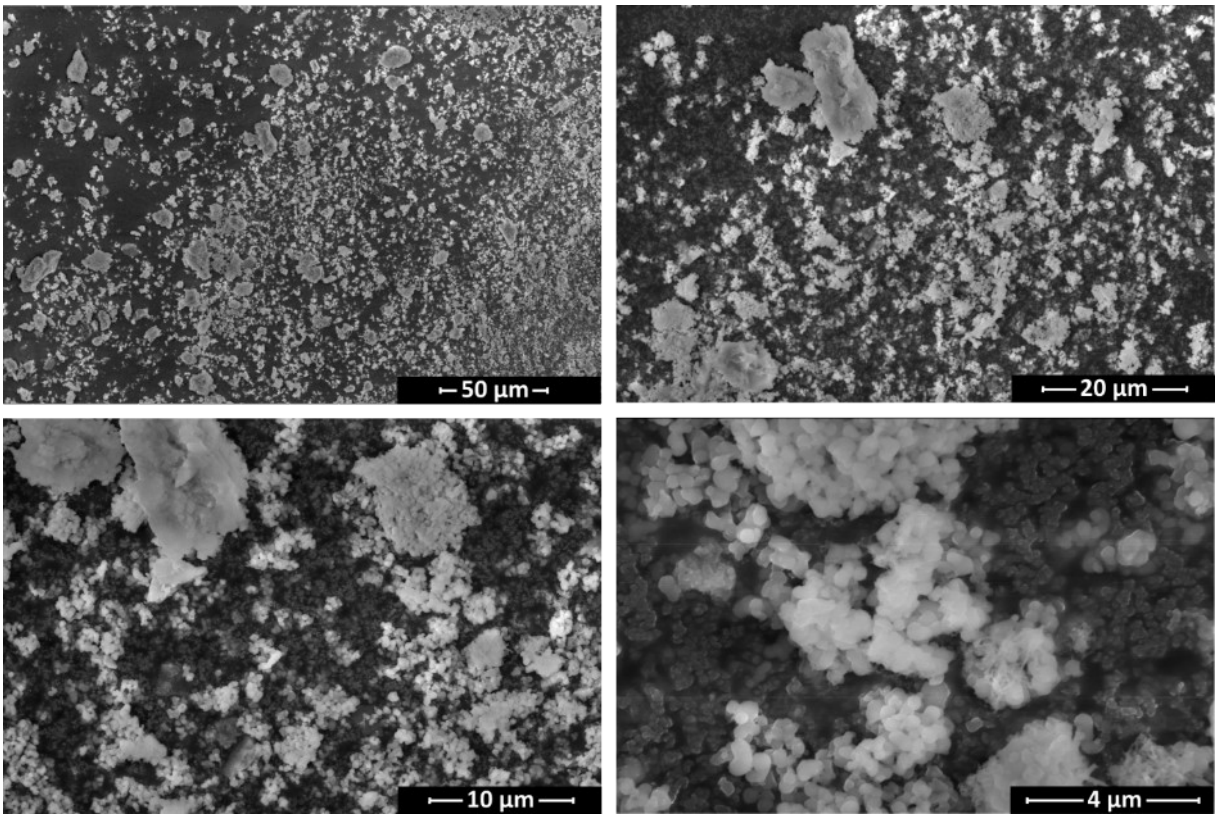

Figure S43. Scanning electron microscopy (SEM) images of the polymer **P1**.

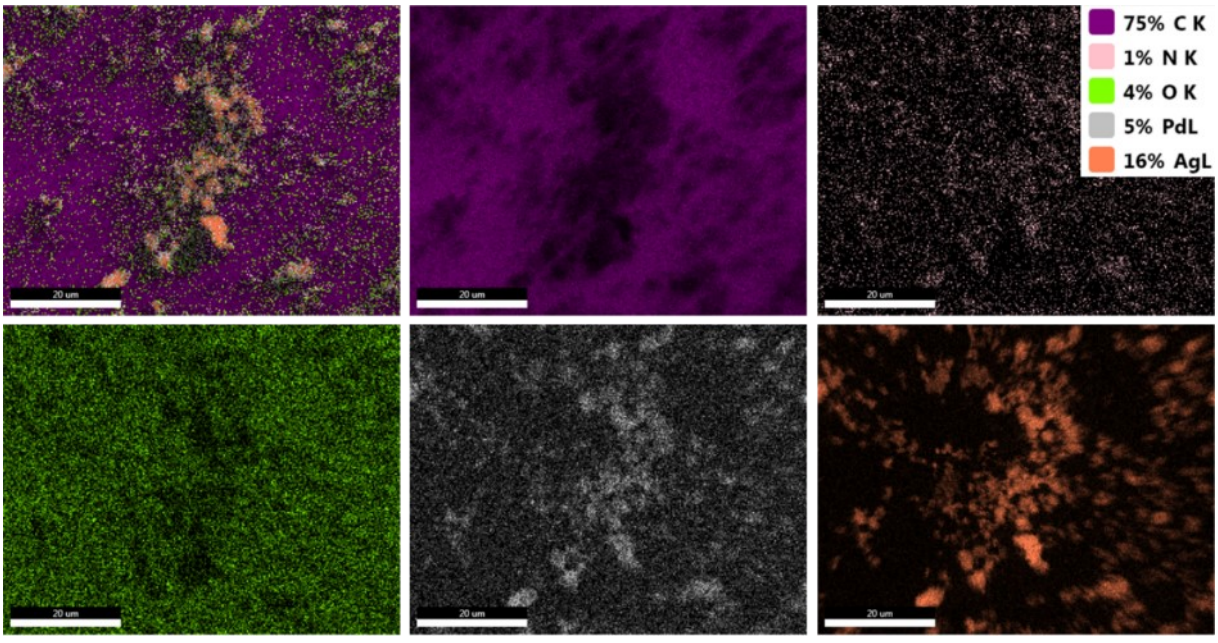

Figure S44. EDS elemental mapping of the sample composition for **P1**.

10.2. Polymer P2

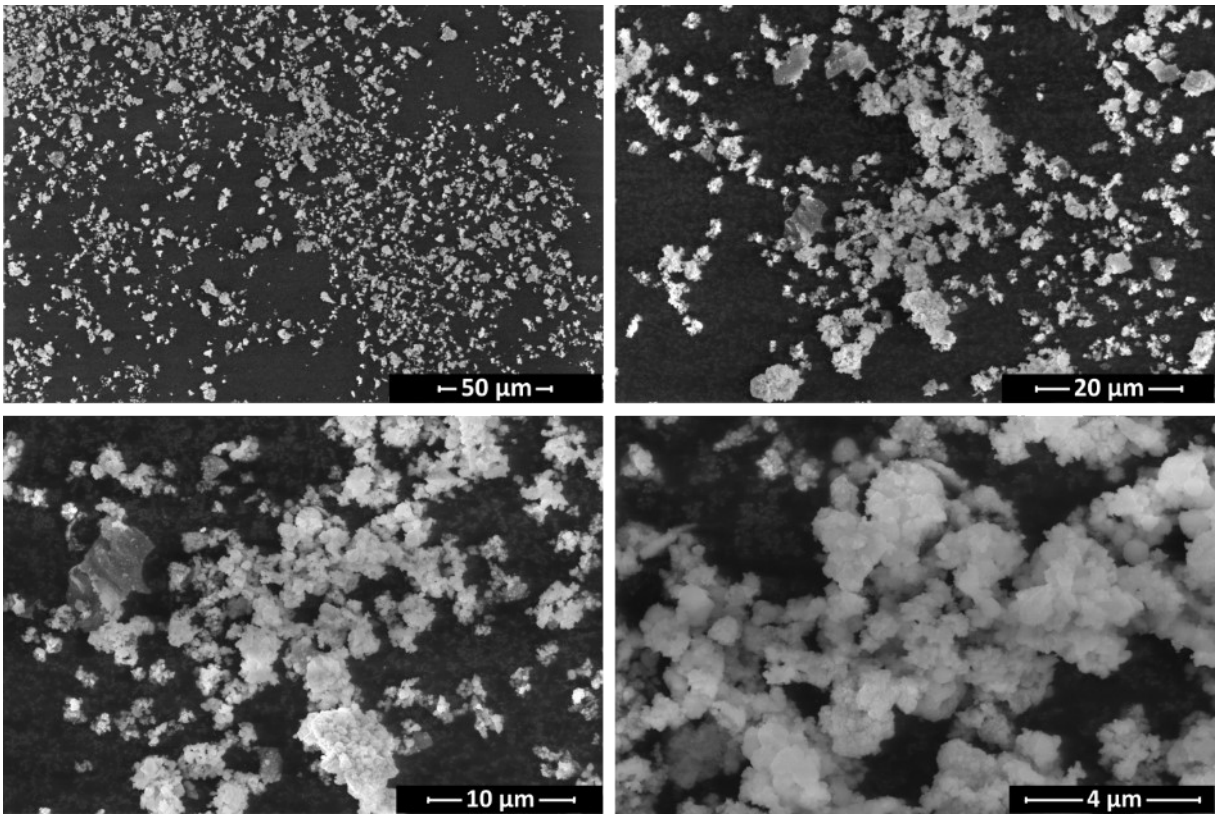

Figure S45. Scanning electron microscopy (SEM) images of the polymer **P2**.

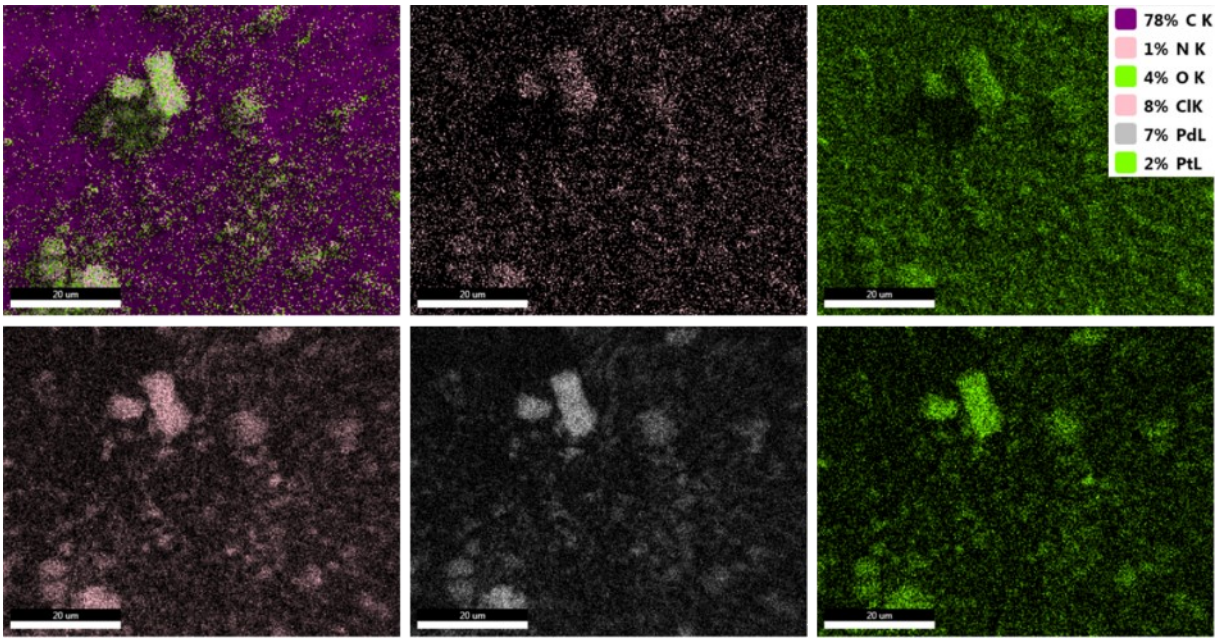

Figure S46. EDS elemental mapping of the sample composition for **P2**.

10.3. Polymer P3

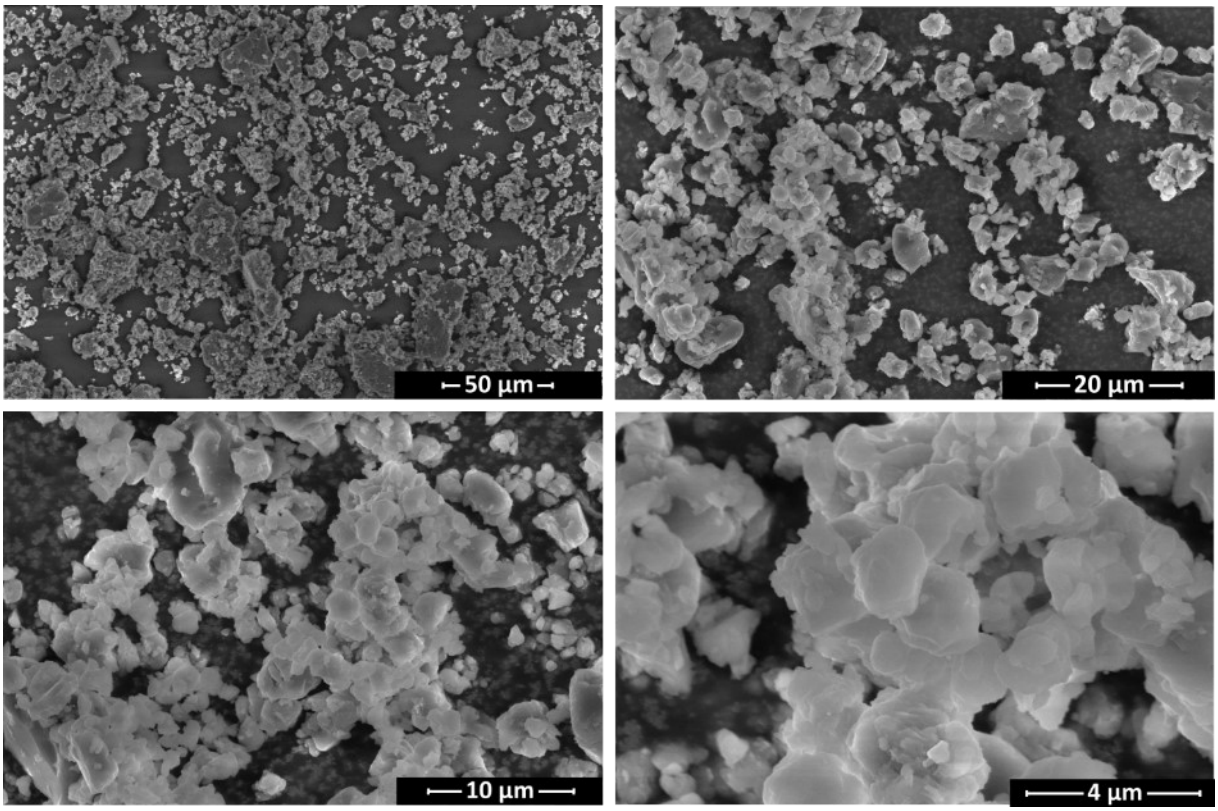

Figure S47. Scanning electron microscopy (SEM) images of the polymer **P3**.

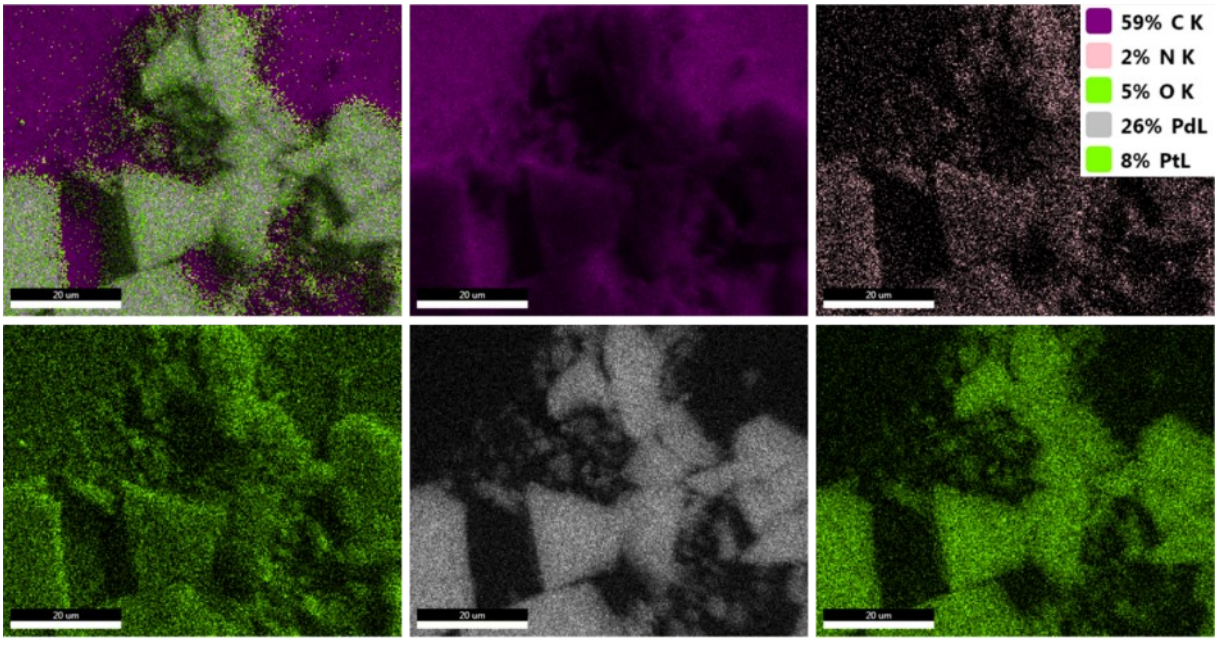

Figure S48. EDS elemental mapping of the sample composition for **P3**.

10.4. Complex C1

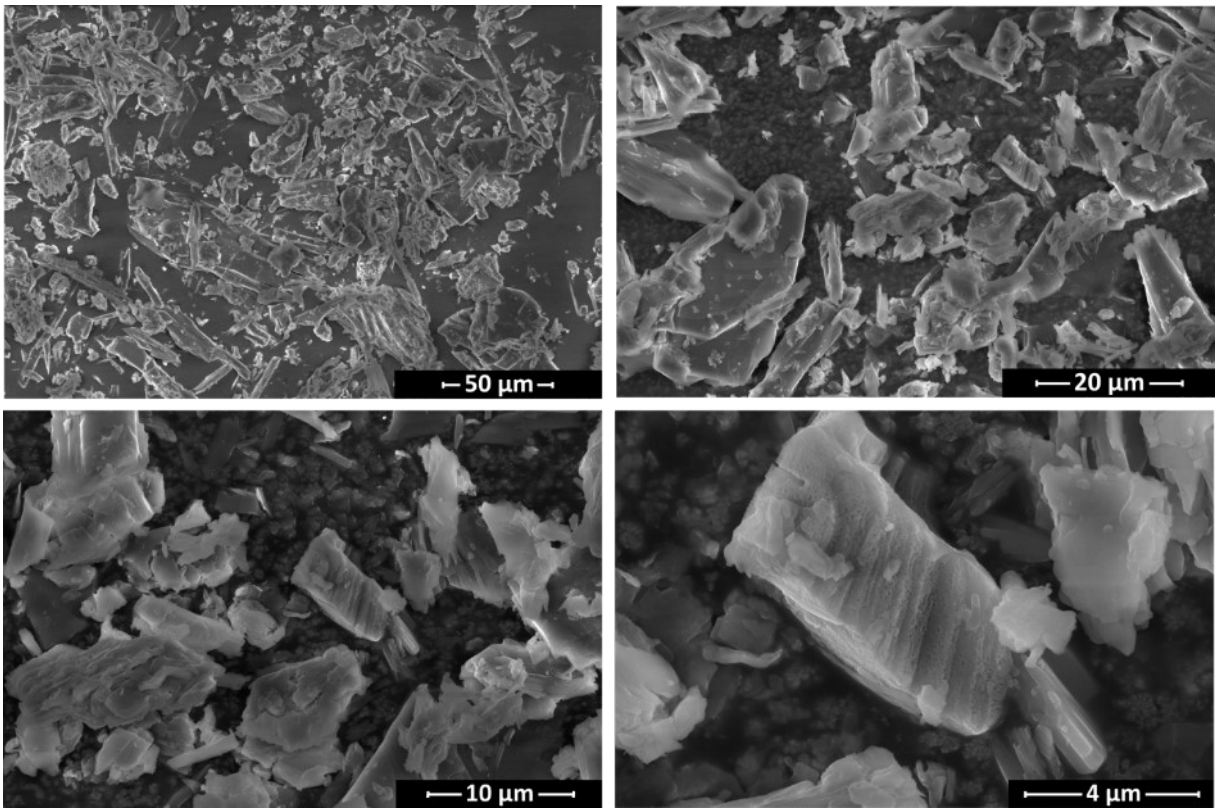

Figure S49. Scanning electron microscopy (SEM) images of the complex **C1**.

10.5. Complex C4

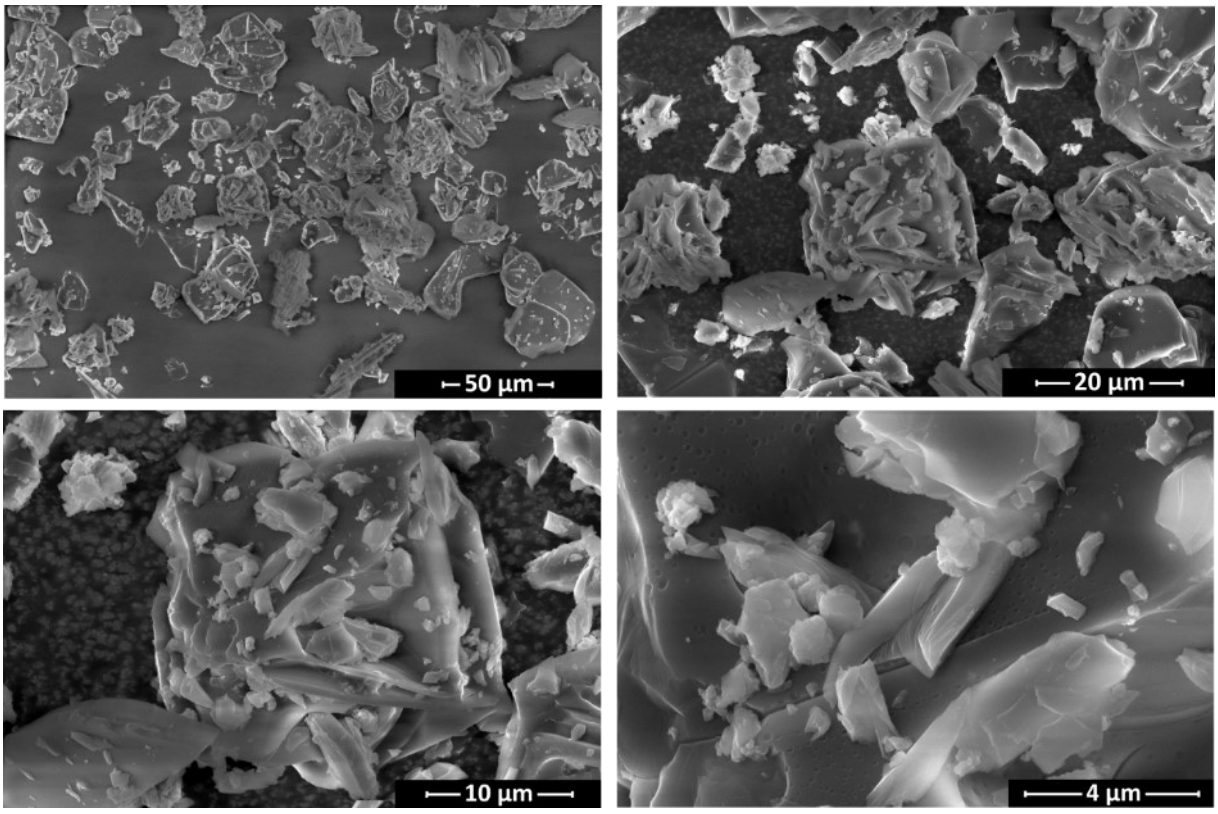

Figure S50. Scanning electron microscopy (SEM) images of the complex **C4**.

10.6. Complex C6

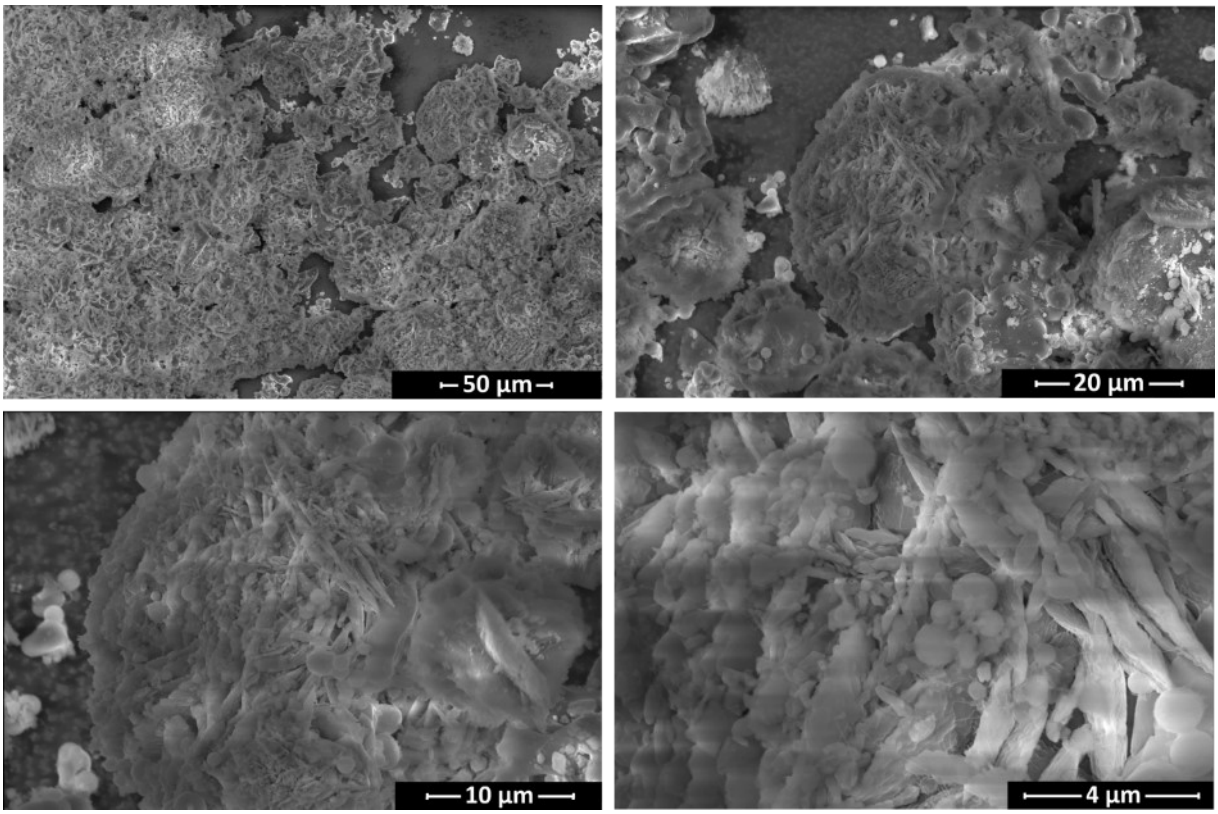

Figure S51. Scanning electron microscopy (SEM) images of the complex **C6**.

11. TG and DTG analysis of the coordination compounds

11.1. Complex C6

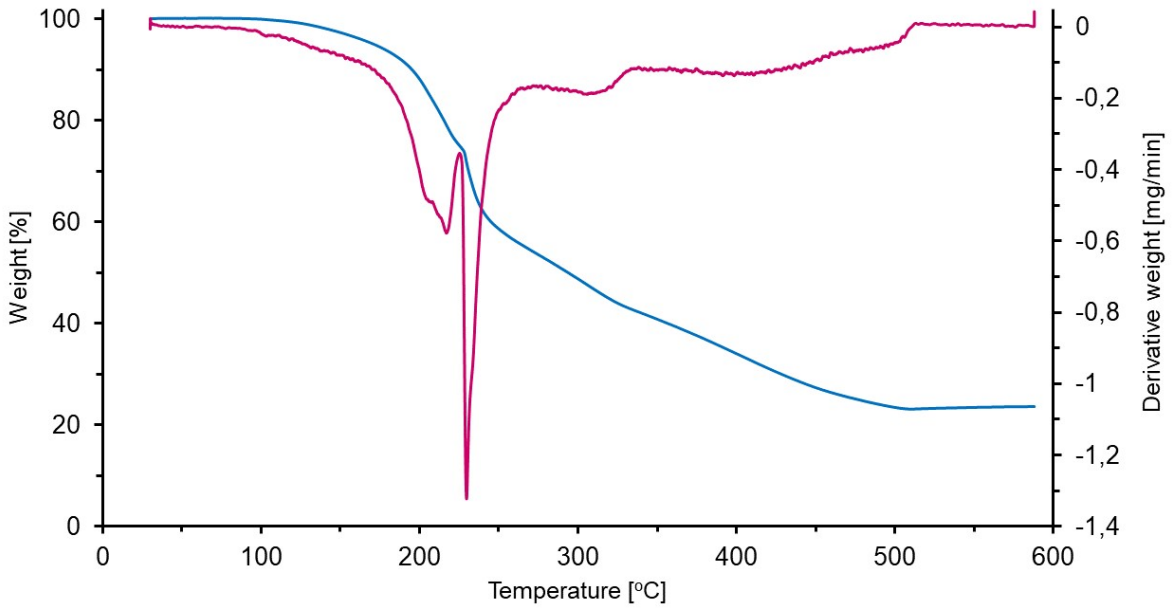

Figure S52. The thermogravimetry (TG) and derivative thermogravimetry (DTG) curves for the complex **C6**.

11.2. Complex C4

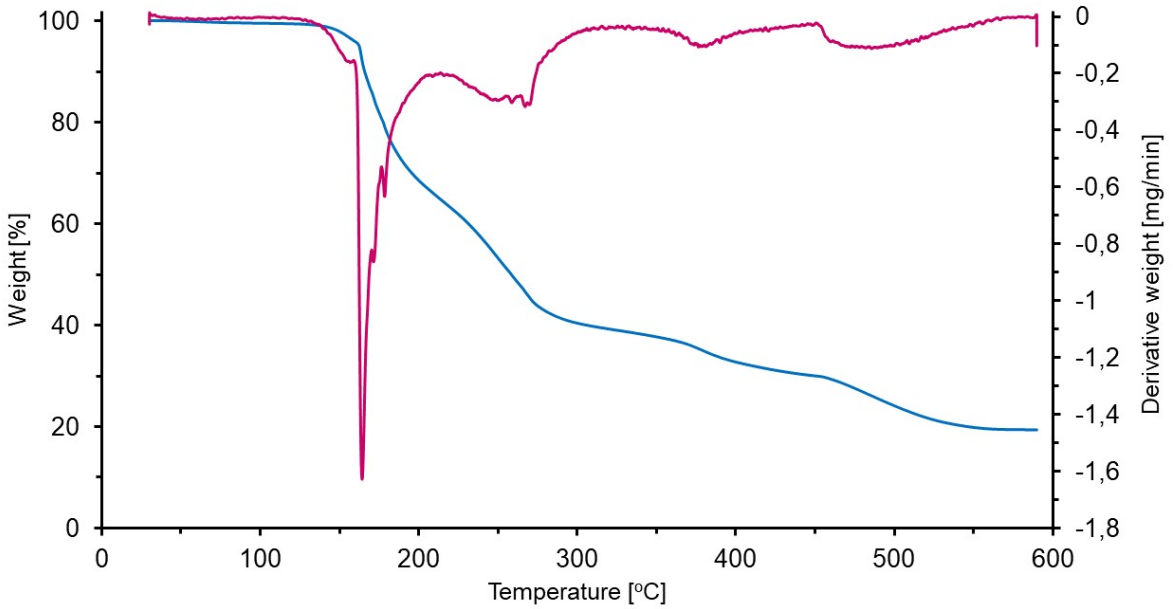

Figure S53. The thermogravimetry (TG) and derivative thermogravimetry (DTG) curves for the complex **C4**.

11.3. Polymer P1

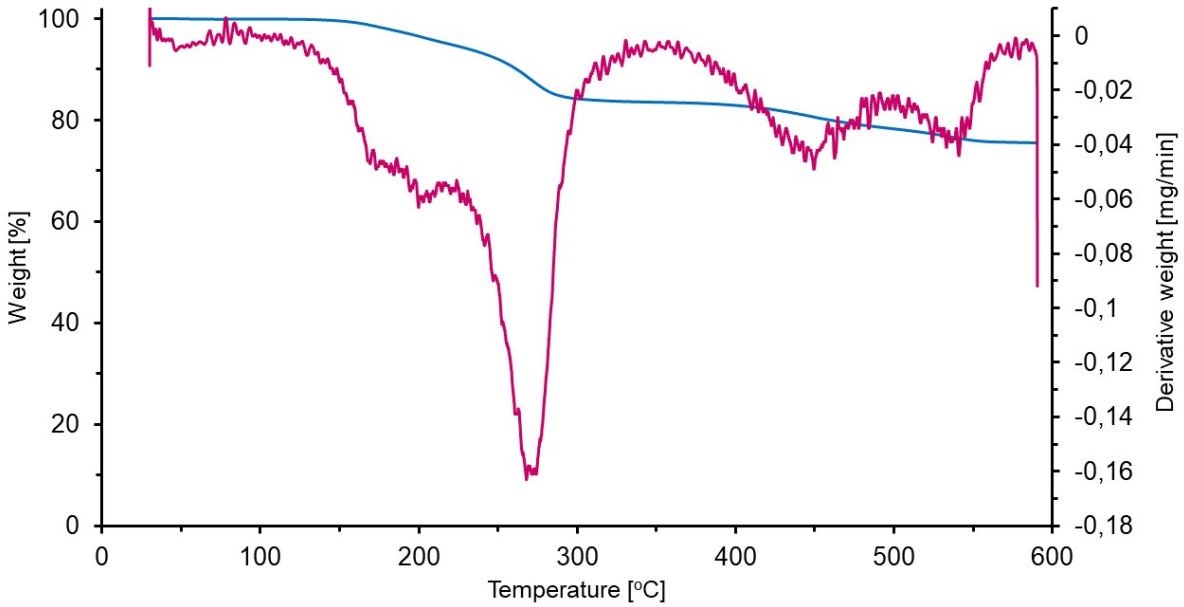

Figure S54. The thermogravimetry (TG) and derivative thermogravimetry (DTG) curves for the polymer **P1**.

11.4. Polymer P2

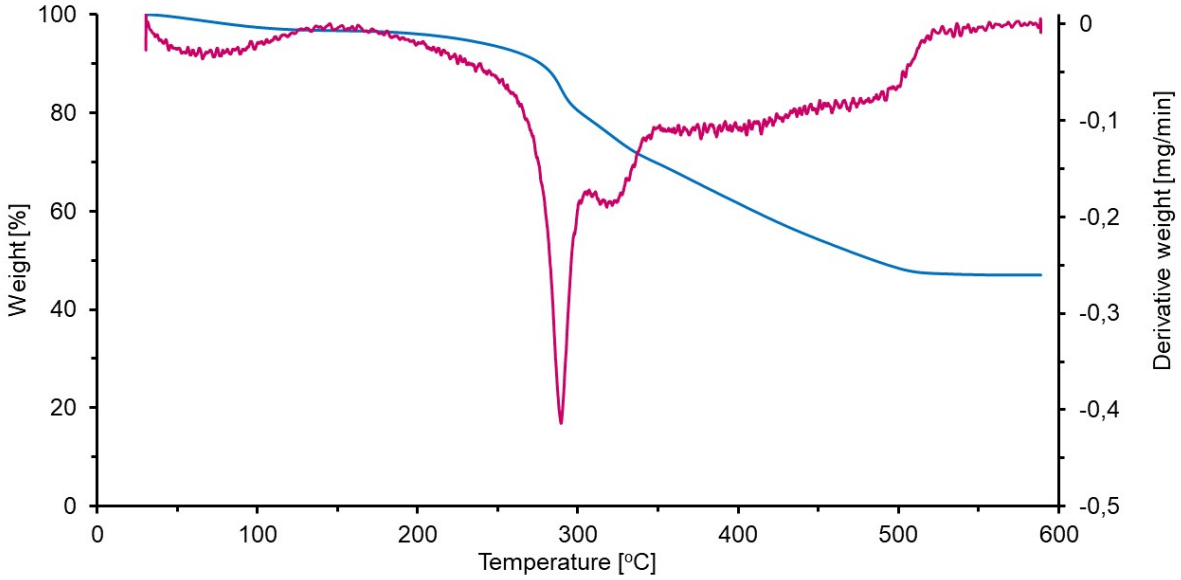

Figure S55. The thermogravimetry (TG) and derivative thermogravimetry (DTG) curves for the polymer **P2**.

11.5. Polymer P3

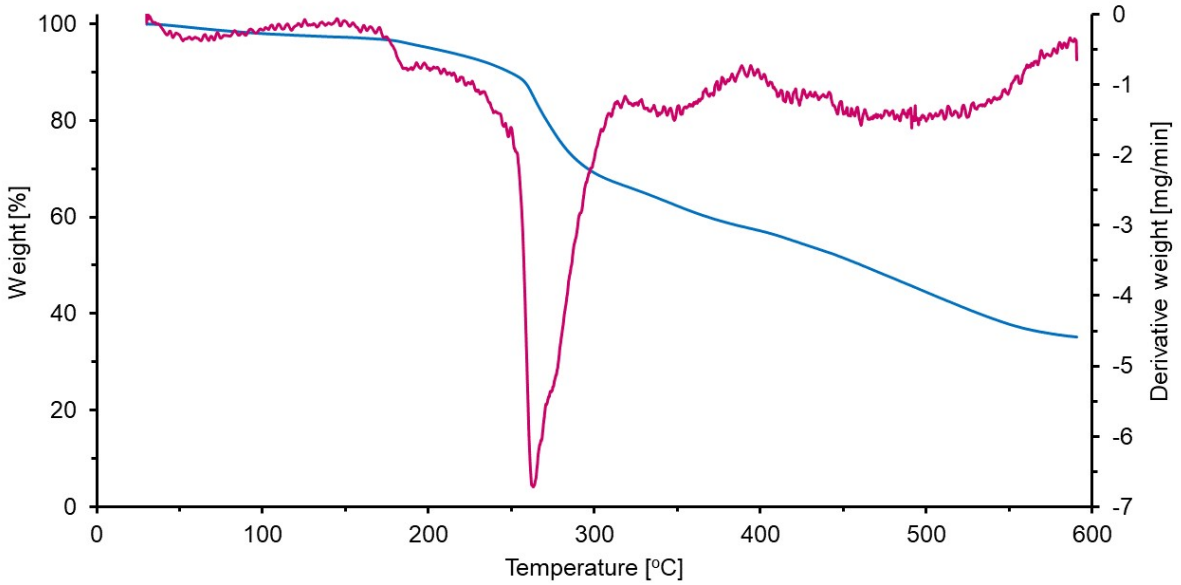

Figure S56. The thermogravimetry (TG) and derivative thermogravimetry (DTG) curves for the polymer **P3**.

11.6. Comparison of TGA curves

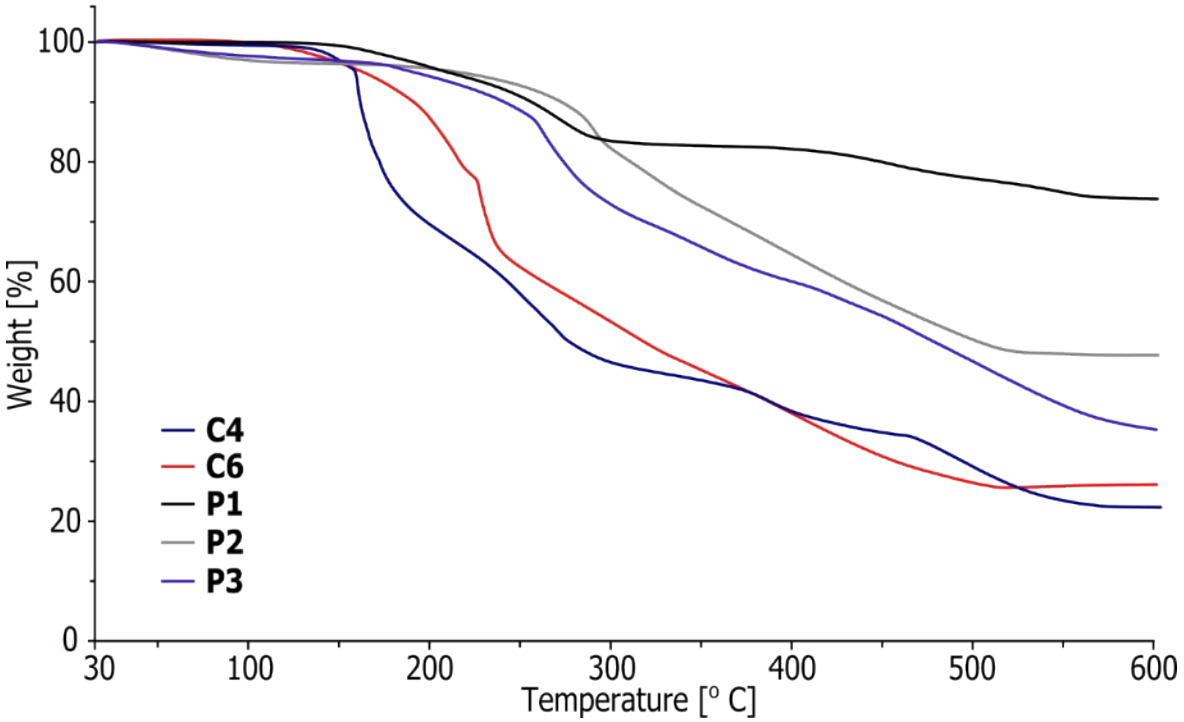

Figure S57. The thermogravimetric analysis (TGA) curves for the complex compounds **C4** and **C6**, and polymeric materials **P1**-**P3**.

11.7. Comparison of DTG curves

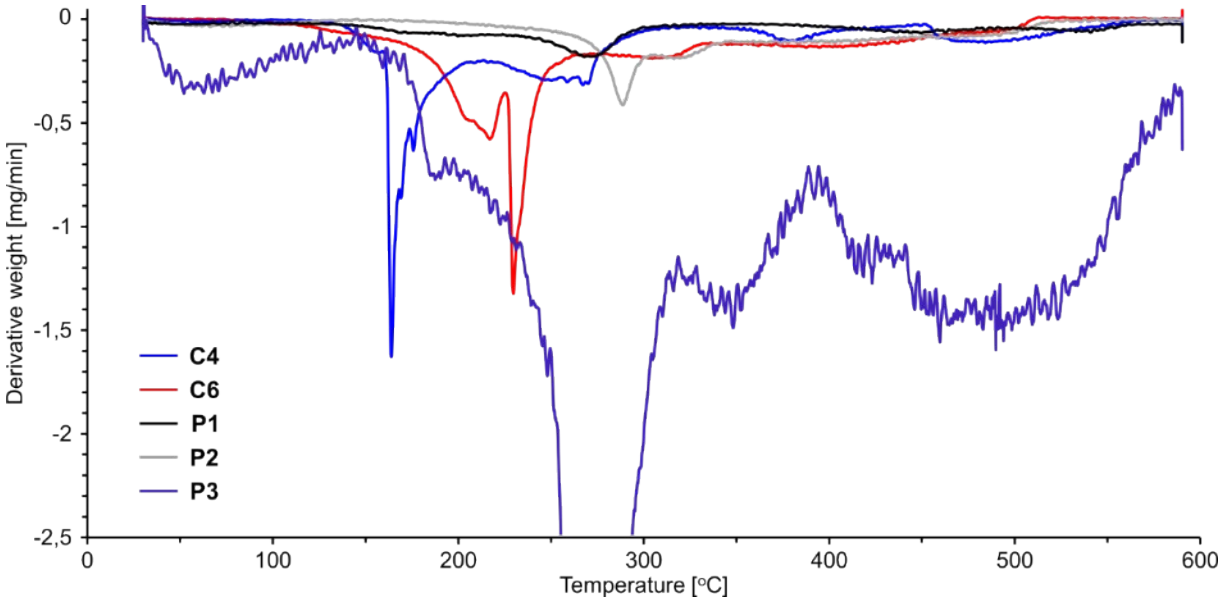

Figure S58. The comparison of derivative thermogravimetry (DTG) curves for the investigated materials.

12. Catalytic studies

12.1. Reaction development for the Heck reaction

Table S3. Reaction development for the Heck cross-coupling between styrene and iodobenzene.[a]

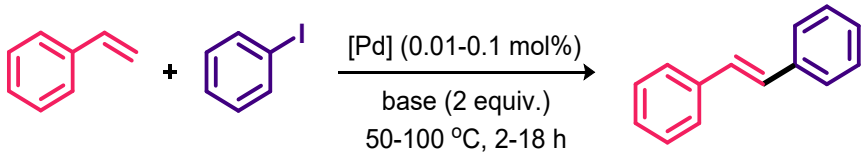

	solvent	base	T [°C]	mol% Pd	time [h]	GC yield [%]
1	DMSO	Et_3N	100	0.1	18	100
2	DMF	Et_3N	100	0.1	18	86
3	MeCN	Et_3N	100	0.1	18	69
4	1,4-dioxane	Et_3N	100	0.1	18	25
5	iPrOH	Et_3N	100	0.1	18	60
6	DMSO	*t*BuONa	100	0.1	18	39
7	DMSO	K_2CO_3	100	0.1	18	64
8	DMSO	NaOH	100	0.1	18	47
9	DMSO	Et_3N	50	0.1	18	23
10	DMSO	Et_3N	100	0.1	6	100
11	DMSO	Et_3N	100	0.1	4	93
12	DMSO	Et_3N	100	0.1	2	78
13	**DMSO**	**Et_3N**	**100**	**0.05**	**6**	**100**
14	DMSO	Et_3N	100	0.01	6	59
15	DMSO	Et_3N	100	0.01	18	99

[a] Reaction conditions: iodobenzene (0.5 mmol, 1 equiv.), styrene (0.5 mmol, 1 equiv.), base (1 mmol, 2 equiv.) and the catalyst **P2** were stirred in appropriate solvent (0.5 M) at indicated temperature under air atmosphere. [b] Determined by GC measurement of iodobenzene decay.

12.2. General synthetic procedure for the Heck cross-coupling

To a reaction vessel equipped with a stirring bar, aryl iodide (0.5 mmol, 1.0 equiv.), olefin (0.5 mmol, 1.0 equiv.), DMSO (1.0 mL), Pd(II) catalyst (0.05 mol% Pd) and Et_3N (1.0 mmol, 2.0 equiv.) were sequentially added. The vial was sealed and the reaction mixture was heated for 6 h at 100°C. The resulting solution was then cooled to room temperature, diluted with ethyl acetate (20 mL) and washed with icy distilled water (10 mL). The collected aqueous phase was extracted with ethyl acetate (2 × 20 mL). The organic layers were gathered, dried over Na_2SO_4, filtered and the solvent was removed under reduced pressure. The residue was purified by column chromatography on silica gel to obtain the desired coupling products **1**-**16**.

12.3. Characterization of the cross-coupling products

12.3.1. (*E*)-stilbene (1)[7]

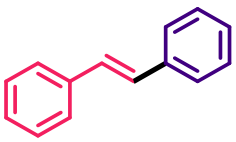

The reaction of iodobenzene (0.5 mmol, 56 µL) with styrene (0.5 mmol, 57 µL) according to the general procedure (flash chromatography: hexane) gave (*E*)-stilbene **1** in the form of white solid. Yield: 93%, 83.8 mg.

^{1}H NMR (600 MHz, $CDCl_3$) δ = 7.54 (d, *J* = 7.3 Hz, 4H), 7.38 (t, *J* = 7.7 Hz, 4H), 7.28 (t, *J* = 7.4 Hz, 2H), 7.13 (s, 2H).

^{13}C NMR (151 MHz, $CDCl_3$) δ = 137.47, 128.83, 128.82, 127.76, 126.65.

12.3.2. (*E*)-4-tert-butylstilbene (2)[8]

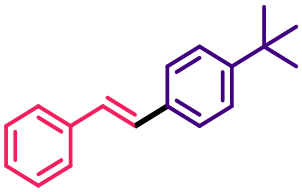

The reaction of 4-tert-butyliodobenzene (0.5 mmol, 89 µL) with styrene (0.5 mmol, 57 µL) according to the general procedure (flash chromatography: hexane) gave (*E*)-4-tert-butylstilbene **2** in the form of white solid. Yield: 90%, 106.4 mg.

^{1}H NMR (600 MHz, $CDCl_3$) δ = 7.56 (d, *J* = 7.3 Hz, 2H), 7.51 (d, *J* = 8.3 Hz, 2H), 7.44 (d, *J* = 8.4 Hz, 2H), 7.40 (t, *J* = 7.7 Hz, 2H), 7.30 (t, *J* = 7.4 Hz, 1H), 7.16 (d, *J* = 16.3 Hz, 1H), 7.13 (d, *J* = 16.3 Hz, 1H), 1.39 (s, 9H).

^{13}C NMR (151 MHz, $CDCl_3$) δ = 150.90, 137.67, 134.70, 128.78, 128.63, 128.06, 127.54, 126.55, 126.39, 125.74, 34.76, 31.44.

12.3.3. (*E*)-4-bromostilbene (3)[9]

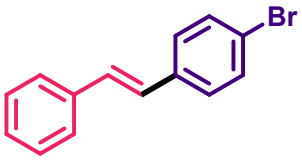

The reaction of 1-bromo-4-iodobenzene (0.5 mmol, 141.5 mg) with styrene (0.5 mmol, 57 µL) according to the general procedure (flash chromatography: hexane) gave (*E*)-4-bromostilbene **3** in the form of white solid. Yield: 76%, 98.5 mg.

^{1}H NMR (600 MHz, $CDCl_3$) δ = 7.51 (d, *J* = 7.2 Hz, 2H), 7.48 (d, *J* = 8.5 Hz, 2H), 7.39 – 7.37 (m, 4H), 7.29 (t, *J* = 6.7 Hz, 1H), 7.10 (d, *J* = 16.3 Hz, 1H), 7.04 (d, *J* = 16.3 Hz, 1H).

^{13}C NMR (151 MHz, $CDCl_3$) δ = 137.19, 136.52, 132.02, 129.67, 128.99, 128.21, 128.15, 127.64, 126.80, 121.55.

12.3.4. (*E*)-4-methoxystilbene (4)[8]

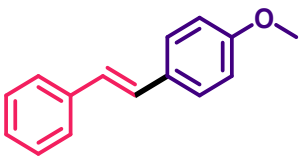

The reaction of 4-iodoanisole (0.5 mmol, 117.0 mg) with styrene (0.5 mmol, 57 µL) according to the general procedure (flash chromatography: hexane/ethyl acetate 95:5) gave (*E*)-4-methoxystilbene **4** in the form of pale yellow solid. Yield: 88%, 92.5 mg.

^{1}H NMR (600 MHz, $CDCl_3$) δ = 7.49 (d, *J* = 7.5 Hz, 2H), 7.46 (d, *J* = 8.7 Hz, 2H), 7.35 (t, *J* = 7.7 Hz, 2H), 7.24 (t, *J* = 7.4 Hz, 1H), 7.07 (d, *J* = 16.3 Hz, 1H), 6.98 (d, *J* = 16.3 Hz, 1H), 6.91 (d, *J* = 8.7 Hz, 2H), 3.84 (s, 3H).

^{13}C NMR (151 MHz, $CDCl_3$) δ = 159.44, 137.79, 130.29, 128.78, 128.35, 127.86, 127.35, 126.76, 126.39, 114.28, 55.48.

12.3.5. (*E*)-4-aminostilbene (5)[10]

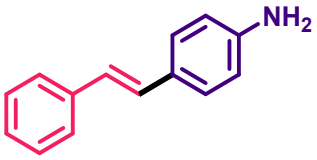

The reaction of 4-iodoaniline (0.5 mmol, 109.5 mg) with styrene (0.5 mmol, 57 µL) according to the general procedure (flash chromatography: hexane/ethyl acetate 95:5) gave (*E*)-4-aminostilbene **5** in the form of brownish solid. Yield: 80%, 78.1 mg.

^{1}H NMR (600 MHz, $CDCl_3$) δ = 7.48 (d, *J* = 7.7 Hz, 2H), 7.37 – 7.32 (m, 4H), 7.22 (t, *J* = 7.3 Hz, 1H), 7.04 (d, *J* = 16.3 Hz, 1H), 6.93 (d, *J* = 16.3 Hz, 1H), 6.68 (d, *J* = 8.4 Hz, 2H), 3.74 (bs, 2H).

^{13}C NMR (151 MHz, $CDCl_3$) δ = 146.27, 138.08, 128.81, 128.73, 128.16, 127.88, 127.02, 126.23, 125.24, 115.33.

12.3.6. (*E*)-4-acetylstilbene (6)[11]

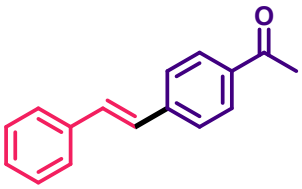

The reaction of 4-iodoacetophenone (0.5 mmol, 123.0 mg) with styrene (0.5 mmol, 57 µL) according to the general procedure (flash chromatography: hexane/ethyl acetate 95:5) gave (*E*)-4-acetylstilbene **6** in the form of white solid. Yield: 70%, 77.8 mg.

^{1}H NMR (600 MHz, $CDCl_3$) δ = 7.96 (d, *J* = 8.4 Hz, 2H), 7.59 (d, *J* = 8.4 Hz, 2H), 7.54 (d, *J* = 7.4 Hz, 2H), 7.39 (t, *J* = 7.7 Hz, 2H), 7.31 (t, *J* = 7.3 Hz, 1H), 7.23 (d, *J* = 16.3 Hz, 1H), 7.14 (d, *J* = 16.3 Hz, 1H), 2.61 (s, 3H).

^{13}C NMR (151 MHz, $CDCl_3$) δ = 197.59, 142.14, 136.83, 136.09, 131.59, 129.01, 128.93, 128.45, 127.58, 126.95, 126.63, 26.74.

12.3.7. (*E*)-4-tert-butylstilbene (7)[8]

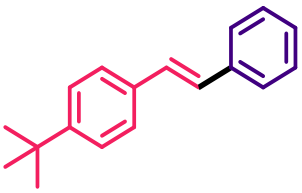

The reaction of iodobenzene (0.5 mmol, 56 µL) with 4-tert-butylstyrene (0.5 mmol, 92 µL) according to the general procedure (flash chromatography: hexane) gave (*E*)-4-tert-butylstilbene **7** in the form of white solid. Yield: 82%, 96.9 mg.

^{1}H NMR (600 MHz, $CDCl_3$) δ = 7.56 (d, *J* = 7.3 Hz, 2H), 7.51 (d, *J* = 8.3 Hz, 2H), 7.44 (d, *J* = 8.4 Hz, 2H), 7.40 (t, *J* = 7.7 Hz, 2H), 7.30 (t, *J* = 7.4 Hz, 1H), 7.16 (d, *J* = 16.3 Hz, 1H), 7.13 (d, *J* = 16.3 Hz, 1H), 1.39 (s, 9H).

^{13}C NMR (151 MHz, $CDCl_3$) δ = 150.90, 137.67, 134.70, 128.78, 128.63, 128.06, 127.54, 126.55, 126.39, 125.74, 34.76, 31.44.

12.3.8. (*E*)-4-bromo-4'-tert-butylstilbene (8)[12]

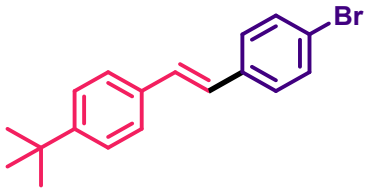

The reaction of 1-bromo-4-iodobenzene (0.5 mmol, 141.5 mg) with 4-tert-butylstyrene (0.5 mmol, 92 µL) according to the general procedure (flash chromatography: hexane) gave (*E*)-4-bromo-4'-tert-butylstilbene **8** in the form of white solid. Yield: 80%, 126.1 mg.

^{1}H NMR (600 MHz, $CDCl_3$) δ = 7.50 – 7.45 (m, 4H), 7.41 (d, *J* = 8.4 Hz, 2H), 7.38 (d, *J* = 8.5 Hz, 2H), 7.10 (d, *J* = 16.3 Hz, 1H), 7.02 (d, *J* = 16.3 Hz, 1H), 1.37 (s, 9H).

^{13}C NMR (151 MHz, $CDCl_3$) δ = 151.23, 136.61, 134.30, 131.85, 129.36, 128.01, 126.74, 126.45, 125.80, 121.18, 34.79, 31.42.

12.3.9. (*E*)-4-methoxy-4'-tert-butylstilbene (9)[13]

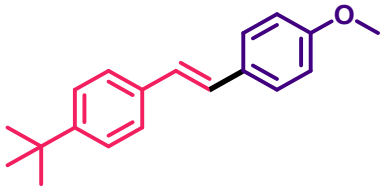

The reaction of 4-iodoanisole (0.5 mmol, 117.0 mg) with 4-tert-butylstyrene (0.5 mmol, 92 µL) according to the general procedure (flash chromatography: hexane) gave (*E*)-4-methoxy-4'-tert-butylstilbene **9** in the form of white solid. Yield: 81%, 107.9 mg.

^{1}H NMR (600 MHz, $CDCl_3$) δ = 7.48 – 7.43 (m, 4H), 7.39 (d, *J* = 8.4 Hz, 2H), 7.05 (d, *J* = 16.3 Hz, 1H), 6.98 (d, *J* = 16.3 Hz, 1H), 6.91 (d, *J* = 8.7 Hz, 2H), 3.84 (s, 3H), 1.35 (s, 9H).

^{13}C NMR (151 MHz, $CDCl_3$) δ = 159.29, 150.46, 135.02, 130.51, 127.73, 127.59, 126.58, 126.11, 125.70, 114.24, 55.46, 34.73, 31.45.

12.3.10. (*E*)-4-acetyl-4'-tert-butylstilbene (10)[14]

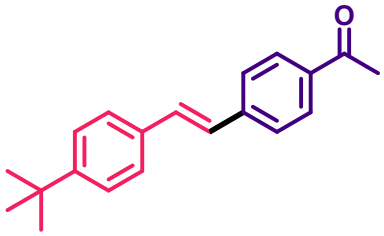

The reaction of 4-iodoacetophenone (0.5 mmol, 123.0 mg) with 4-tert-butylstyrene (0.5 mmol, 92 µL) according to the general procedure (flash chromatography: hexane/ethyl acetate 95:5) gave (*E*)-4-acetyl-4'-tert-butylstilbene **10** in the form of white solid. Yield: 83%, 115.5 mg.

^{1}H NMR (600 MHz, $CDCl_3$) δ = 7.95 (d, *J* = 8.3 Hz, 2H), 7.58 (d, *J* = 8.3 Hz, 2H), 7.49 (d, *J* = 8.3 Hz, 2H), 7.41 (d, *J* = 8.4 Hz, 2H), 7.22 (d, *J* = 16.3 Hz, 1H), 7.10 (d, *J* = 16.3 Hz, 1H), 2.61 (s, 3H), 1.35 (s, 9H).

^{13}C NMR (151 MHz, $CDCl_3$) δ = 197.58, 151.74, 142.38, 135.88, 134.05, 131.43, 128.98, 126.77, 126.71, 126.50, 125.87, 34.84, 31.39, 26.71.

12.3.11. (*E*)-4-bromostilbene (11)[9]

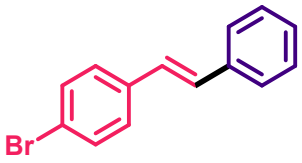

The reaction of iodobenzene (0.5 mmol, 56 µL) with 4-bromostyrene (0.5 mmol, 66 µL) according to the general procedure (flash chromatography: hexane) gave (*E*)-4-bromostilbene **11** in the form of white solid. Yield: 87%, 112.7 mg.

^{1}H NMR (600 MHz, $CDCl_3$) δ = 7.51 (d, *J* = 7.2 Hz, 2H), 7.48 (d, *J* = 8.5 Hz, 2H), 7.39 – 7.37 (m, 4H), 7.29 (t, *J* = 6.7 Hz, 1H), 7.10 (d, *J* = 16.3 Hz, 1H), 7.04 (d, *J* = 16.3 Hz, 1H).

^{13}C NMR (151 MHz, $CDCl_3$) δ = 137.19, 136.52, 132.02, 129.67, 128.99, 128.21, 128.15, 127.64, 126.80, 121.55.

12.3.12. (*E*)-4,4'-dibromostilbene (12)[15]

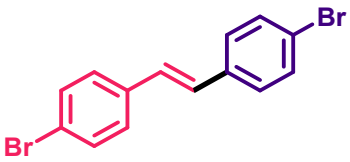

The reaction of 1-bromo-4-iodobenzene (0.5 mmol, 141.5 mg) with 4-bromostyrene (0.5 mmol, 66 µL) according to the general procedure (flash chromatography: hexane) gave (*E*)-4,4'-dibromostilbene **12** in the form of white solid. Yield: 82%, 138.6 mg.

^{1}H NMR (600 MHz, $CDCl_3$) δ = 7.48 (d, *J* = 8.5 Hz, 4H), 7.36 (d, *J* = 8.5 Hz, 4H), 7.02 (s, 2H).

^{13}C NMR (151 MHz, $CDCl_3$) δ = 136.05, 132.00, 128.27, 128.15, 121.79.

12.3.13. Methyl (*E*)-cinnamate (13)[7]

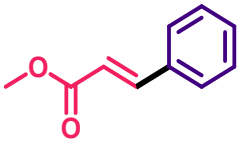

The reaction of iodobenzene (0.5 mmol, 56 µL) with methyl acrylate (0.5 mmol, 45 µL) according to the general procedure (flash chromatography: hexane/ethyl acetate 90:10) gave methyl (*E*)-cinnamate **13** in the form of light yellow solid. Yield: 95%, 77.0 mg.

^{1}H NMR (600 MHz, $CDCl_3$) δ = 7.70 (d, *J* = 16.0 Hz, 1H), 7.53 – 7.52 (m, 2H), 7.39 – 7.38 (m, 3H), 6.45 (d, *J* = 16.0 Hz, 1H), 3.81 (s, 3H).

^{13}C NMR (151 MHz, $CDCl_3$) δ = 167.56, 145.00, 134.52, 130.43, 129.02, 128.20, 117.94, 51.84.

12.3.14. Methyl (*E*)-4-bromocinnamate (14)[16]

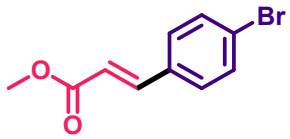

The reaction of 1-bromo-4-iodobenzene (0.5 mmol, 141.5 mg) with methyl acrylate (0.5 mmol, 45 µL) according to the general procedure (flash chromatography: hexane/ethyl acetate 95:5) gave methyl (*E*)-4-bromocinnamate **14** in the form of pale yellow solid. Yield: 92%, 110.9 mg.

^{1}H NMR (600 MHz, $CDCl_3$) δ = 7.62 (d, *J* = 16.0 Hz, 1H), 7.52 (d, *J* = 8.4 Hz, 2H), 7.38 (d, *J* = 8.5 Hz, 2H), 6.42 (d, *J* = 16.0 Hz, 1H), 3.81 (s, 3H).

^{13}C NMR (151 MHz, $CDCl_3$) δ = 167.29, 143.62, 133.43, 132.29, 129.58, 124.69, 118.64, 51.95.

12.3.15. Methyl (*E*)-4-methoxycinnamate (15)[17]

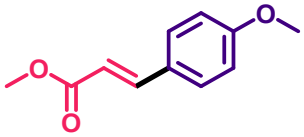

The reaction of 4-iodoanisole (0.5 mmol, 117.0 mg) with methyl acrylate (0.5 mmol, 45 µL) according to the general procedure (flash chromatography: hexane/ethyl acetate 90:10) gave methyl (*E*)-4-methoxycinnamate **15** in the form of pale yellow solid. Yield: 85%, 81.7 mg.

^{1}H NMR (600 MHz, $CDCl_3$) δ = 7.65 (d, *J* = 16.0 Hz, 1H), 7.47 (d, *J* = 8.7 Hz, 2H), 6.90 (d, *J* = 8.8 Hz, 2H), 6.30 (d, *J* = 16.0 Hz, 1H), 3.83 (s, 3H), 3.79 (s, 3H).

^{13}C NMR (151 MHz, $CDCl_3$) δ = 167.86, 161.50, 144.63, 129.83, 127.22, 115.37, 114.43, 55.48, 51.68.

12.3.16. Methyl (*E*)-4-acetylcinnamate (16)[17]

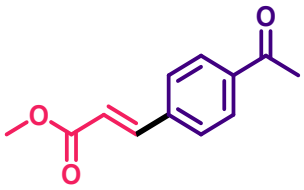

The reaction of 4-iodoacetophenone (0.5 mmol, 123.0 mg) with methyl acrylate (0.5 mmol, 45 µL) according to the general procedure (flash chromatography: hexane/ethyl acetate 80:20) gave methyl (*E*)-4-acetylcinnamate **16** in the form of pale yellow solid. Yield: 93%, 95.0 mg.

^{1}H NMR (600 MHz, $CDCl_3$) δ = 7.96 (d, *J* = 8.4 Hz, 2H), 7.70 (d, *J* = 16.0 Hz, 1H), 7.60 (d, *J* = 8.4 Hz, 2H), 6.52 (d, *J* = 16.0 Hz, 1H), 3.82 (s, 3H), 2.61 (s, 3H).

^{13}C NMR (151 MHz, $CDCl_3$) δ = 197.40, 167.04, 143.42, 138.82, 138.17, 128.98, 128.27, 120.46, 52.04, 26.82.

12.4. NMR spectra of the isolated reaction products

All NMR data were compared with the data available in the literature to confirm their consistency.

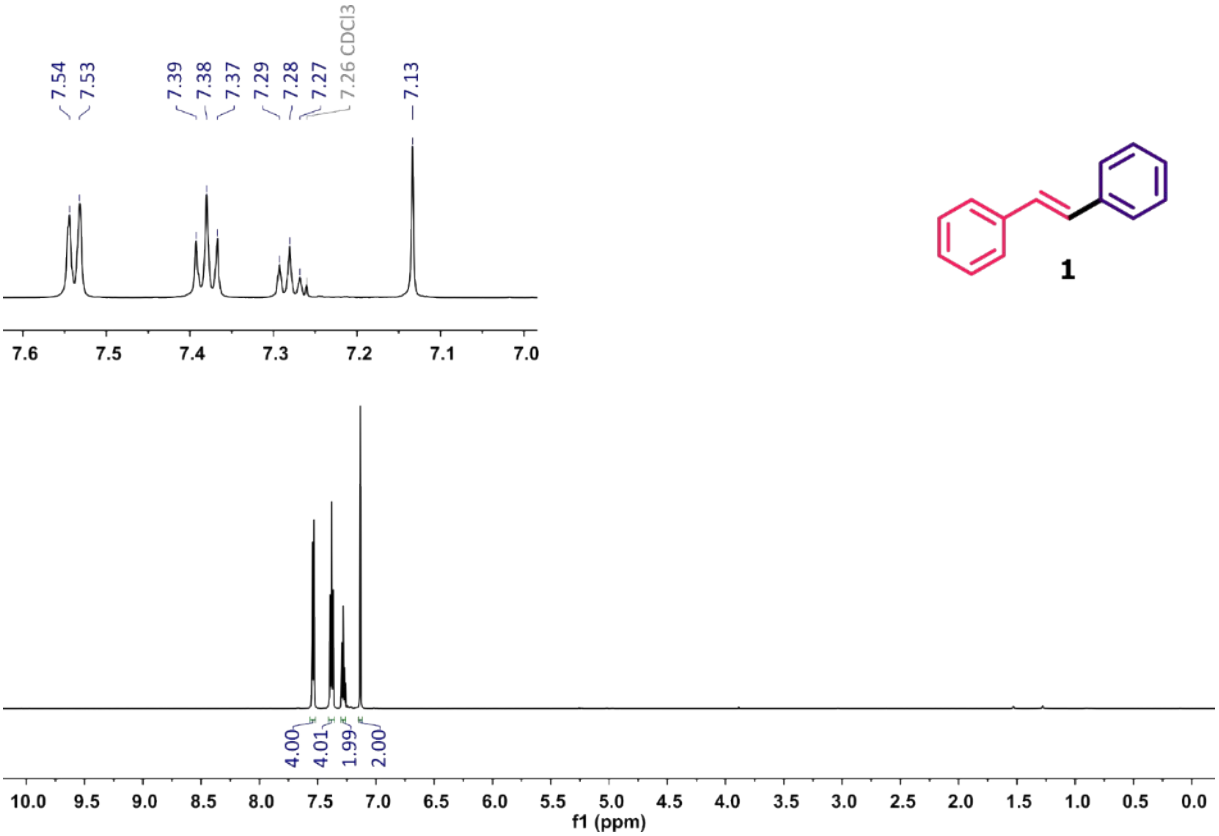

Figure S59. ^{1}H NMR spectrum (600 MHz, $CDCl_3$) of (*E*)-stilbene **1**.

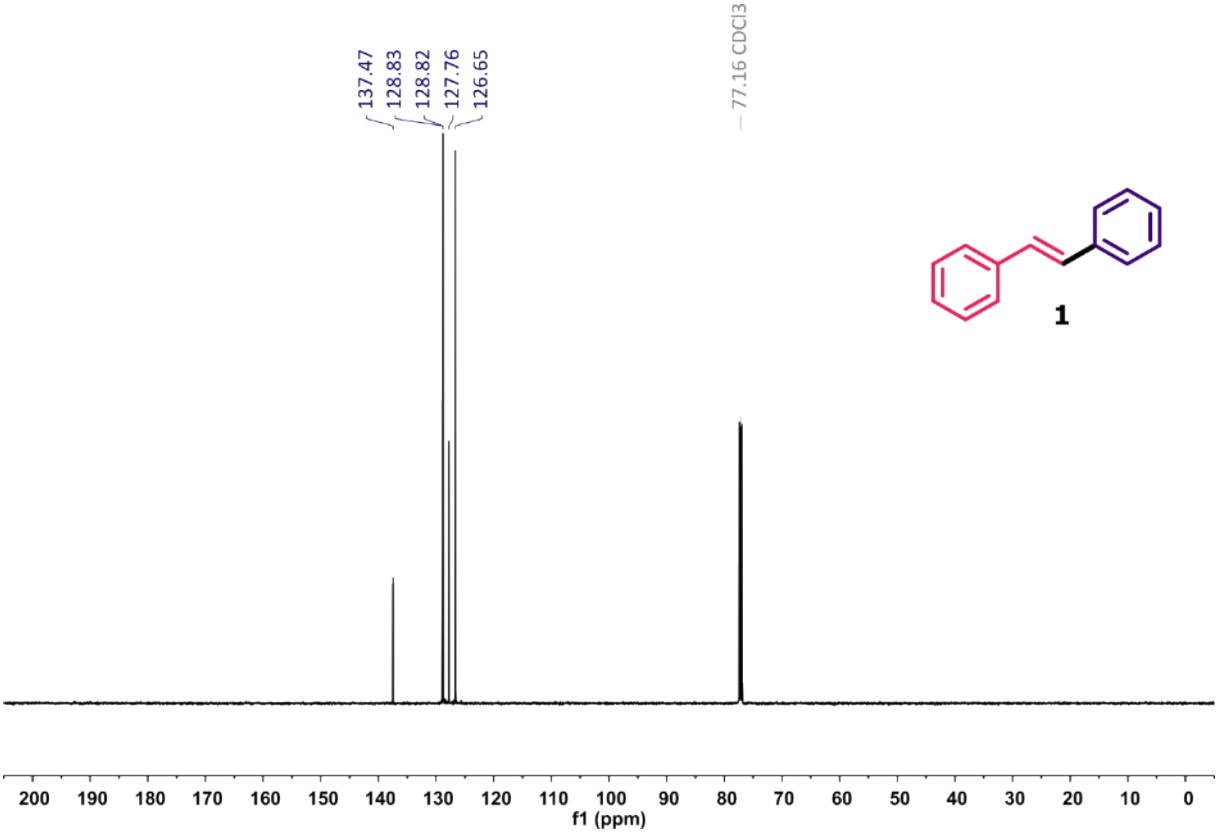

Figure S60. ^{13}C NMR spectrum (151 MHz, $CDCl_3$) of (*E*)-stilbene **1**.

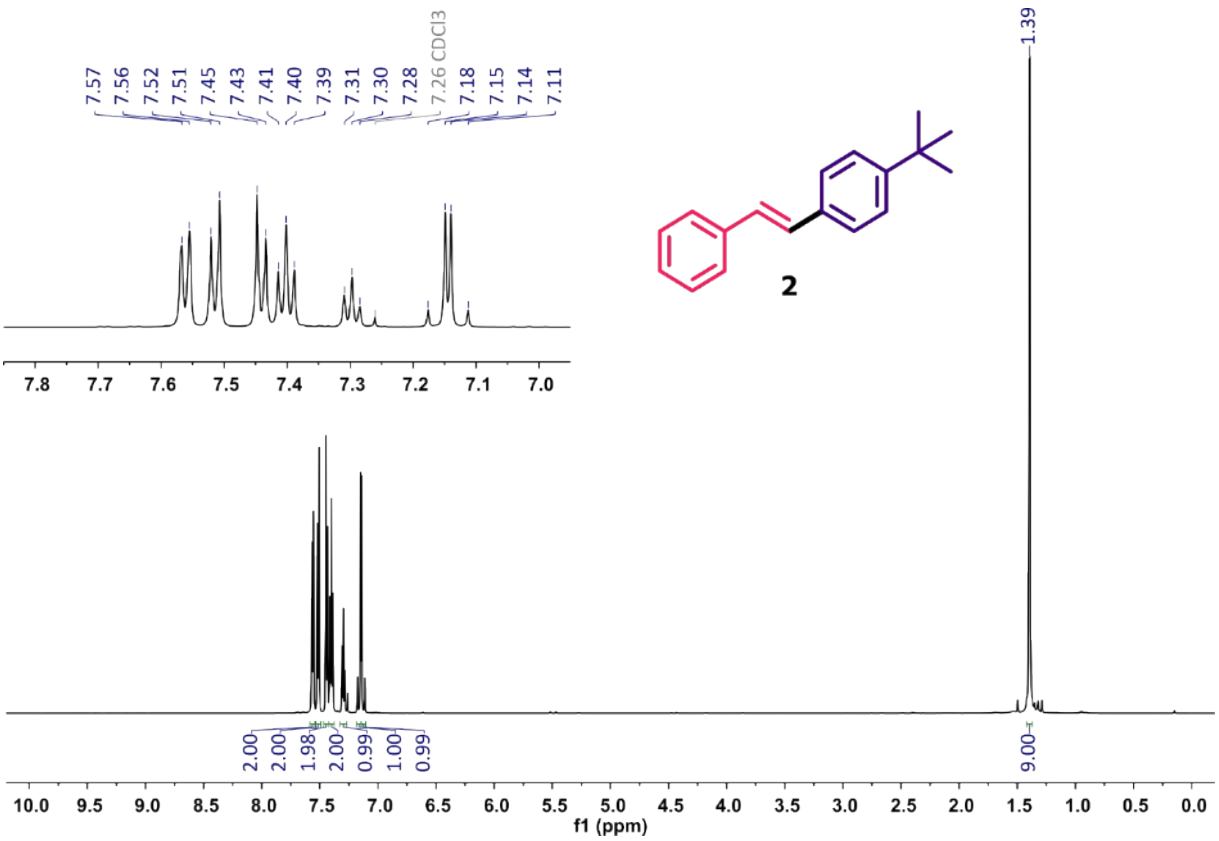

Figure S61. ^{1}H NMR spectrum (600 MHz, $CDCl_3$) of (*E*)-4-tert-butylstilbene **2**.

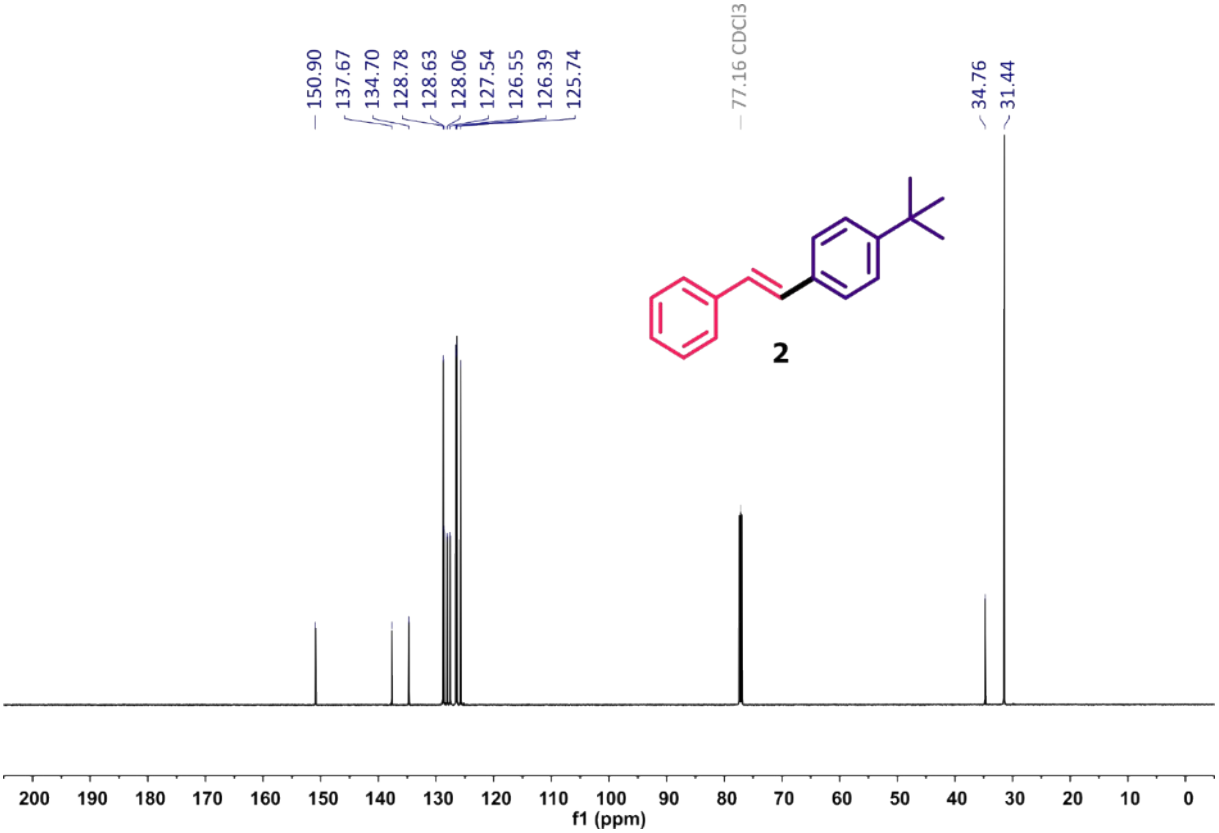

Figure S62. ^{13}C NMR spectrum (151 MHz, $CDCl_3$) of (*E*)-4-tert-butylstilbene **2**.

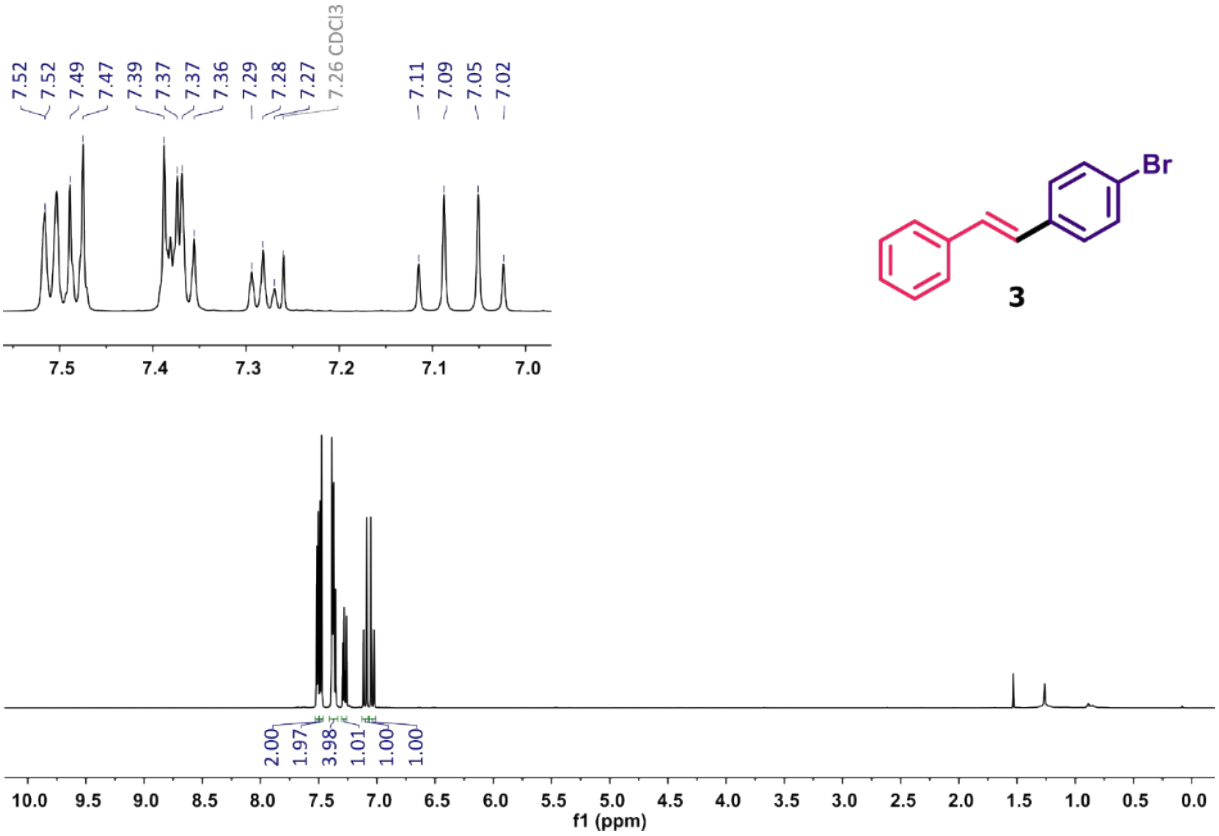

Figure S63. ^{1}H NMR spectrum (600 MHz, $CDCl_3$) of (*E*)-4-bromostilbene **3**.

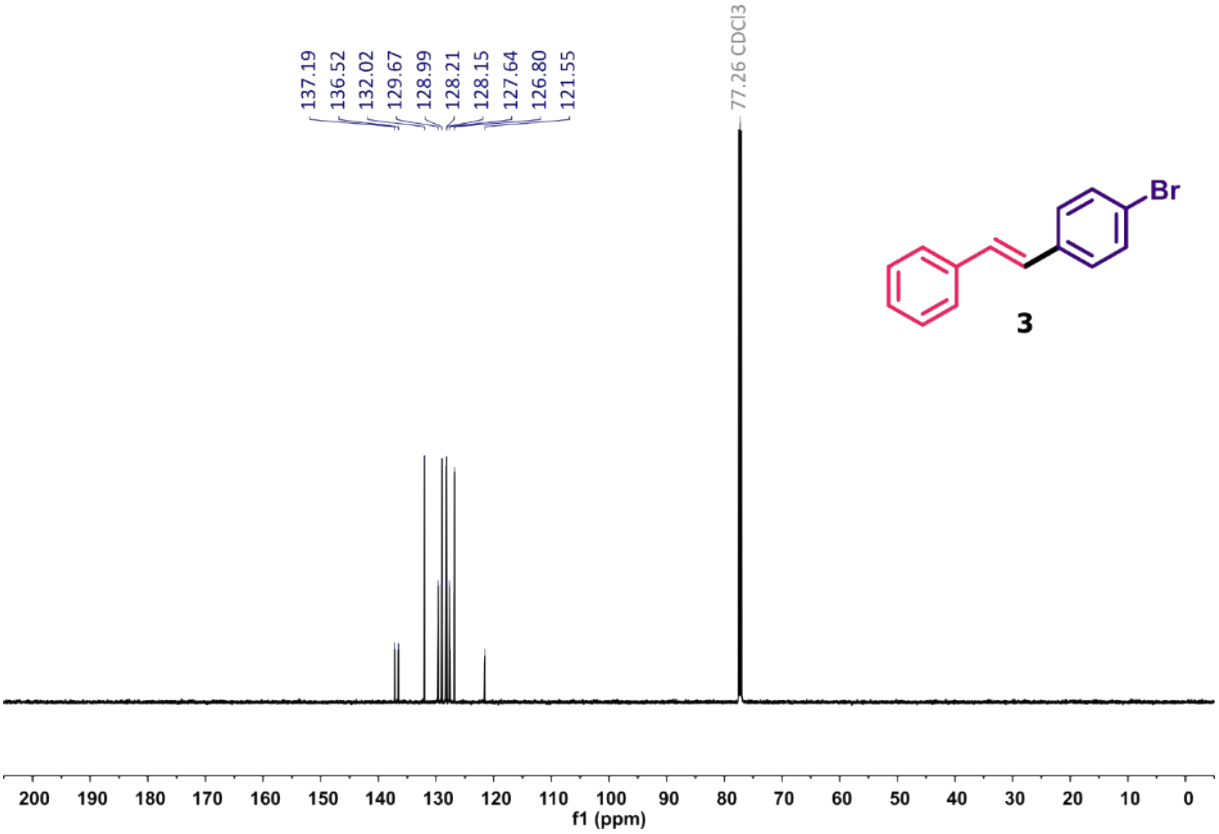

Figure S64. ^{13}C NMR spectrum (151 MHz, $CDCl_3$) of (*E*)-4-bromostilbene **3**.

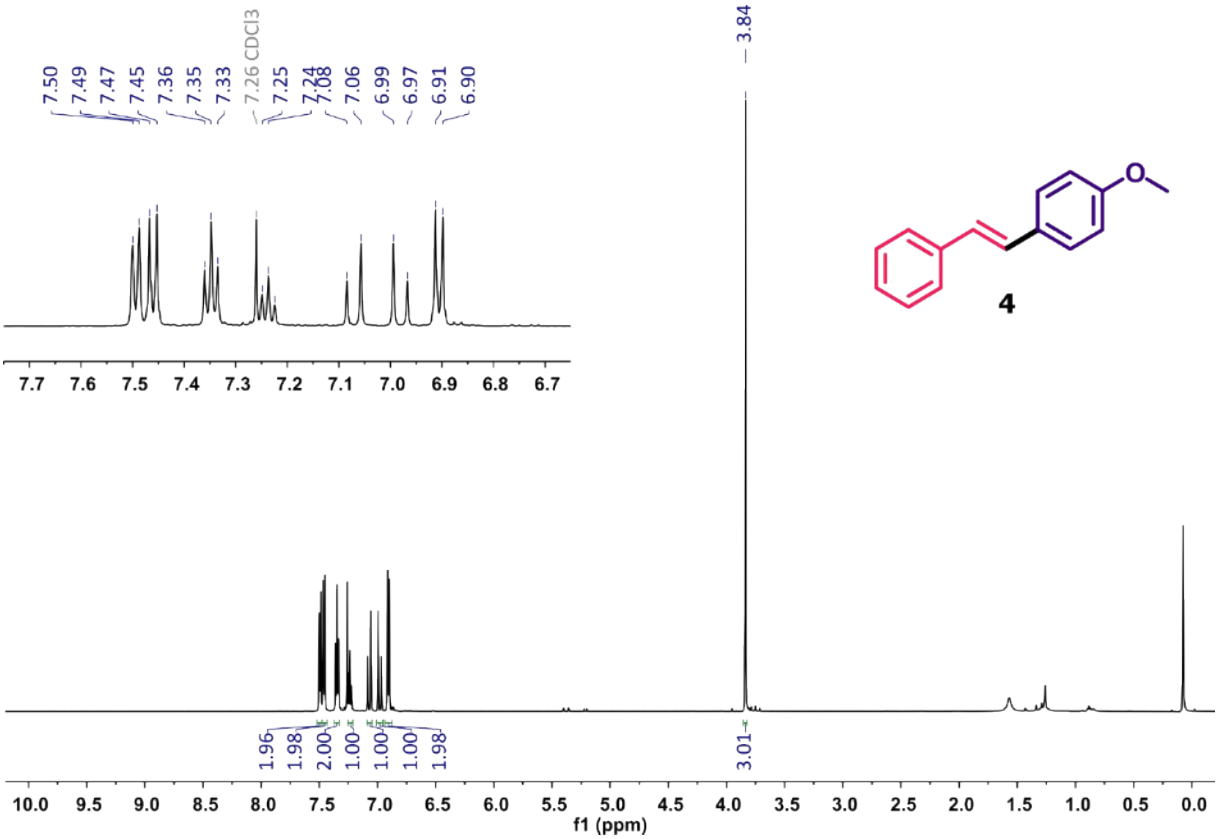

Figure S65. ^{1}H NMR spectrum (600 MHz, $CDCl_3$) of (*E*)-4-methoxystilbene **4**.

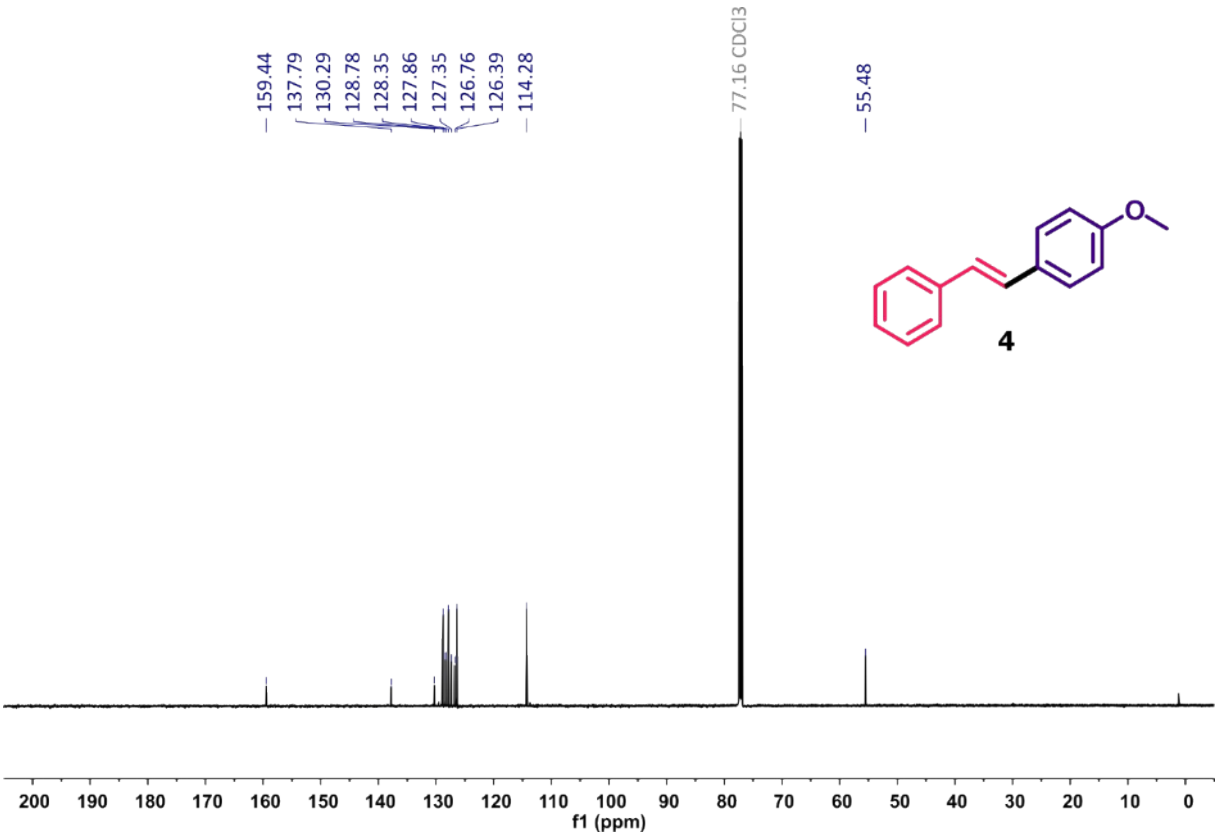

Figure S66. ^{13}C NMR spectrum (151 MHz, $CDCl_3$) of (*E*)-4-methoxystilbene **4**.

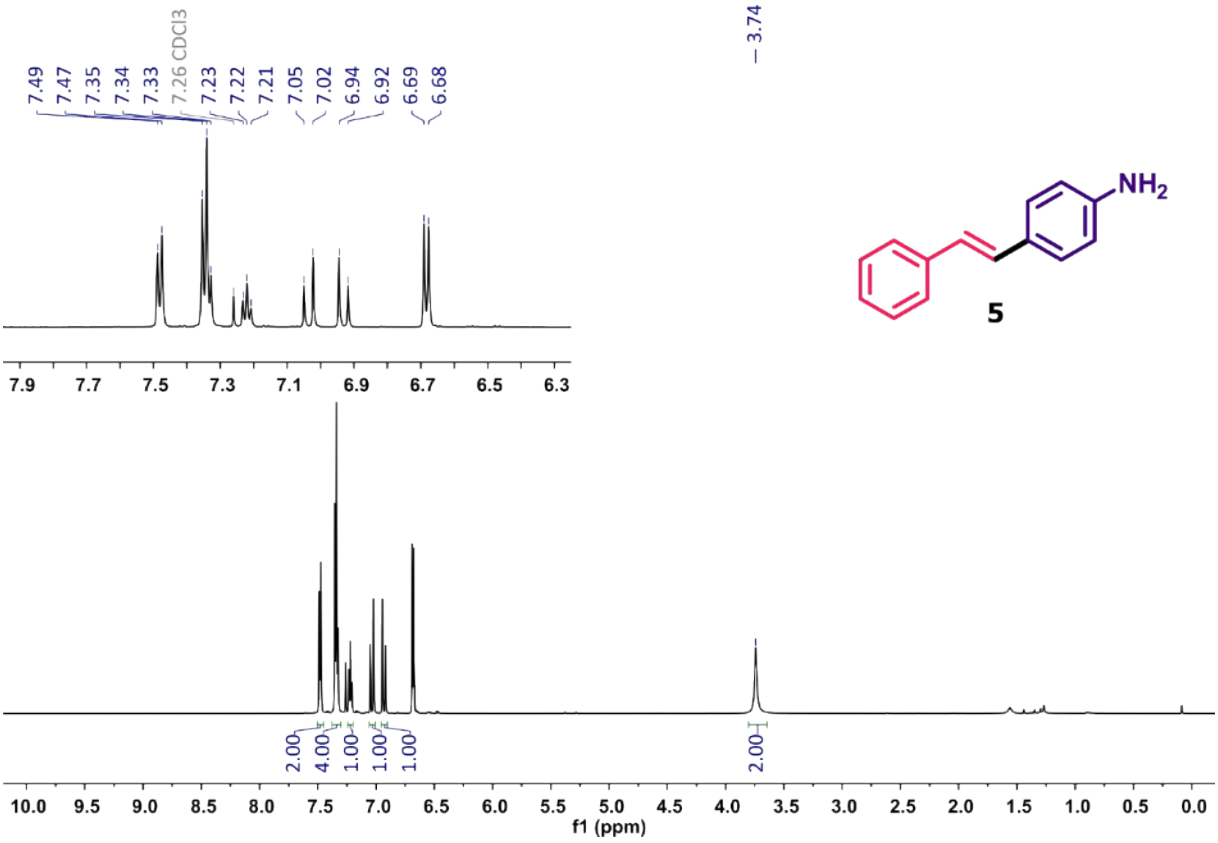

Figure S67. ^{1}H NMR spectrum (600 MHz, $CDCl_3$) of (*E*)-4-aminostilbene **5**.

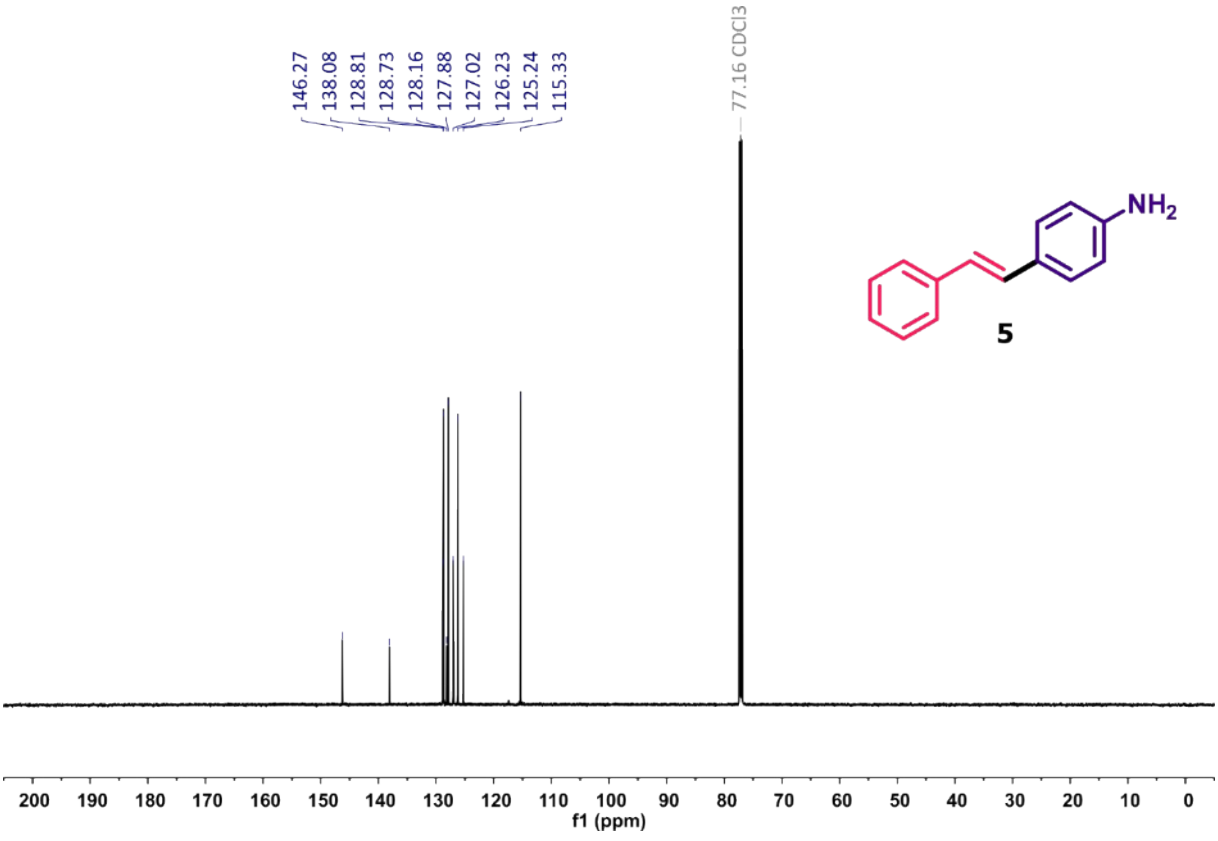

Figure S68. ^{13}C NMR spectrum (151 MHz, $CDCl_3$) of (*E*)-4-aminostilbene **5**.

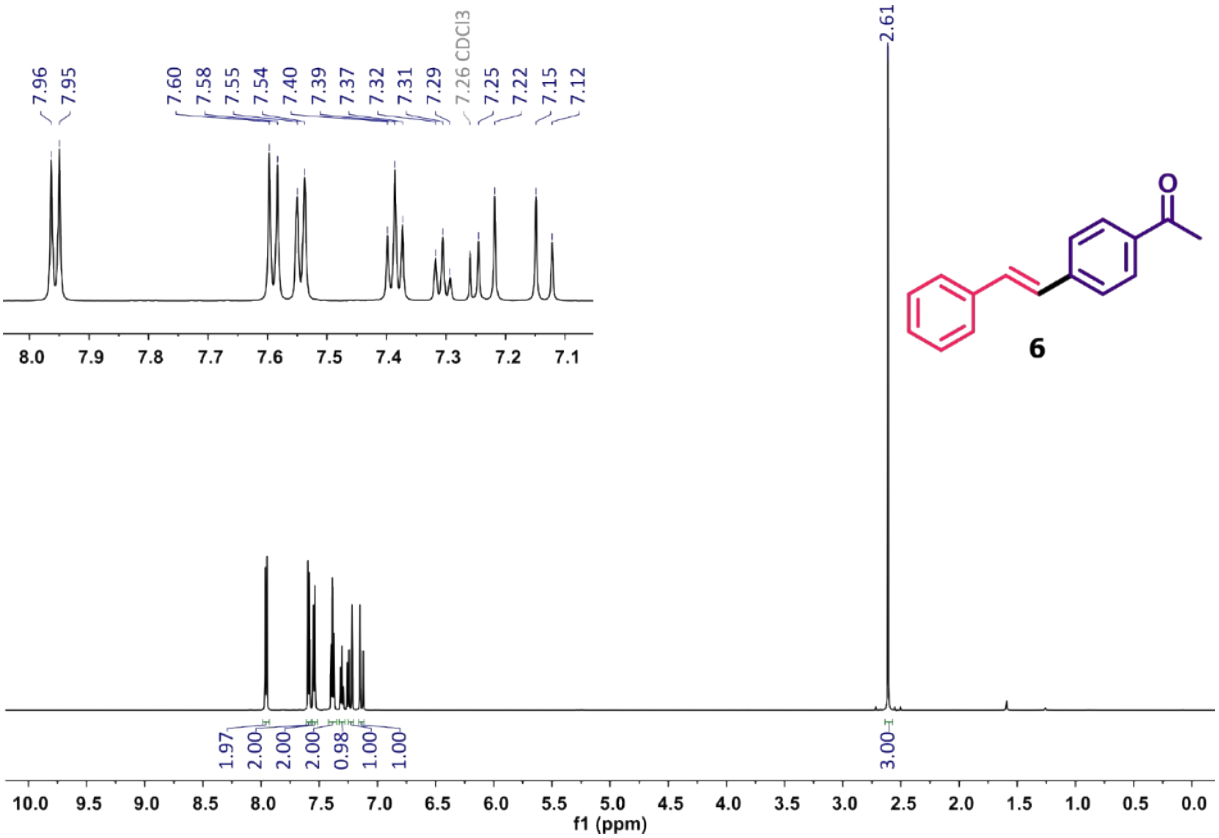

Figure S69. ^{1}H NMR spectrum (600 MHz, $CDCl_3$) of (*E*)-4-acetylstilbene **6**.

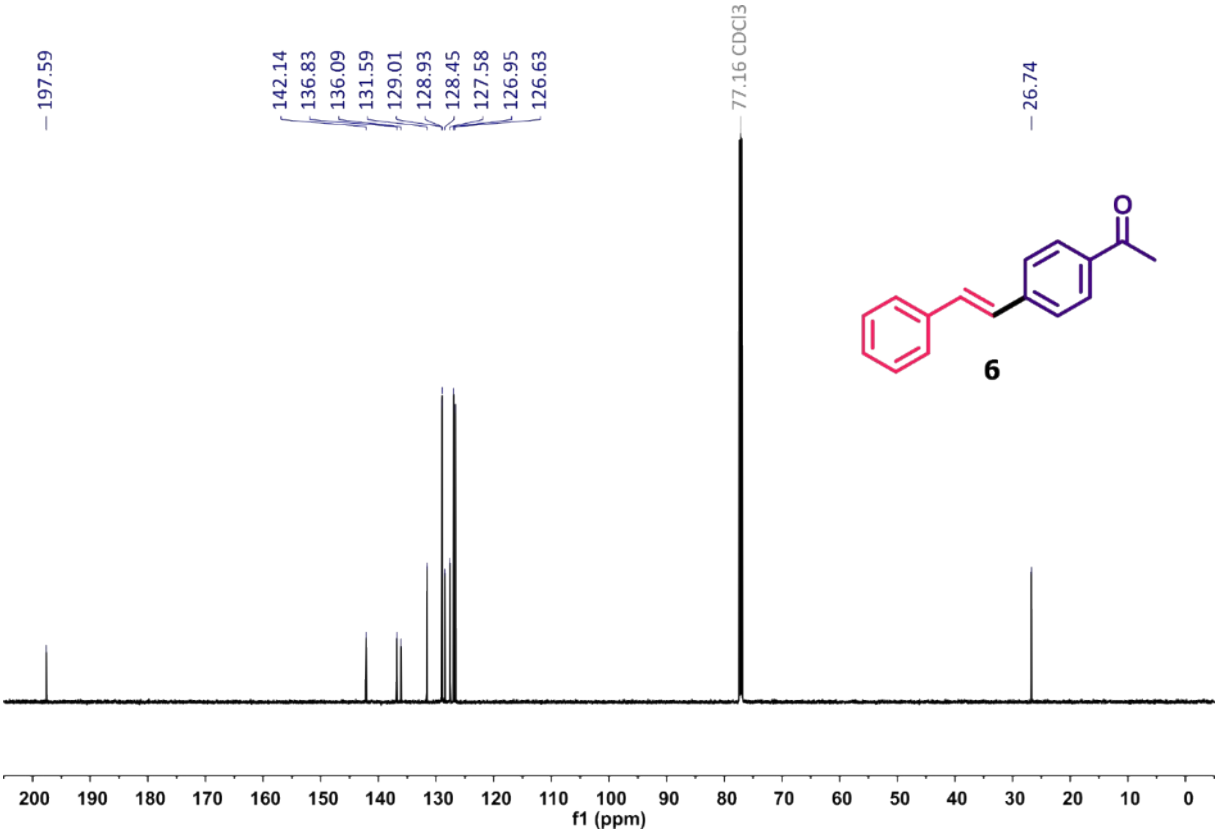

Figure S70. ^{13}C NMR spectrum (151 MHz, $CDCl_3$) of (*E*)-4-acetylstilbene **6**.

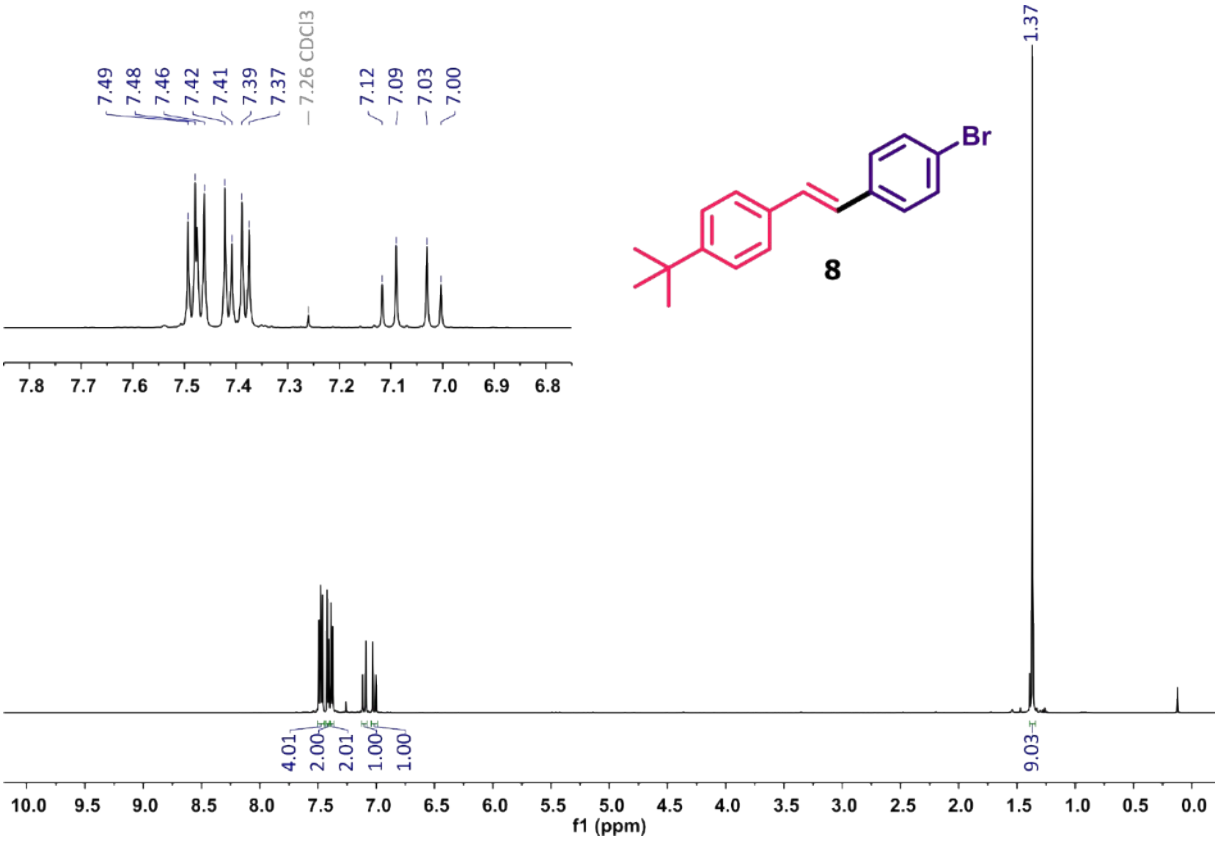

Figure S71. ^{1}H NMR spectrum (600 MHz, $CDCl_3$) of (*E*)-4-bromo-4'-tert-butylstilbene **8**.

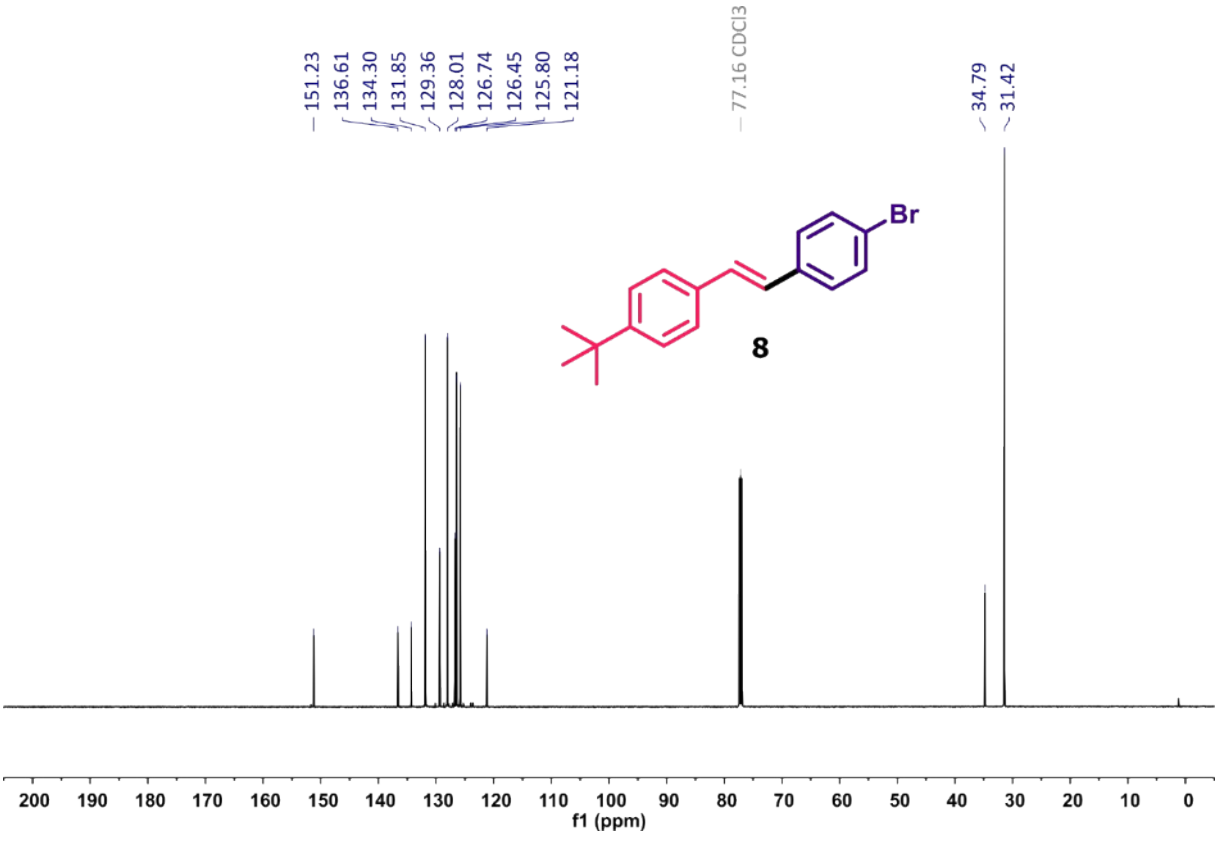

Figure S72. ^{13}C NMR spectrum (151 MHz, $CDCl_3$) of (*E*)-4-bromo-4'-tert-butylstilbene **8**.

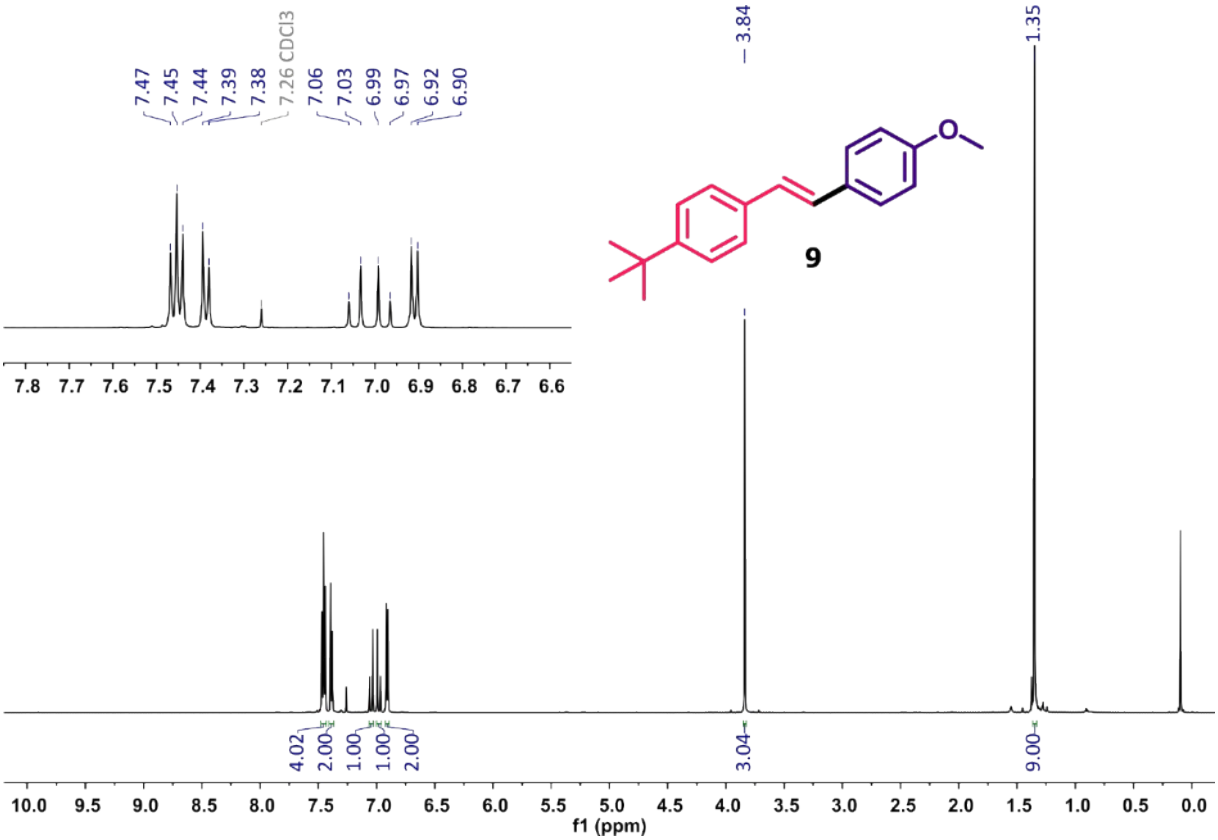

Figure S73. ^{1}H NMR spectrum (600 MHz, $CDCl_3$) of (*E*)-4-methoxy-4'-tert-butylstilbene **9**.

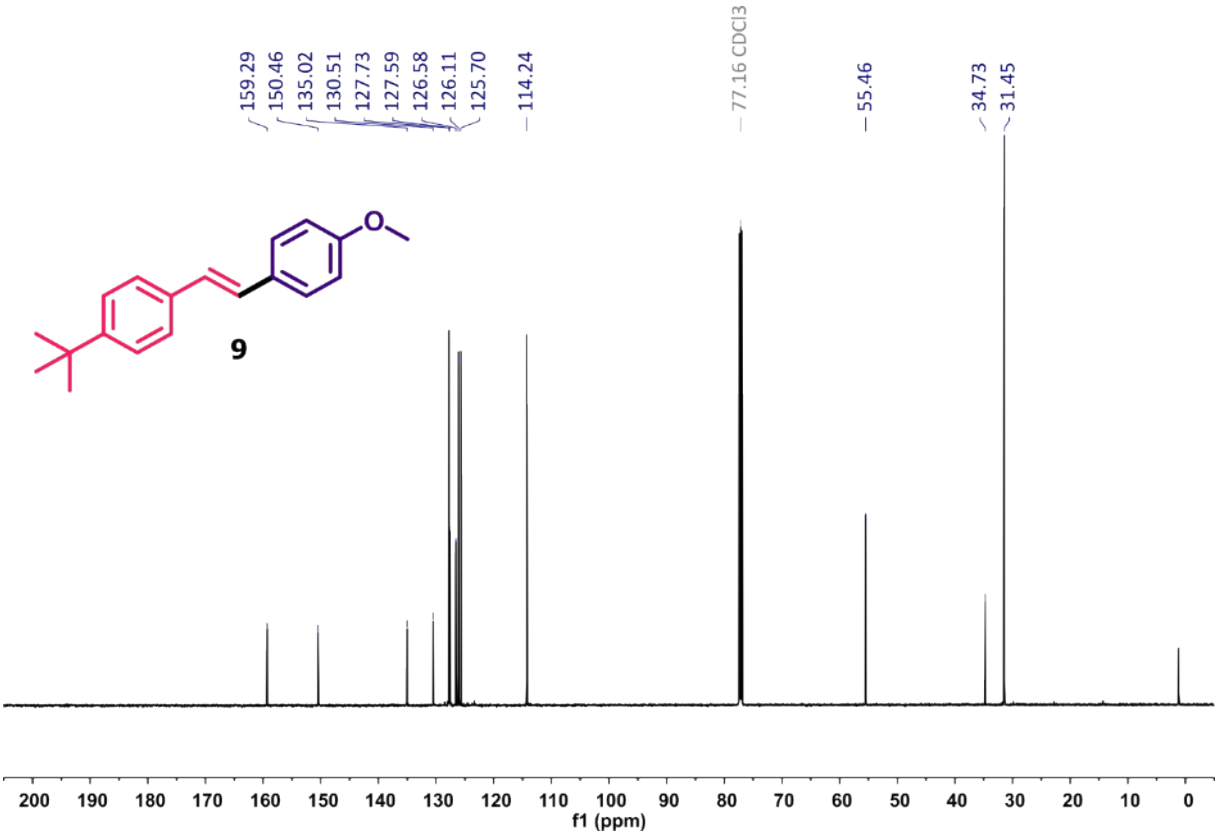

Figure S74. ^{13}C NMR spectrum (151 MHz, $CDCl_3$) of (*E*)-4-methoxy-4'-tert-butylstilbene **9**.

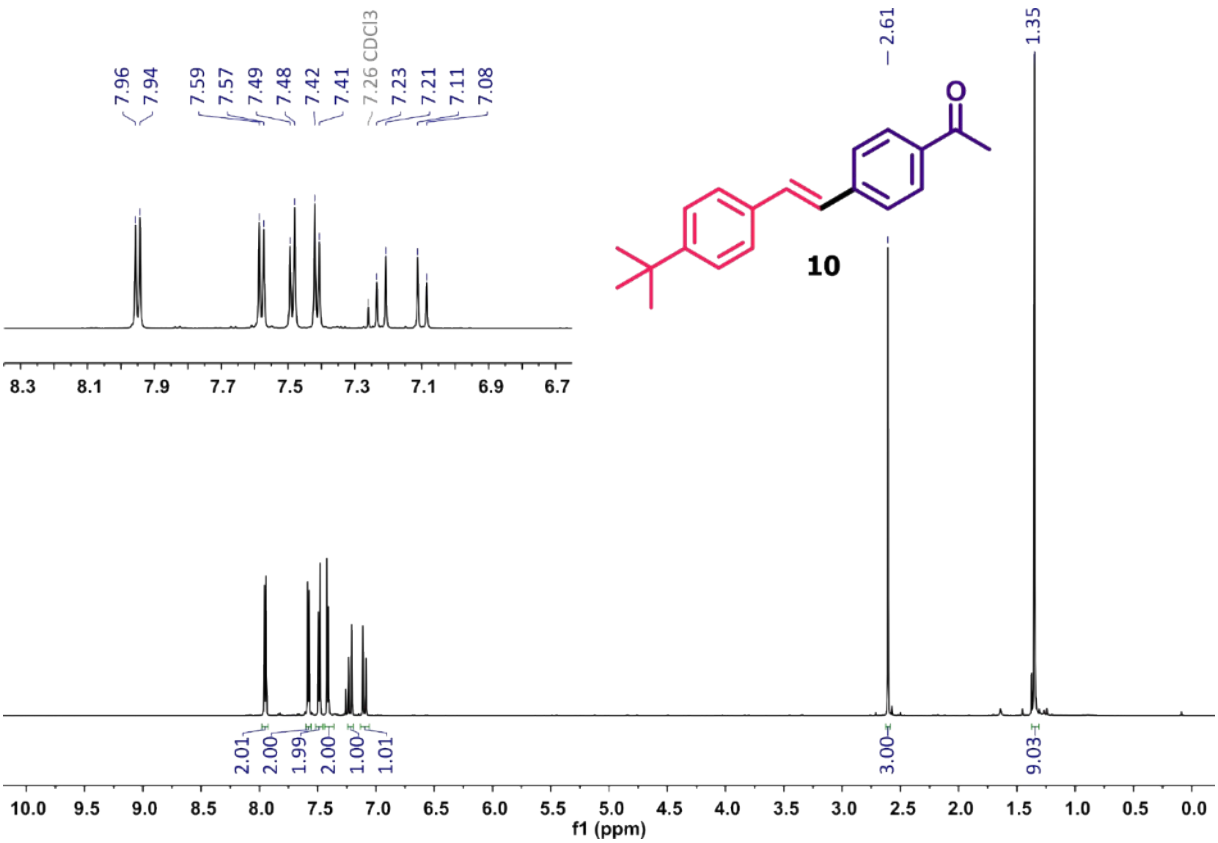

Figure S75. ^{1}H NMR spectrum (600 MHz, $CDCl_3$) of (*E*)-4-acetyl-4'-tert-butylstilbene **10**.

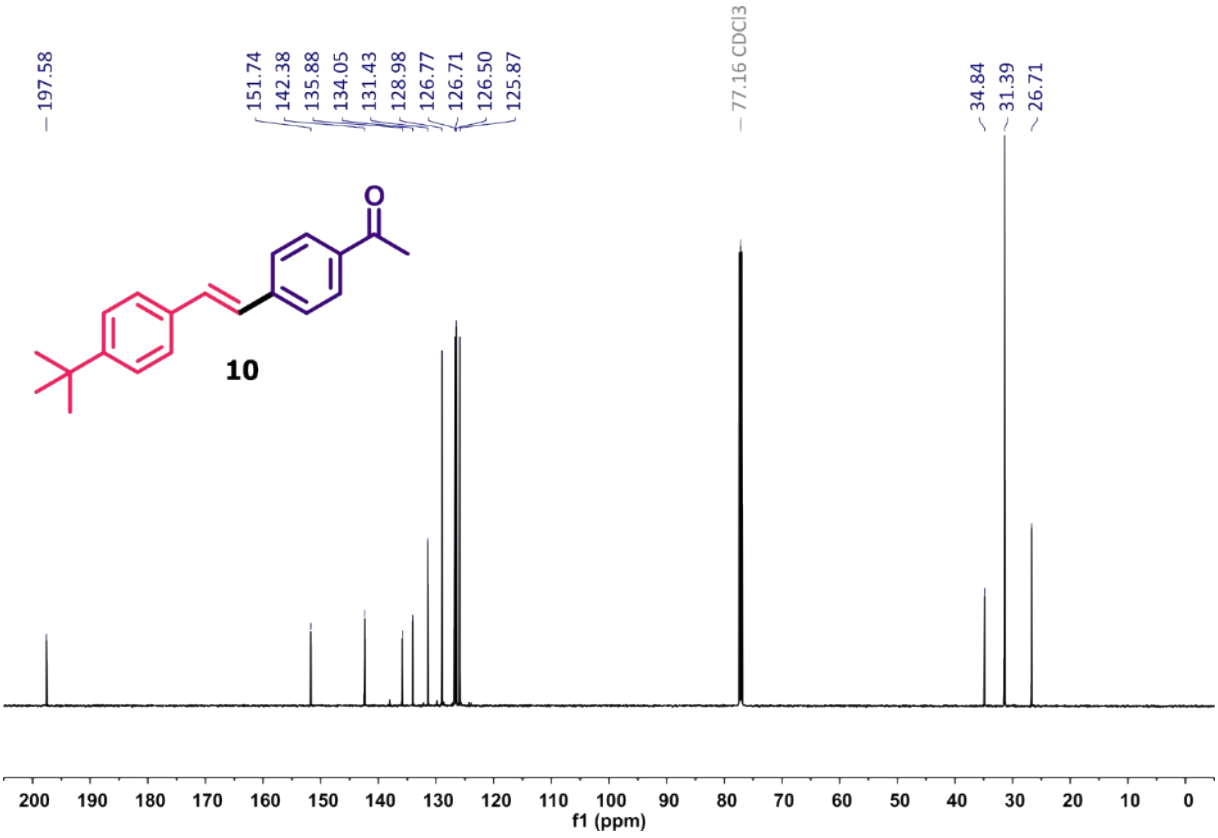

Figure S76. ^{13}C NMR spectrum (151 MHz, $CDCl_3$) of (*E*)-4-acetyl-4'-tert-butylstilbene **10**.

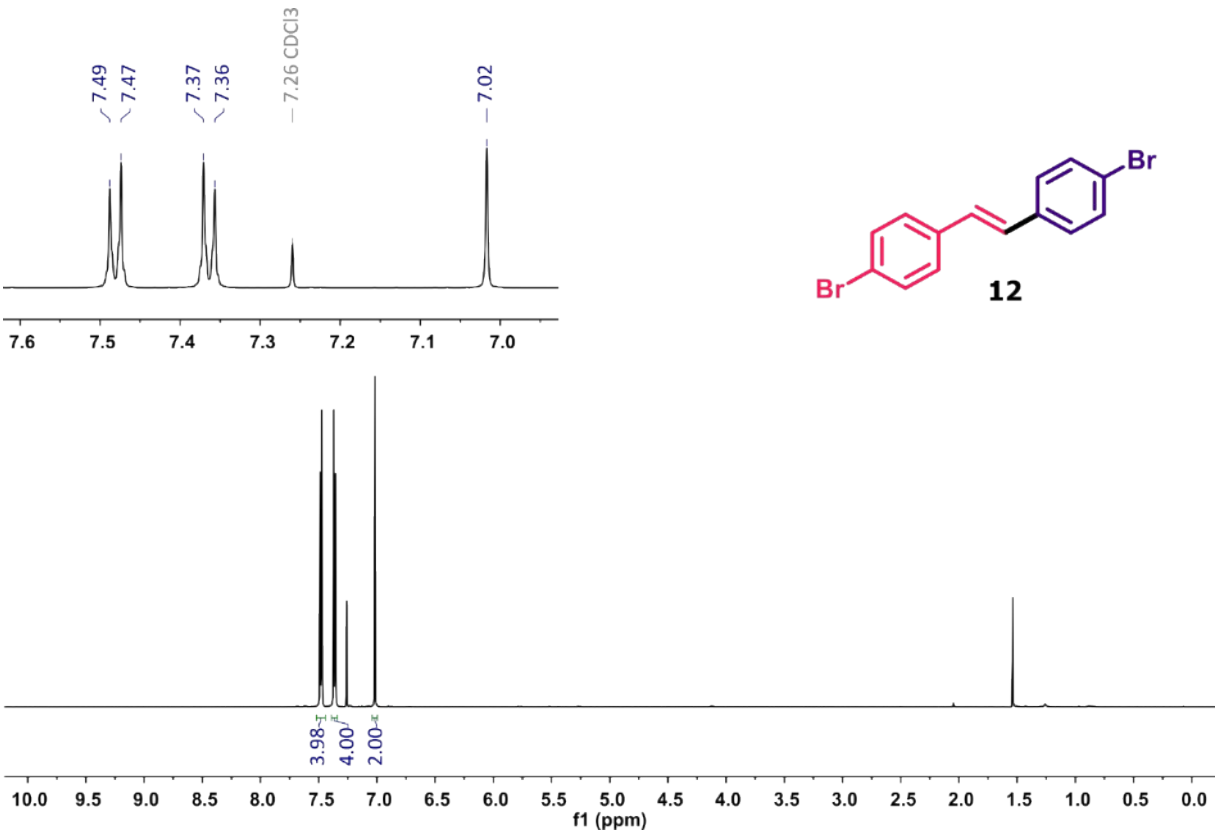

Figure S77. ^{1}H NMR spectrum (600 MHz, $CDCl_3$) of (*E*)-4,4'-dibromostilbene **12**.

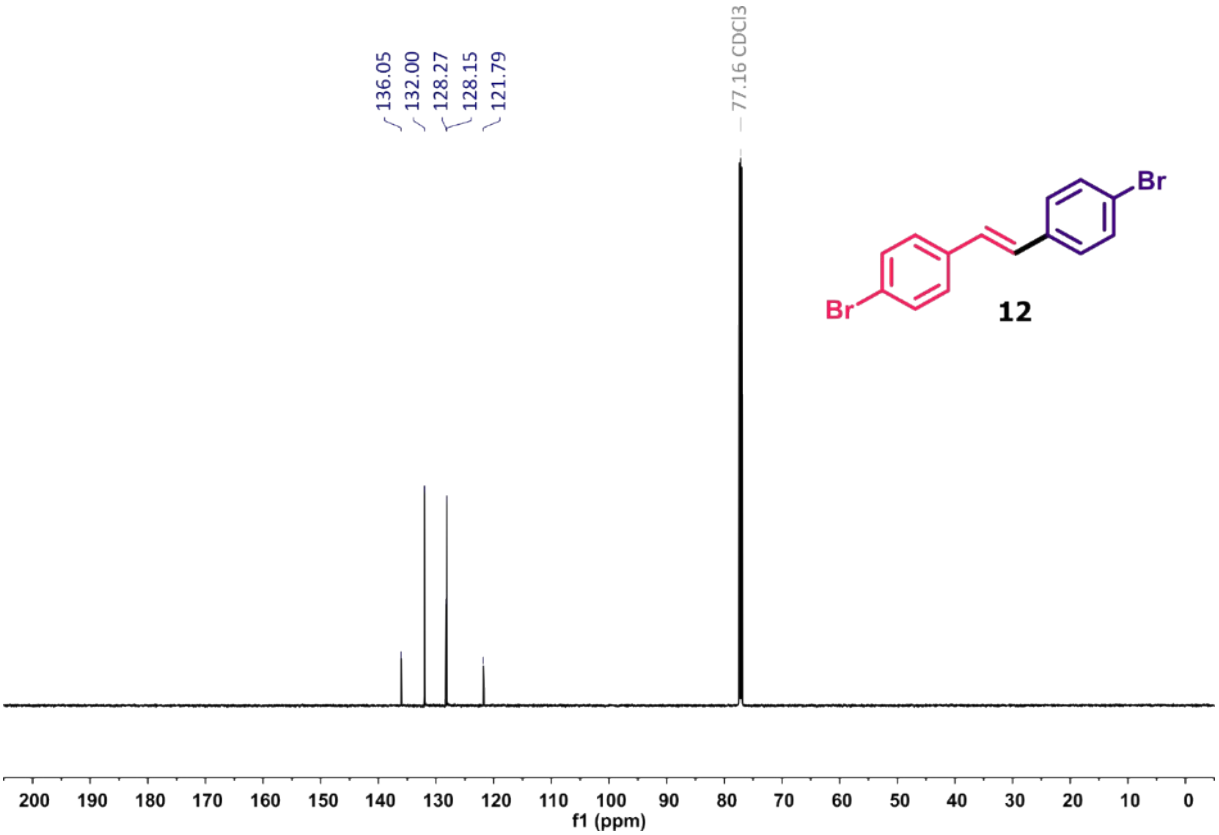

Figure S78. ^{13}C NMR spectrum (151 MHz, $CDCl_3$) of (*E*)-4,4'-dibromostilbene **12**.

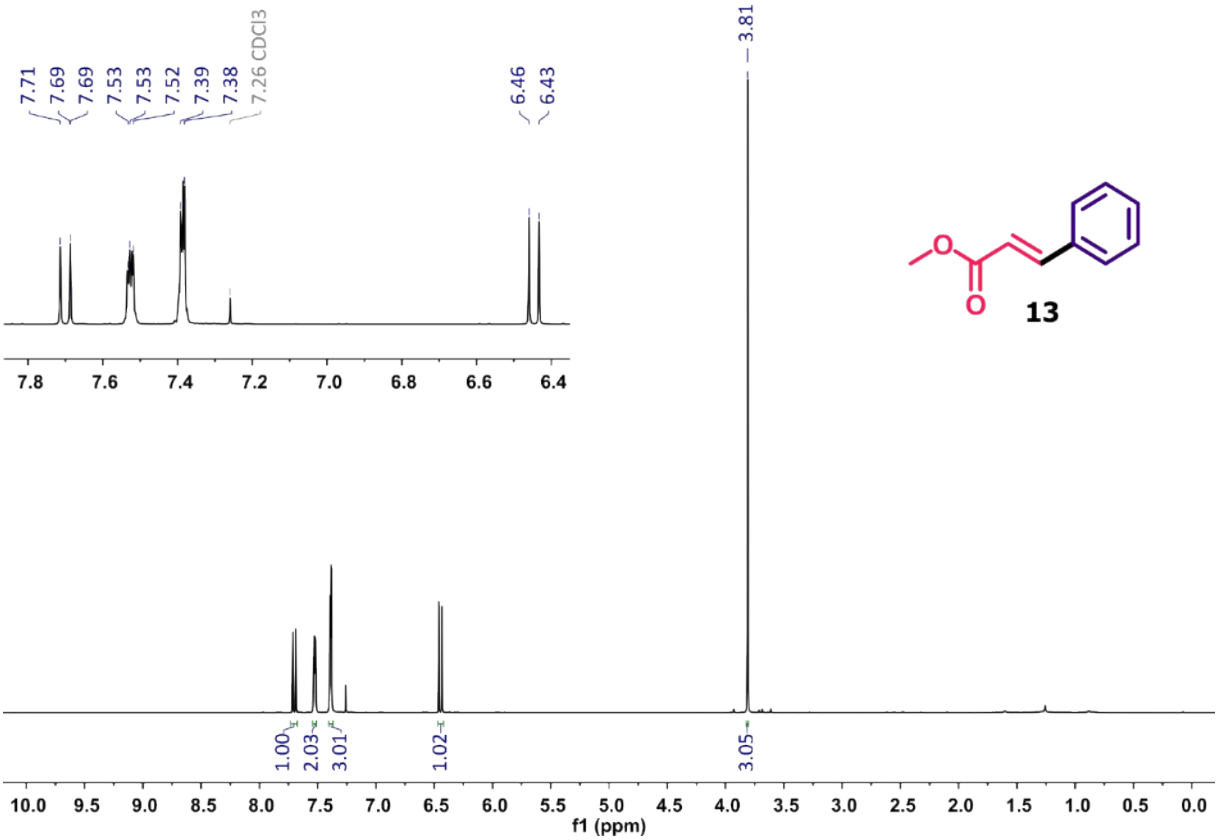

Figure S79. ^{1}H NMR spectrum (600 MHz, $CDCl_3$) of methyl (*E*)-cinnamate **13**.

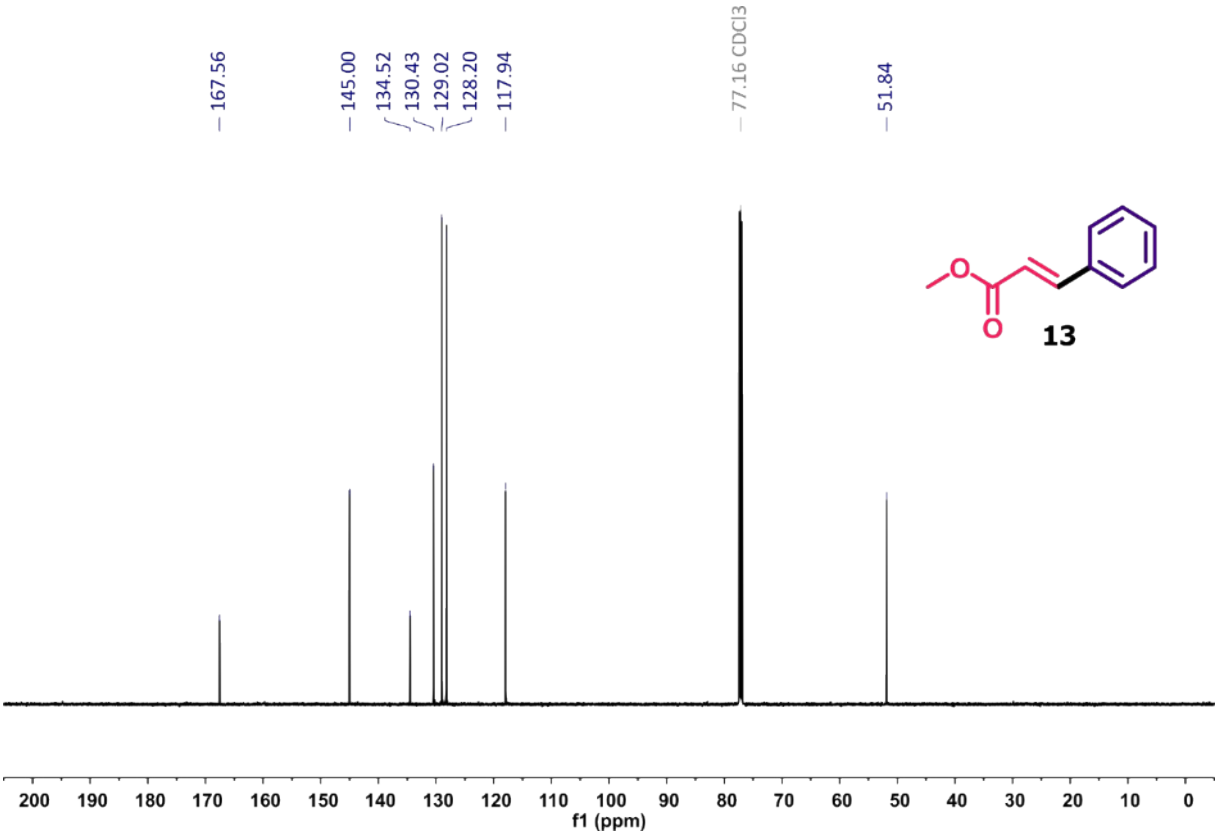

Figure S80. ^{13}C NMR spectrum (151 MHz, $CDCl_3$) of methyl (*E*)-cinnamate **13**.

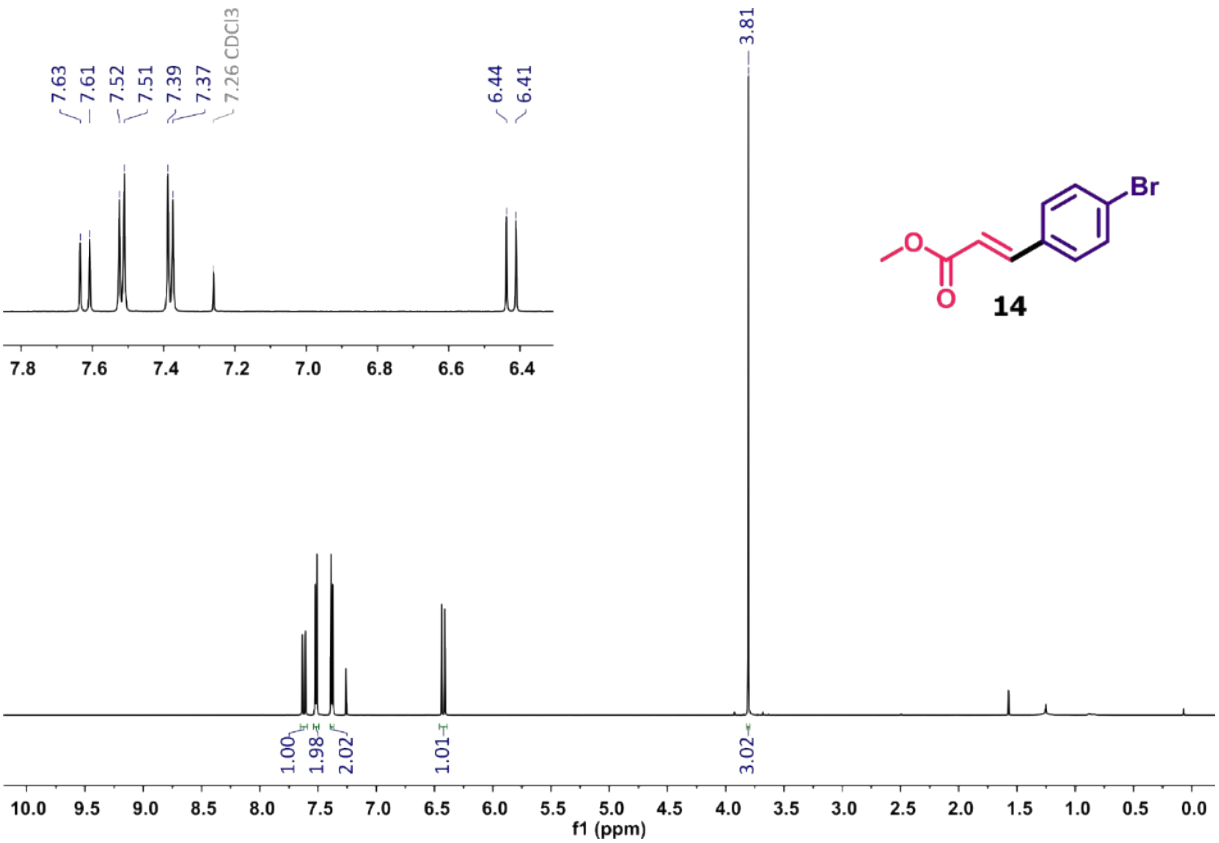

Figure S81. ^{1}H NMR spectrum (600 MHz, $CDCl_3$) of methyl (*E*)-4-bromocinnamate **14**.

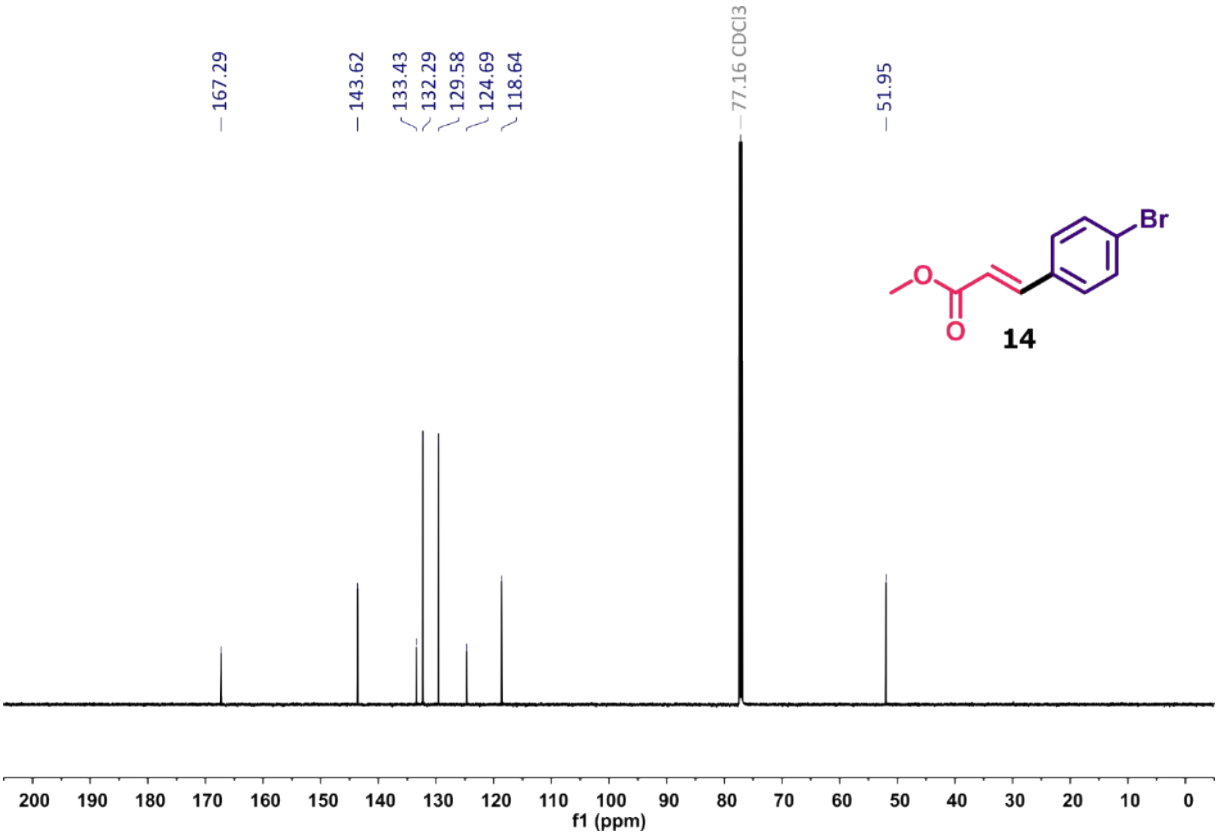

Figure S82. ^{13}C NMR spectrum (151 MHz, $CDCl_3$) of methyl (*E*)-4-bromocinnamate **14**.

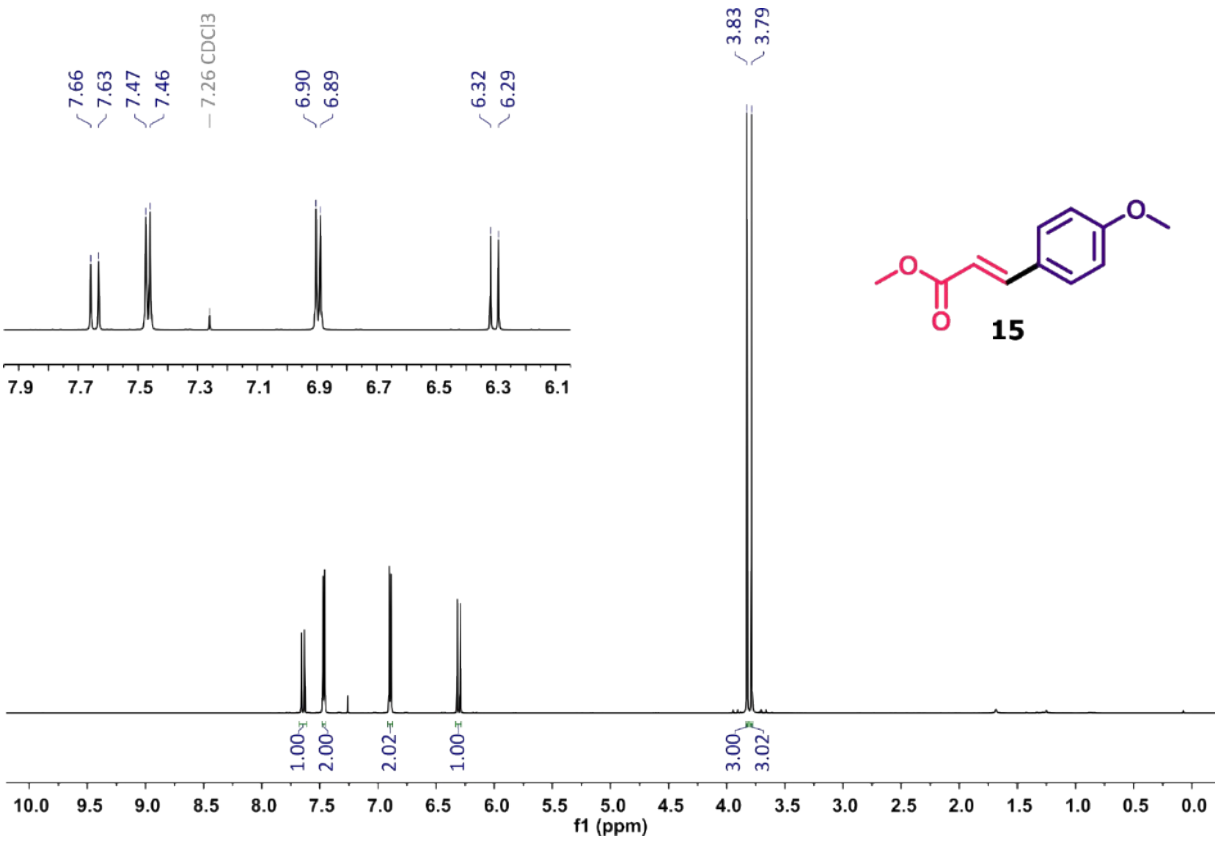

Figure S83. ^{1}H NMR spectrum (600 MHz, $CDCl_3$) of methyl (*E*)-4-methoxycinnamate **15**.

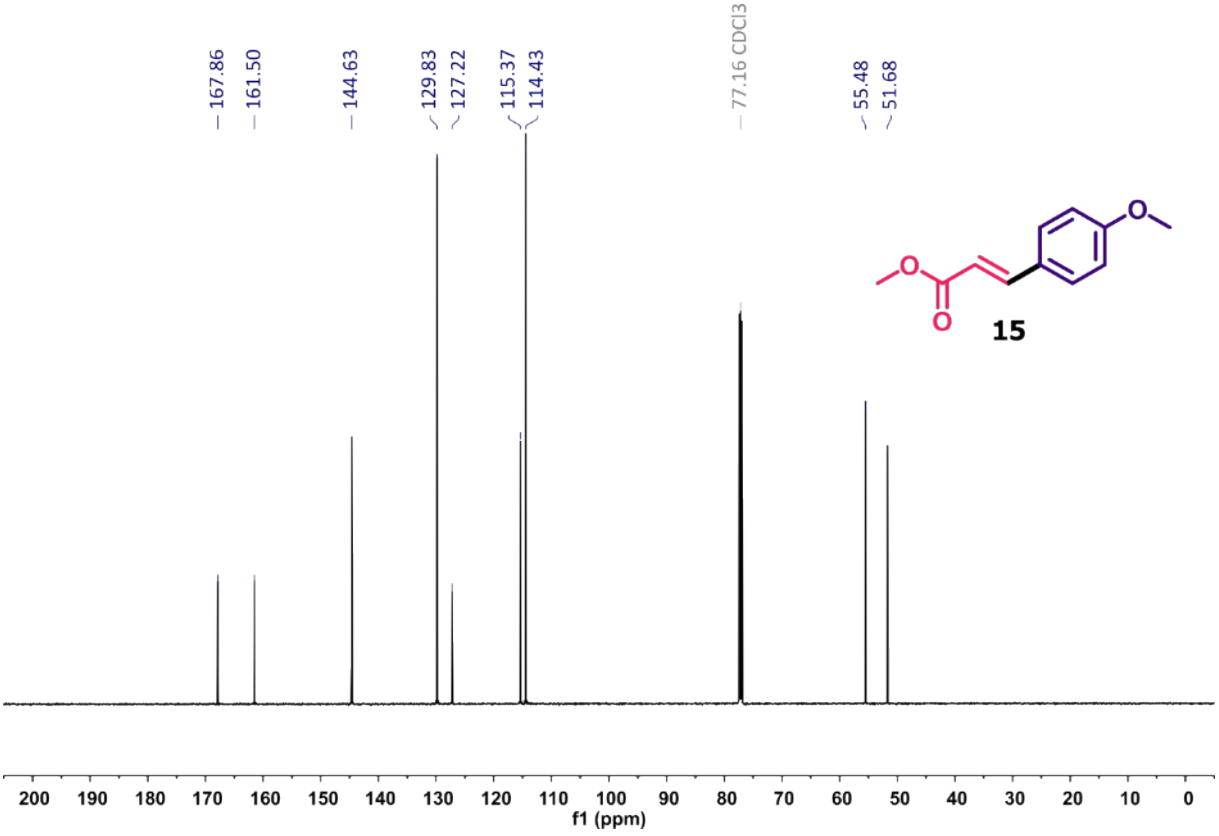

Figure S84. ^{13}C NMR spectrum (151 MHz, $CDCl_3$) of methyl (*E*)-4-methoxycinnamate **15**.

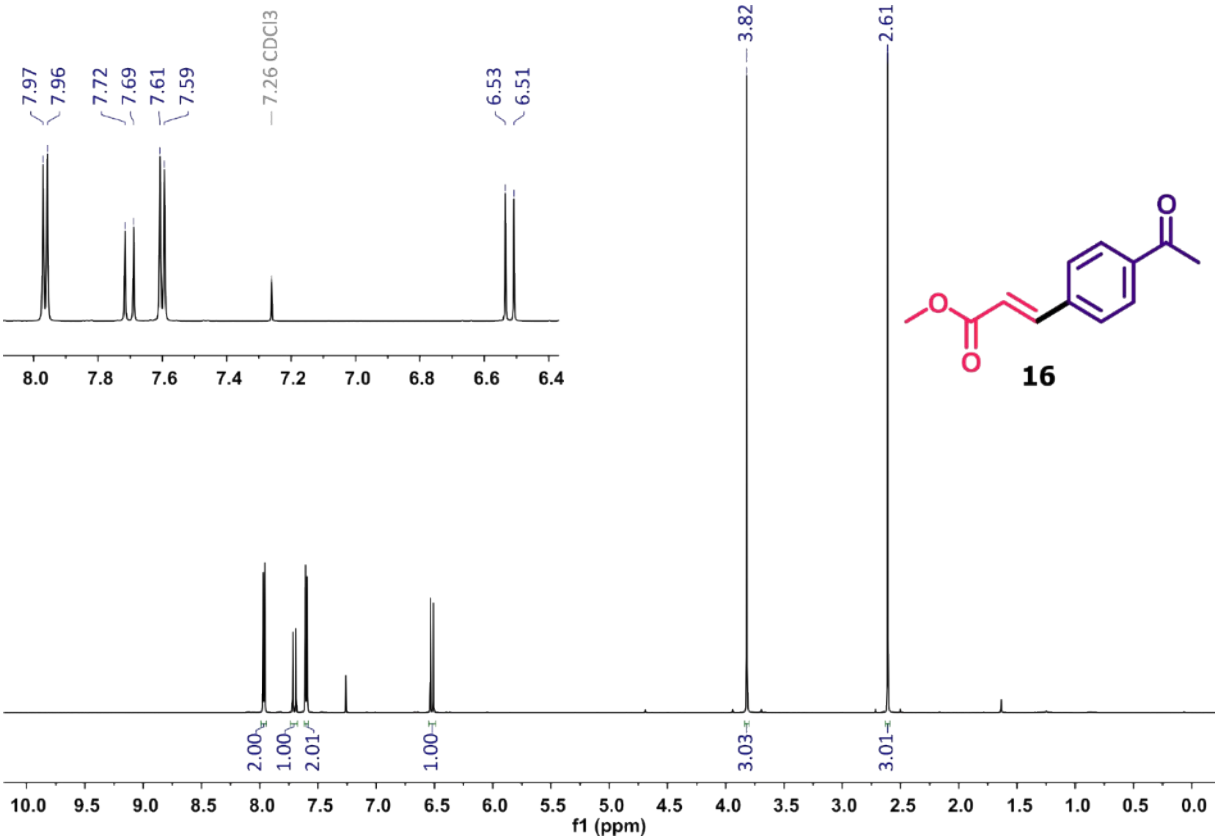

Figure S85. ^{1}H NMR spectrum (600 MHz, $CDCl_3$) of methyl (*E*)-4-acetylcinnamate **16**.

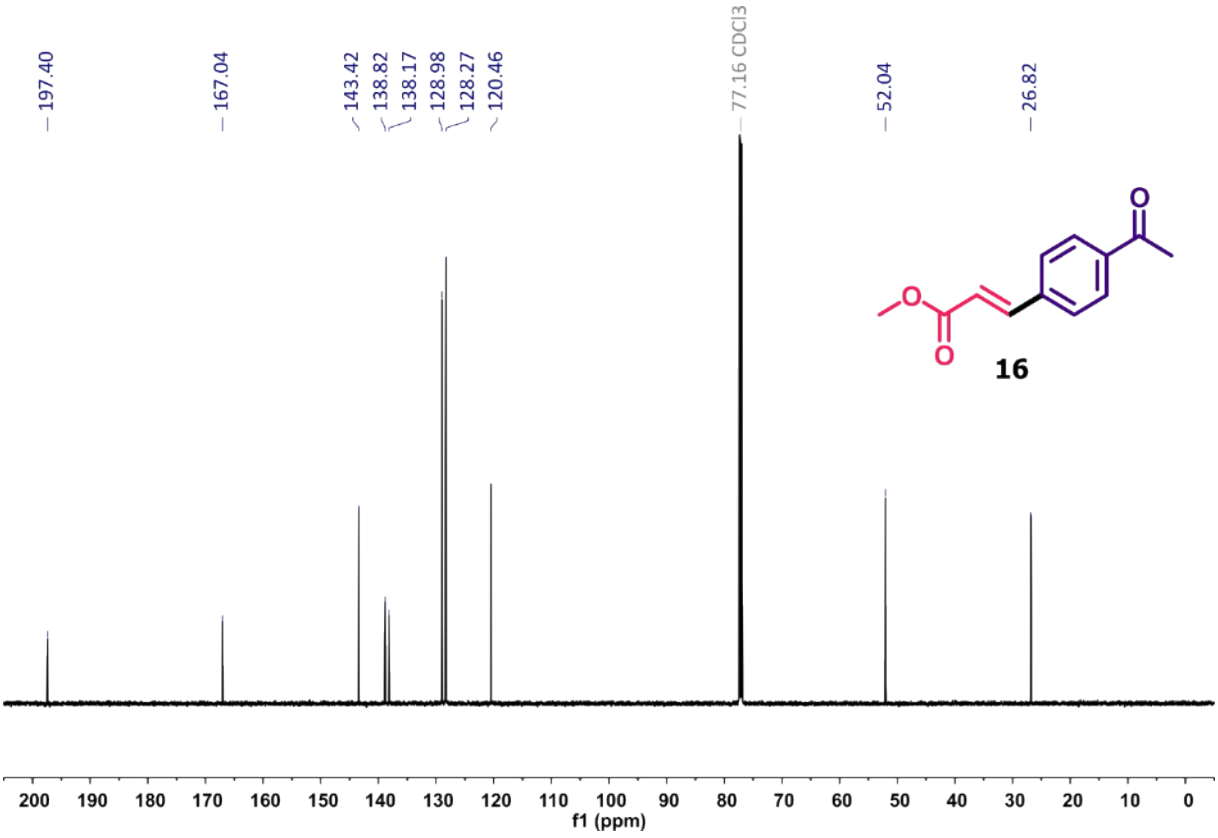

Figure S86. ^{13}C NMR spectrum (151 MHz, $CDCl_3$) of methyl (*E*)-4-acetylcinnamate **16**.

13. References

S1. Walczak, A.; Stefankiewicz, A. R., pH-Induced Linkage Isomerism of Pd(II) Complexes: A Pathway to Air- and Water-Stable Suzuki–Miyaura-Reaction Catalysts. *Inorganic Chemistry* **2018,** *57* (1), 471-477.

S2. Walczak, A.; Stachowiak, H.; Kurpik, G.; Kaźmierczak, J.; Hreczycho, G.; Stefankiewicz, A. R., High catalytic activity and selectivity in hydrosilylation of new Pt(II) metallosupramolecular complexes based on ambidentate ligands. *Journal of Catalysis* **2019,** *373*, 139-146.

S3. CrysAlisPRO, *Oxford Diffraction., Agilent CrysAlis PRO. Agilent Technologies Ltd* **2014**, Yarnton, Oxfordshire, England.

S4. Dolomanov, O. V.; Bourhis, L. J.; Gildea, R. J.; Howard, J. A. K.; Puschmann, H., OLEX2: a complete structure solution, refinement and analysis program. *J. Appl. Crystallogr.* **2009,** *42* (2), 339-341.

S5. Sheldrick, G., SHELXT - Integrated space-group and crystal-structure determination. *Acta Crystallographica Section A* **2015,** *71* (1), 3-8.

S6. Sheldrick, G., Crystal structure refinement with SHELXL. *Acta Crystallographica Section C* **2015,** *71* (1), 3-8.

S7. Ye, Z.; Chen, F.; Luo, F.; Wang, W.; Lin, B.; Jia, X.; Cheng, J., Palladium-Catalyzed Mizoroki-Heck-Type Reaction of Aryl Trimethoxysilanes. *Synlett* **2009,** *2009* (13), 2198-2200.

S8. Lerch, S.; Fritsch, S.; Strassner, T., The Mizoroki-Heck Reaction in Tunable Aryl Alkyl Ionic Liquids. *European Journal of Organic Chemistry* **2022,** *2022* (6), e202200008.

S9. Jia, X.; Frye, L. I.; Zhu, W.; Gu, S.; Gunnoe, T. B., Synthesis of Stilbenes by Rhodium-Catalyzed Aerobic Alkenylation of Arenes via C–H Activation. *Journal of the American Chemical Society* **2020,** *142* (23), 10534-10543.

S10. Chen, Z.; Luo, M.; Wen, Y.; Luo, G.; Liu, L., Transition-Metal-Free Semihydrogenation of Diarylalkynes: Highly Stereoselective Synthesis of trans-Alkenes Using Na2S·9H2O. *Organic Letters* **2014,** *16* (11), 3020-3023.

S11. Zhong, J.-J.; Liu, Q.; Wu, C.-J.; Meng, Q.-Y.; Gao, X.-W.; Li, Z.-J.; Chen, B.; Tung, C.-H.; Wu, L.-Z., Combining visible light catalysis and transfer hydrogenation for in situ efficient and selective semihydrogenation of alkynes under ambient conditions. *Chemical Communications* **2016,** *52* (9), 1800-1803.

S12. Mai, J.; Arkhypchuk, A. I.; Gupta, A. K.; Ott, S., Reductive coupling of two aldehydes to unsymmetrical E-alkenes via phosphaalkene and phosphinate intermediates. *Chemical Communications* **2018,** *54* (52), 7163-7166.

S13. Song, K.; Liu, P.; Wang, J.; Pang, L.; Chen, J.; Hussain, I.; Tan, B.; Li, T., Controlled synthesis of uniform palladium nanoparticles on novel micro-porous carbon as a recyclable heterogeneous catalyst for the Heck reaction. *Dalton Transactions* **2015,** *44* (31), 13906-13913.

S14. Yang, K.; Song, Q., Pd-Catalyzed Regioselective Arylboration of Vinylarenes. *Organic Letters* **2016,** *18* (21), 5460-5463.

S15. Desai, S. P.; Ye, J.; Zheng, J.; Ferrandon, M. S.; Webber, T. E.; Platero-Prats, A. E.; Duan, J.; Garcia-Holley, P.; Camaioni, D. M.; Chapman, K. W.; Delferro, M.; Farha, O. K.; Fulton, J. L.; Gagliardi, L.; Lercher, J. A.; Penn, R. L.; Stein, A.; Lu, C. C., Well-Defined Rhodium–Gallium Catalytic Sites in a Metal–Organic Framework: Promoter-Controlled Selectivity in Alkyne Semihydrogenation to E-Alkenes. *Journal of the American Chemical Society* **2018,** *140* (45), 15309-15318.

S16. Pape, S.; Daukšaitė, L.; Lucks, S.; Gu, X.; Brunner, H., An in Situ Generated Palladium on Aluminum Oxide: Applications in Gram-Scale Matsuda–Heck Reactions. *Organic Letters* **2016,** *18* (24), 6376-6379.

S17. Mahmoudi, H.; Valentini, F.; Ferlin, F.; Bivona, L. A.; Anastasiou, I.; Fusaro, L.; Aprile, C.; Marrocchi, A.; Vaccaro, L., A tailored polymeric cationic tag–anionic Pd(ii) complex as a catalyst for the low-leaching Heck–Mizoroki coupling in flow and in biomass-derived GVL. *Green Chemistry* **2019,** *21* (2), 355-360.